LAS

Jahresbericht / Annual Report 2020/2021

Neubau des "Anwendungszentrums Fluiddynamik, AZFD"

Prof. Dr.-Ing. Christoph Egbers
Lehrstuhl Aerodynamik und Strömungslehre (LAS)
Institut für Verkehrstechnik
Fakultät 3
Maschinenbau, Elektro- und Energiesysteme
BTU Cottbus-Senftenberg
Siemens-Halske-Ring 15a
03046 Cottbus

Brandenburgische Technische Universität Cottbus - Senftenberg

Vorwort

Der *Lehrstuhl Aerodynamik und Strömungslehre (LAS)* wurde im Juli 2000 mit der Berufung von Dr.-Ing. Christoph Egbers an die Brandenburgische Technische Universität (BTU) Cottbus neu gegründet. Der Lehrstuhl gehört zum *Institut für Verkehrstechnik (IVT),* welches im Jahr 1999 gegründet wurde. Diesem Institut gehören z.Zt. folgende Lehrstühle an:

- LS Aerodynamik und Strömungslehre (LAS)
- LS Technische Mechanik und Fahrzeugdynamik
- LS Strukturmechanik und Fahrzeugschwingungen
- LS Verbrennungskraftmaschinen und Flugantriebe
- LS Fahrzeugtechnik- und Antriebe
- FG Technische Akustik
- LS Triebwerksdesign
- LS Numerische Strömungs- und Gasdynamik
- LS Bildgebende Messverfahren (neu: gemeinsame Berufung DLR-BTU)

Der Lehrstuhl für Aerodynamik und Strömungslehre (LAS) beschäftigt 21 Mitarbeiter/innen und ist in vier Abteilungen gegliedert, in denen z.Zt. folgende Forschungsthemen bearbeitet werden:

Aerodynamik
- Triebwerks-Flügel-Wechselwirkungen
- Grenzschichtströmungen
- Strömungsbeeinflussung

Strömungsmechanik
- Strukturbildung und Stabilität in hydrodynamischen Systemen
- Rotierende Strömungen
- Turbulente Strömungen
- Geophysikalisch motivierte Strömungen
- Meteorologisch motivierte Strömungen
- Gleitlagerströmungen
- Partikelströmungen
- Thermoelektrohydrodynamik (TEHD)

Raumfahrtanwendungen
- Fluid-Experimente unter Schwerelosigkeit (Raumstation ISS, Parabelflüge, TEXUS)

Messtechnik
- Entwicklung von Strömungsmessverfahren zur Strömungsbeeinflussung
- Partikelmesstechnik
- Zeitreihenanalyse und nichtlineare Datenanalyse
- Koppelung von PIV und Thermographie (simultane Temperatur- und Geschwindigkeitsmessung)

Ich bedanke mich mit diesem Jahresbericht bei meinen Mitarbeiterinnen und Mitarbeitern für die sehr erfolgreich geleistete Arbeit am Lehrstuhl sowie bei unseren Kooperationspartnern und bei allen Förderinstitutionen, von denen der Lehrstuhl Aerodynamik und Strömungslehre (LAS) an der BTU Cottbus-Senftenberg Projektförderung erhalten hat.

Cottbus, im März 2022 Prof. Dr.-Ing. Christoph Egbers

Inhaltsverzeichnis / Index

Mitarbeiter / Staff at the Chair of Aerodynamics and Fluid Mechanics

Prof. Dr.-Ing. Christoph Egbers	Leiter des Lehrstuhls
Silke Kaschwich	Sekretariat
Wissenschaftliche Mitarbeiter	**Aufgabengebiet**
M.Sc. Yann Gaillard-Röpke	Strömungsmechanik (Doktorand)
M.Sc. Zeinab Hallol	Strömungsmechanik (Doktorandin)
M.Sc. Mohammed Hamede	Strömungsmechanik (Doktorand)
apl. Prof. Dr. rer. nat. habil. Uwe Harlander	Strömungsmechanik, Meteorologie
Dr.-Ing. Gazi Hasanuzzaman	Aerodynamik (Postdoc)
M.Sc. Peter Haun	Strömungsmechanik (Doktorand)
Dr. rer. nat. Andreas Krebs	Rechneradministration CFTMM und HLRN
Dr.-Ing. Martin Meier	Raumfahrtanwendungen (Postdoc)
Dr.-Ing. Sebastian Merbold	Strömungsmechanik (Postdoc)
Dr. Antoine Meyer	Strömungsmechanik (Postdoc)
Dr.-Ing Vasyl Motuz	Aerodynamik, (Postdoc)
M.Sc. Stefan Richter	Aerodynamik (Doktorand)
M.Sc. Yaraslau Sliavin	Strömungsmechanik (Doktorand)
Dr. Peter Szabo	Strömungsmechanik (Postdoc)
Dr.-Ing. Vadim Travnikov	Strömungsmechanik (Postdoc)
M.Sc. Mohammed Yousry	Aerodynamik (Doktorand)
Dr.-Ing. El-Sayed Zanoun	Aerodynamik
Technische Mitarbeiter	**Aufgabengebiet**
B. Eng. Tark Raj Bista	Parabelflug-/TEXUS-Experimente
Techniker Stefan Rohark	Werkstatt-Leitung
Dipl.-Ing. Robin Stöbel	Labore, Windkanäle, Messtechnik
Dipl.-Ing. Andreas Stöckert	Systemadministration, Messtechnik

Wissenschaftliche Kooperationen und Partner
Scientific contacts and co-operation with industrial partner

Prof. Dr. Detlef Lohse	Physics of Fluids, University of Twente, The Netherlands
Prof. Dr. Vincent Heuveline	URZ, Heidelberg, Universität Heidelberg
Prof. Dr. Peter Read	Dept. of Atmospheric, Oceanic and Planetary Physics University of Oxford, UK
Dr. Wolf-Gerrit Früh	Heriot-Watt University, Edinborough, UK
Prof. Dr. Rainer Hollerbach	Dept. of Mathematics, University of Leeds, UK
Prof. Dr. Daniel Lathrop	Institute for Physical Sciences and Technology, University of Maryland, USA
Prof. Dr. Richard M. Lueptow	Dept. of Mech. Engineering Northwestern University, Chicago, USA
Prof. Dr. Laurette Tuckerman	ESPCI, Paris, France
Prof. Dr. Patrice LeGal	IRPHE, Université Marseille, France
Prof. Dr. Innocent Mutabazi	LOMC, CNRS Université du Havre, France
Prof. Dr. Pascal Chossat	Directeur Centre International de Rencontres Mathématiques, Luminy (Marseille), France
Prof. Dr. Philippe Cardin	Institut des Sciences de la Terre, Grenoble, France
Prof. Dr. Antony Randriamampianina	CNRS, Université Marseille, France
Prof. Dr. rer. nat. Doris Breuer	DLR-Inst. (Planetary Atmospheres), Berlin
Prof. Dr.-Ing. habil. Antonio Delgado	Lehrstuhl für Strömungsmechanik Universität Erlangen-Nürnberg
Prof. Dr. Jörg Schumacher	Institut für Thermo- und Fluiddynamik, TU Ilmenau
Prof. Dr. rer. nat. habil. Andre Thess	Institut für Technische Thermodynamik, DLR, Stuttgart
Prof. Dr. Andreas Tilgner	Institut für Geophysik,, Universität Göttingen
Prof. Dr. Eberhard Bodenschatz	MPI für Dynamik und Selbstorganisation, Göttingen
Prof. Dr. Uwe Hampel	HZDR Rossendorf und TU Dresden
Prof. Dr. Jeanette Hussong	FG Strömungslehre und Aerodynamik, TU Darmstadt
Prof. Dr.-Ing. Ulrich Riebel	Lehrstuhl für Mech. Verfahrenstechnik, BTU Cottbus

Fluid-Centrum / Fluid-Center

Das Fluid-Centrum des Lehrstuhls Aerodynamik und Strömungslehre wurde 2004 in Betrieb genommen. Dort sind folgende Labore sowie Prüf- und Versuchsstände des Lehrstuhls untergebracht

Halle I (Aerodynamik- und Aeroakustik-Halle, 400qm):
- Großer Rohrströmungskanal (Cottbus Large Pipe Test Facility, CoLa-Pipe)
- Kleiner Rohrströmungskanal (Cottbus Small Pipe Test Facility, CoSma-Pipe)
- Kleiner Lehr- und Forschungswindkanal für hochpräzise Strömungskalibration
- Windkanal für Fahrzeugmodell- bzw. Flugzeughalbmodelluntersuchungen
- Aeroakustik-Prüfstand/Freistrahlgebläse

Halle II (Strömungsprüfstands- / Raumfahrt-Halle, 400qm):
- Labore für rotierende Strömungen (150 qm)
- Laserlabor (75 qm)
- Strömungsprüfstandslabore (75 qm)
- 3 Schülerlabore (je 45-50 qm)

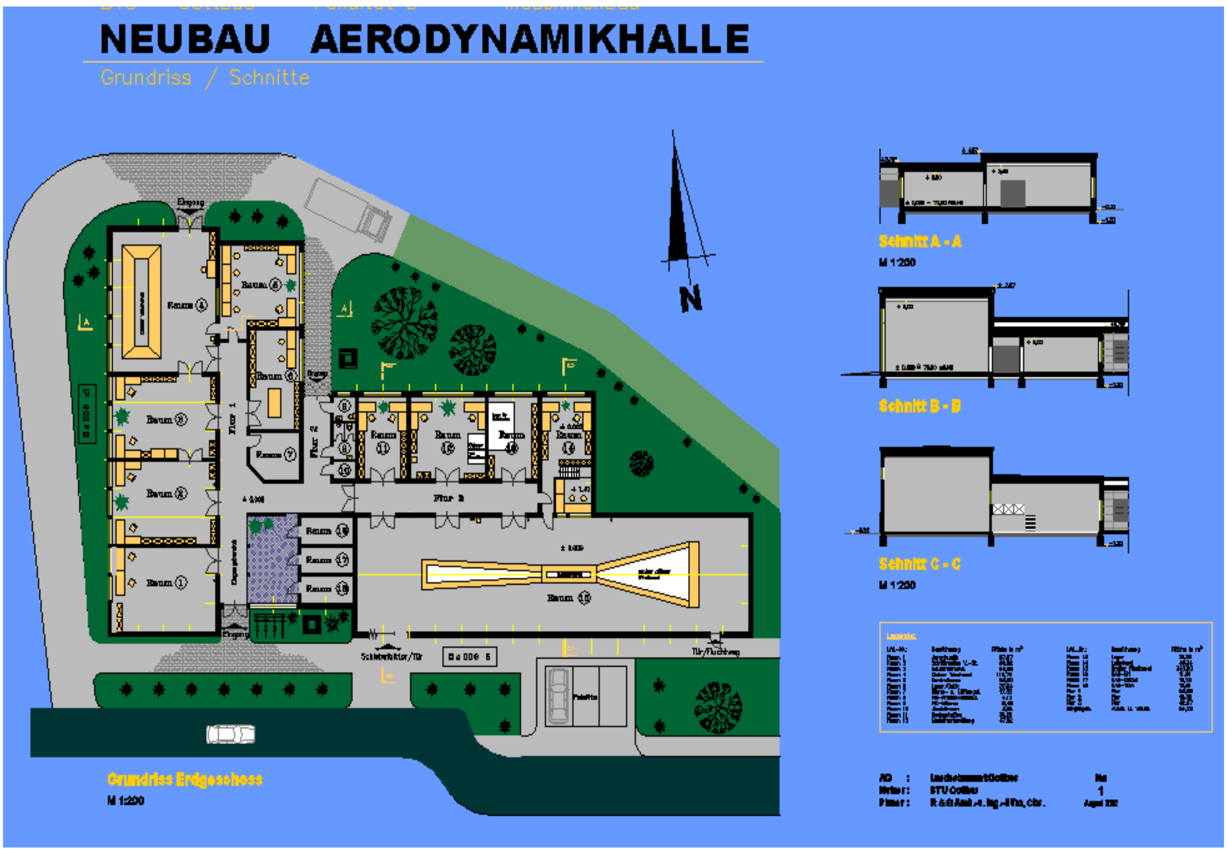

Ansicht des Fluid-Centrums (Aerodynamik- und Strömungsprüfstandshalle)

Neubau des „Anwendungszentrums Fluiddynamik“
New Building „Center of Applied Fluid Dynamics“

EUROPÄISCHE UNION
Europäischer Fonds für regionale Entwicklung

M. Meier, C. Egbers (EFRE-Förderung, Antrags-Nr.: 85001205))

Zusammenfassung
Ziel des Ende 2017 genehmigten EFRE-Vorhabens in Höhe von 7.2 Mio. € ist der Neubau des "Anwendungszentrums Fluiddynamik", eines neuen Labor- und Bürogebäudes, neben dem Fluid-Centrum (LH3D) der Brandenburgischen Technischen Universität Cottbus-Senftenberg (BTU) auf dem Zentralcampus in Cottbus. Das neue Gebäude soll die Anzahl der Projekte, insbesondere die Kooperationsvorhaben im Bereich der Energietechnik mit der regionalen Industrie und damit den Technologietransfer maßgeblich erhöhen. Einen vergleichbaren Standort in Brandenburg gibt es nicht.
Neben neuen Büros für die bisher in verschiedenen Gebäuden verteilten Mitarbeiter der Lehrstühle LAS, LTA und LNSG sowie dem CFTM² wird auch Platz für 7 weitere Labore geschaffen. Dies sind u. a. ein Labor für Parabelflug-Vorbereitung, ein Labor für akustische Messtechnik und ein Laserlabor.
Damit wird das neue Anwendungszentrum zu einem zentralen Forschungspartner für die Energietechnik in der Region und überregional. Baubeginn war Februar 2018, Fertigstellung und Übernahme der BTU fand im März 2020 statt.

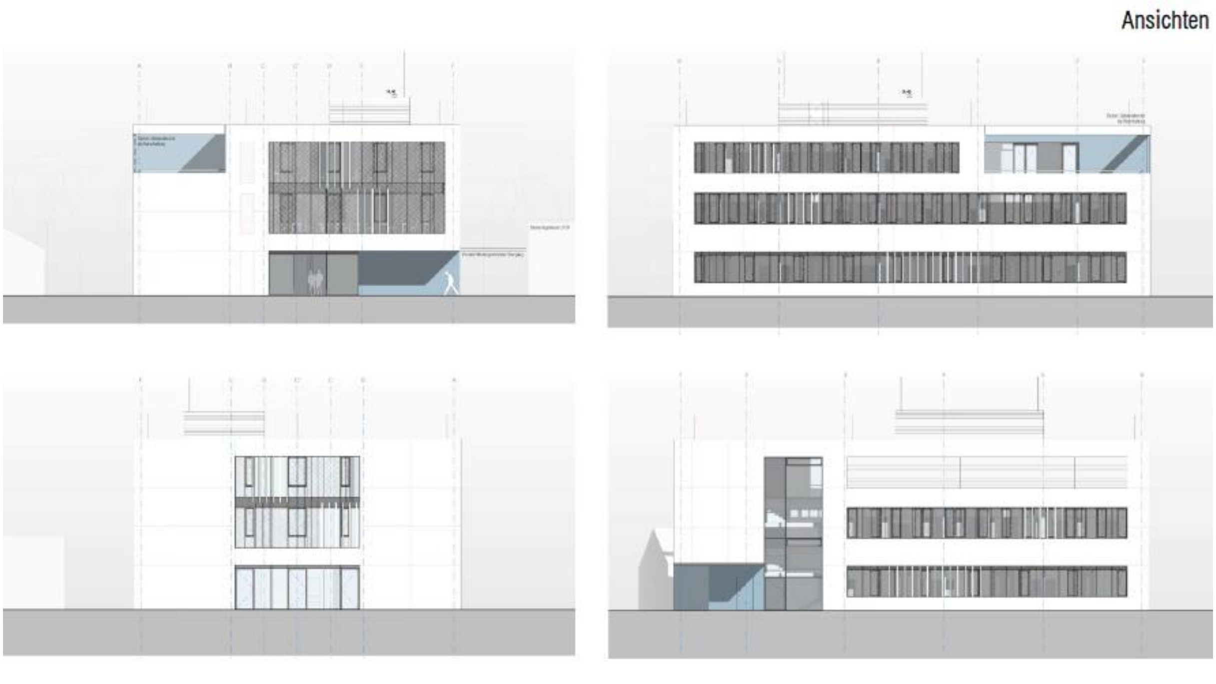

Abb. 1: Ansichten des neuen AZFD-Gebäudes (Quelle: AWB Architekten, Dresden)

Ziele des Bau-Vorhabens
Am Lehrstuhl für Aerodynamik und Strömungslehre (LAS, Institut für Verkehrstechnik, BTU Cottbus-Senftenberg) werden national und international anerkannte grundlagen- und anwendungsorientierte Forschungsarbeiten auf dem Gebiet der experimentellen, theoretischen und numerischen Strömungsmechanik, Aerodynamik sowie Messtechnik durchgeführt.
Der Lehrstuhl gehört ebenso wie die beiden anderen mitbeantragenden Lehrstühle für Technische Akustik (LTA) und Numerische Strömungs- und Gasdynamik, (LNSG), zum BTU-weiten Zentrum für Strömungs- und Transportphänomene, Modellierung und Messtechnik (CFTM2). Das Fluid-Centrum mit seiner Laborhalle steht dabei zentral im Mittelpunkt interdisziplinärer Forschung der beteiligten und weiteren BTU-Lehrstühle.

Das neue Gebäude „Anwendungszentrum Fluiddynamik“
New Building „Center of Applied Fluid Dynamics“

EUROPÄISCHE UNION
Europäischer Fonds für
regionale Entwicklung

Das neue Gebäude "Anwendungszentrum Fluiddynamik (AZFD)", ein kombiniertes Labor- und Bürogebäude, konnte 2020 in Betrieb genommen werden. Es liegt direkt neben dem „Fluid-Centrum“ (LH3D) der Brandenburgischen Technischen Universität Cottbus-Senftenberg (BTU) auf dem Zentralcampus in Cottbus. Das Ende 2017 genehmigte Bauvorhaben mit Baukosten von insgesamt ca. 8.3 Mio. € ist durch das Land Brandenburg und im Rahmen einer EFRE-Förderung finanziert worden. Das AZFD soll die Anzahl der Projekte, insbesondere die Kooperationsvorhaben im Bereich der Energietechnik mit der regionalen Industrie und damit den Technologietransfer maßgeblich erhöhen und steht dabei zentral im Mittelpunkt interdisziplinärer angewandter Forschung der beteiligten und weiteren BTU-Lehrstühle. Das Anwendungszentrum Fluiddynamik war zunächst im benachbarten Fluidcentrum tätig und wurde mit der Fertigstellung des AZFD-Gebäudes deutlich erweitert. Mit den Baumaßnahmen wurde Anfang 2018 begonnen, die Übernahme durch die BTU erfolgte am 28.2. 2020. Der Umzug in die neuen Räume erfolgte auf Grund der Pandemie-bedingten Einschränkungen nach und nach in den folgenden Monaten und war im Sommer abgeschlossen. Sowohl die Erarbeitung des Antrages für die EFRE- Förderung (2015), die Beschaffung der Laboreinrichtungen und des Mobiliars als auch die Begleitung der Baumaßnahme über die gesamte Bauzeit hinweg (z.B. mit zeitweise wöchentlichen Bausitzungen) in Vertretung aller (zukünftigen) Gebäudenutzer erfolgte durch die Autoren. Sowohl die Planungs- (ab 7/2016) als auch die Bauphase wurde vom BLB (Brandenburgischer Landesbetrieb für Liegenschaften und Bauen) mit dem verantwortlichen Architekturbüro AWB Werner Bauer, Dresden, koordiniert und BTU-seitig durch die Abteilung „Infrastrukturelles Gebäudemanagement“ sowie bei Bedarf weiteren Abteilungen der BTU (z.B. Technisches Gebäudemanagement, Facility Management, Sicherheitsingenieur) begleitet. Die Zusammenarbeit mit allen Beteiligten – BLB, AWB, BTU, den Systemplanern, der Feuerwehr und nahezu allen Firmen – war konstruktiv, effizient und im Allgemeinen sehr gut.

Das kompakte Gebäude im Passivhaus-Standard wurde nach dem Gebot des kostensparenden Bauens bei gleichzeitig hoher Robustheit, Langlebigkeit und geringen Betriebskosten errichtet. Die Erscheinung des Gebäudes wird durch die vorgehängte Fassade aus Metallpaneelen bestimmt. Im Bereich der großformatigen Fensterbänder und Verglasungen nach Süden hin löst sich mit dem notwendigen Sonnenschutz die Metallfassade in bewegliche Einzelelemente auf. Die Fassadentafeln wurden feuerverzinkt ausgeführt, die fortlaufend variierende Erscheinung soll dem Forschungsansatz des Hauses folgend die ebenso wenig endgültig vorhersagbaren Forschungsergebnisse widerspiegeln und so zum Sinnbild künftiger Entwicklungen einer technisch und technoid geprägten Umgebung werden.

Der Lehrstuhl für Aerodynamik und Strömungslehre (LAS) gehört ebenso wie die anderen im Gebäude ansässigen Fachgebiete für Technische Akustik (TA), Numerische Strömungs- und Gasdynamik (NSG) und Bildgebende Messverfahren zum BTU-weiten Zentrum für Strömungs- und Transportphänomene, Modellierung und Messtechnik (CFTM^2). Neben neuen Büros für die bisher in verschiedenen Gebäuden verteilten Mitarbeiter der Fachgebiete und des CFTM^2 wurde auch Platz für 7 weitere Labore, einen Rechnerpoolraum, 2 Besprechungsräume und einen Seminarraum geschaffen. Damit können verstärkt national und international anerkannte grundlagen- und anwendungsorientierte Forschungsarbeiten auf dem Gebiet der experimentellen, theoretischen und numerischen Strömungsmechanik, Aerodynamik sowie Messtechnik durchgeführt werden. Ergänzt wird das AZFD durch das benachbarte Fluid-Centrum mit seiner großen und kleinen Laborhalle mit verschiedenen Wind- bzw. Strömungskanälen, Laboren für Rotationsexperimente und einer mechanischen Werkstatt. Damit ist das neue Anwendungszentrum ein zentraler Forschungspartner für alle strömungstechnischen Fragestellungen in der Region und überregional.

Das neue Gebäude „Anwendungszentrum Fluiddynamik“
New Building „Center of Applied Fluid Dynamics“

EUROPÄISCHE UNION
Europäischer Fonds für
regionale Entwicklung

Abb. 2: AZFD-Eingang und Eingang Fluid-Centrum

Abb. 3: AZFD Nordwestseite

Abb. 4: Blick in eins der sieben Labore - das Parabelfluglabor

Für die künstlerische Gestaltung des Neubaus hatte das Land Brandenburg einen eingeladenen Wettbewerb mit sieben Teilnehmenden ausgelobt, die aus einer Liste mit 22 in Frage kommenden Künstlern und Künstlerinnen ausgewählt wurden. Ziel war es, das Bauvorhaben durch Kunst am Bau zu bereichern, dem kulturellen Anspruch des Landes Ausdruck zu verleihen und Kunst zugänglich zu machen. Die Installation der Künstlerin polnischen Marlena Kudlicka wurde schließlich ausgewählt und gewann den mit 1.500 Euro dotierten Wettbewerb. Ihr dreidimensionales Werk soll einen Algorithmus abbilden und mit „0 Komma A“ Ungenauigkeiten und Messfehler thematisieren. Das Werk ist nun an einer Wand im Treppenhaus des AZFD angebracht, siehe Abb. 5.

Abb. 5: Installation „0 Komma A“ der polnischen Künstlerin Marlena Kudlicka im 2. Stockwerk.

Abb. 6: Eingangsbereich des AZFD

Abb. 7: Foyer im 2. Stockwerk des AZFD

Lehre / Courses offered

Vorlesungen des Lehrstuhls für Aerodynamik und Strömungslehre im SS 2021

Strömungslehre (2 SWS VL + 2 SWS UE)
Prof. Egbers / Dr. Merbold

- Grundlagen (Stoffgrößen und physikalische Eigenschaften von Fluiden)
- Hydrostatik (Druck, Auftrieb)
- Kinematik der Flüssigkeiten (Kontinuitätsgleichung)
- Kinetik der Fluide (Bernoulli-Gleichung, Massenerhaltung, Impulssatz, Drehimpuls)
- Materialgleichungen (Navier-Stokes Gleichungen, Newtonsche Fluide)
- Schichtenströmungen (Couette-, Poiseuille-Strömung)
- Grenzschichttheorie
- Ausgewählte Strömungsbeispiele

Fahrzeug-Aerodynamik I (2 SWS VL + 2 SWS UE)
Prof. Egbers / Dr. Zanoun / M.Sc. Peter Haun

- Grundlagen der Strömungslehre
- Übertragbarkeitsregeln von Modellmessungen auf Originalausführungen
- Fahrzeugaerodynamik und Design
- Windkanaltechnik
- Messtechnik in der Fahrzeugaerodynamik

Raumfahrtanwendungen (2 SWS VL + 2 SWS UE)
Prof. Egbers / Dr. Martin Meier

- Physikalische Grundlagen der Schwerelosigkeit
- Übersicht zu Forschung unter Schwerelosigkeit
- Verschiedene Experimentierplattformen (Fallturm, Parabelflüge, TEXUS, ISS)

Analyse und Visualisierung von Strömungen mit MATLAB (2 SWS VL + 2 SWS UE)
apl. Prof. Harlander

- MATLAB Tutorial
- Strömungslehre Tutorial
- Statistische Analyse von Strömungsdaten
- Zeitreihenanalyse
- bi- und multivariate Verfahren; nichtlineare Verfahren
- Visualisierung von Strömungen
- Darstellung statistischer Ergebnisse

Convection in Fluids and Gases (2 SWS VL + 2 SWS UE)
apl. Prof. Harlander

- Convection between heated/cooled plates
- The Rayleigh-Bernard experiment
- The differentially heated rotating annulus
- Convection with local sources
- Centrifugal- and Coriolis-effects in rotating convection
- Convection in spheres and spherical shells
- Applications in technical and environmental flows

Lehre / Courses offered

<u>Vorlesungen des Lehrstuhls für Aerodynamik und Strömungslehre im WS 2021</u>

<u>Experiments in Aerodynamics and Fluid Mechanics</u> (2 SWS VL + 2 SWS UE)
Dr. Merbold
Einführung in Modellexperimente der Aerodynamik und der Strömungsmechanik: Taylor-Couette Strömungen, Rayleigh-Bénard-Konvektion, Flügelprofil, Windkanalmessmethoden, Reynolds´scher Rohrströmungsversuch, Karman´sche Wirbelstraße, Radhausmodell, Wsserkanal, Particle-Image-Velocimetrie, Laser-Doppler-Anemometrie

<u>Höhere Strömungsmechanik</u> (2 SWS VL + 2 SWS UE)
Prof. Egbers / Dr. Szabo
Einführung, Theoretische Grundlagen; Methoden der Stabilitätsanalyse; Methoden der Zeitreihenanalyse und Chaosdynamik; Modell-Systeme (Strömungsinstabilitäten in Natur und Technik); Experimentelle Methoden; Praktische Beispiele (Rayleigh-Bénard-Konvektion, Taylor-Couette-Strömungen), Turbulente Strömungen

<u>Strömungsmesstechnik</u> (2 SWS VL + 2 SWS UE)
Prof. Egbers / Dr.-Ing. Merbold
- Verfahren zur Sichtbarmachung von Strömungen / Übersicht zu optischen Messverfahren
- LDA-, PIV- und PTV-Strömungsmessverfahren
- Flüssigkristall-Messtechnik
- Farbinjektion
- Hitzdraht- und Heißfilm-Technik
- Verfahren zur Messung von Zustandsgrößen (Temperatur, Druck, Feuchte)
- Windkanalmesstechnik (6-Komponentenwaage, Drucksonden, Drucksensitive Farben)

<u>Aerothermodynamik</u> (2 SWS VL + 2 SWS UE)
Prof. Egbers / Dr. Zanoun / M.Sc. Peter Haun
Einführung; Kompressible Strömungen (Gasdynamik), Grenzschichtströmungen, Übersicht über die Tragflügeltheorie; Singularitätenverfahren für Überschallströmungen; Energiesatz für materielles Volumen, Energiesatz für Stromfaden, Gibbsche Gleichung und Entropieungleichung, Ideale Gase, Thermische und kalorische Zustandsgleichung, Schallgeschwindigkeit und Schallausbreitung, Bernoulli Gleichung für ideales Gas, Isentrope stationäre Stromfadentheorie, Flächen-/Geschwindigkeitsbeziehung, Durchflussfunktion, Verdichtungsstoß, Lavaldüse

<u>Wellen in Flüssigkeiten</u> (2 SWS VL + 2 SWS UE)
apl. Prof. Harlander
- Oberflächenwellen
- Reflexion und Refraktion
- WKB Analyse
- Flachwasserwellen, Interne Schwerewellen, Planetare Wellen, Trägheitswellen
- Numerische Verfahren zur Lösung von Wellenphänomenen

<u>Parallel Rechnen</u> (2 SWS VL + 2 SWS UE)
Dr. Krebs
- Die Studierenden lernen grundlegende Konzepte paralleler Rechnerarchitektur (Hardwareaspekt) und der parallelen Programmierung (Softwareaspekt) kennen. Typische Aufgabenstellungen numerischer Simulation aus den Bereichen Computational Physics, CFD und Image Processing können selbständig parallel implementiert werden.

Infrastruktur des Lehrstuhls / Laboratories and research facilities

Laboreinrichtungen	Laboratory facilities
• Labor für exp. Strömungsmechanik • Elektronik-/Messtechnik-Labor • Mechanik-Labor • Laser-Labor • Labor für Weltraumexperimente • Rechnerraum	• Fluid laboratory • Electronic laboratory • Mechanical workshop • Laseroptical laboratory • Space experiments laboratory • Computation room

Experimenteinrichtungen	Experiment facilities
• Taylor-Couette Apparaturen (DFG) • Strato-Rotations-Experiment (DFG) • QBO-Experiment / Rotor-Stator (DFG) • Kugelspalt-Anlagen (DLR, DFG) • Rayleigh-Bénard Experiment (BTU) • Rotierende Zylinder-Konus-Apparaturen • Barokliner Wellentank (DFG, DLR) • MS-GWave Tank (DFG) • Turbulente Rohrströmung (DFG) • Lehr-und Forschungswindkanal (BTU) • Aeroakustik-Freistrahl-Prüfstand	• Taylor Couette apparatus (DFG) • Strato-Rotational experiment (DFG) • QBO-experiment, rotor-stator (DFG) • Spherical gap flow experiment (DLR, DFG) • Rotating Rayleigh-Bénard tank (BTU) • Rotating cone facilities • Baroclinic-wave tank facility (DFG, DLR) • MS-GWave tank (DFG) • Turbulent pipe flow facility (DFG) • Wind tunnel (aerodynamics, BTU) • Aeroacoustic-Test-Facility

Messtechnik	Measuring techniques
• Laserlichtschnitt-Technik • PIV-Technik (2D-Messungen) • LIF-Technik • LDA-Technik (2D-Messung) • He-Ne Laser, Ar-Ion Laser • Schlieren-/Schattenverfahren und Interferometrie • Heissfilm- und Hitzdraht-Technik • Ölfilm-Methode • Thermographie	• Laser light sheet technique • PIV-technique (2D velocity measurements) • LIF technique • LDA-techniques (2D measurements) • He-Ne laser, Ar-Ion laser • Shadowgraph- Schlieren and interferometer optics • Hotfilm- and hot wire measuring technique • Oilfilm-technique • Thermography

Numerik / Software	Numerics / Software
• 3D zeitabhängige Codes zur Berechnung isothermer und thermisch getriebener Strömungen, FORTRAN • Zeitreihenanalyse- und nicht-lineare Analysemethoden • CREO CAD-tool • OpenFOAM • FLUENT, Matlab • PV wave, Tecplot (Visualisierung)	• 3D time dependent computational code (isothermal and thermal flows), FORTRAN • Time series analysis- and non-linear analysis tools • CREO-CAD-tool • OpenFOAM • FLUENT, Matlab • PV wave, Tecplot (visualization)

Infrastruktur des Lehrstuhls / Laboratories and research facilities

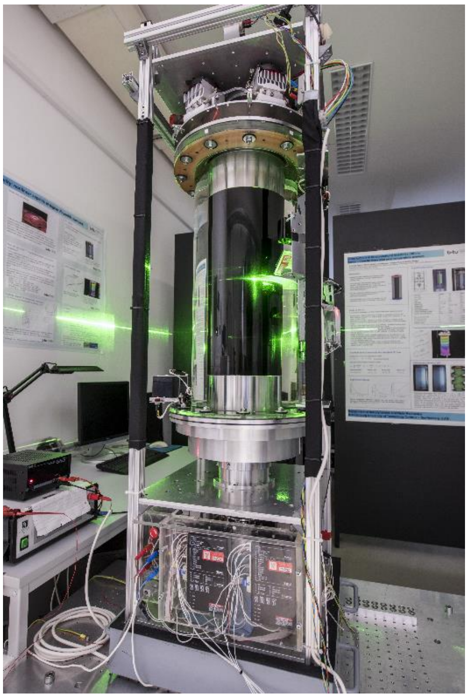

Taylor-Couette-experiment (SRI)

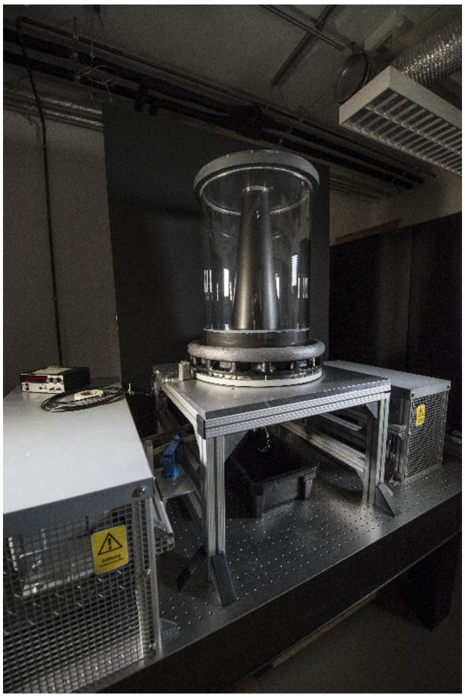

Taylor-Couette experiment (QBO)

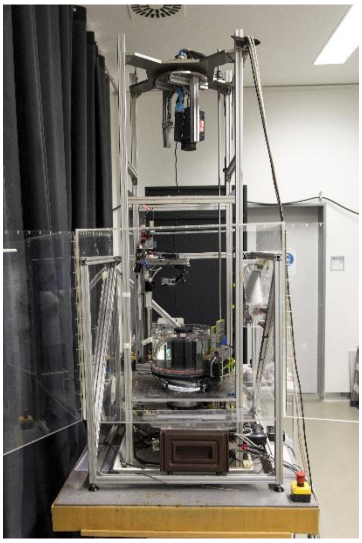

Baroclinic wave tank

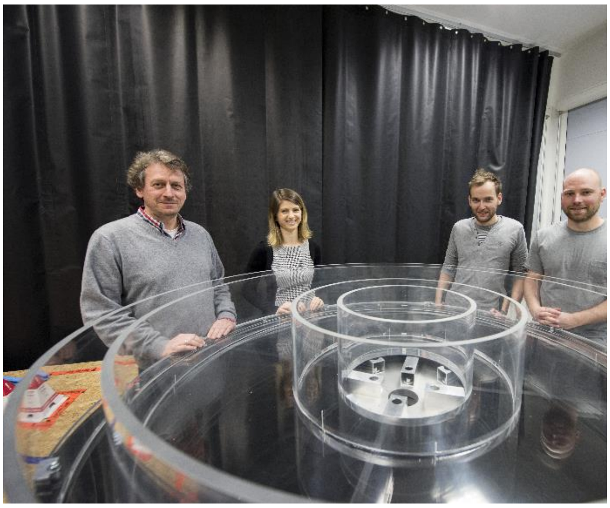

MS-GWaves experiment

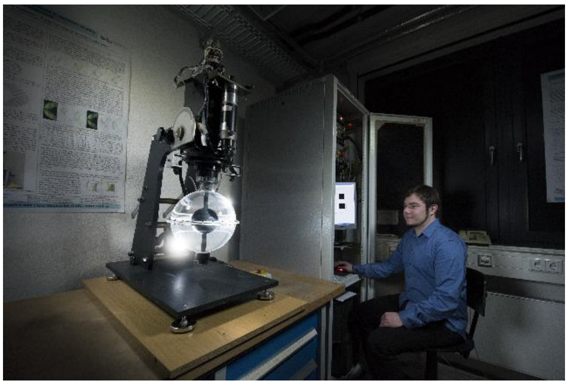

Concentric spherical gap apparatus

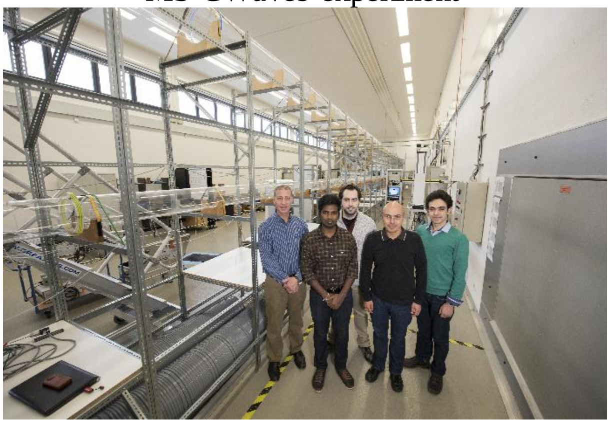

Cottbus Large Pipe Test Facility CoLa-Pipe

Infrastruktur des Lehrstuhls / Laboratories and research facilities

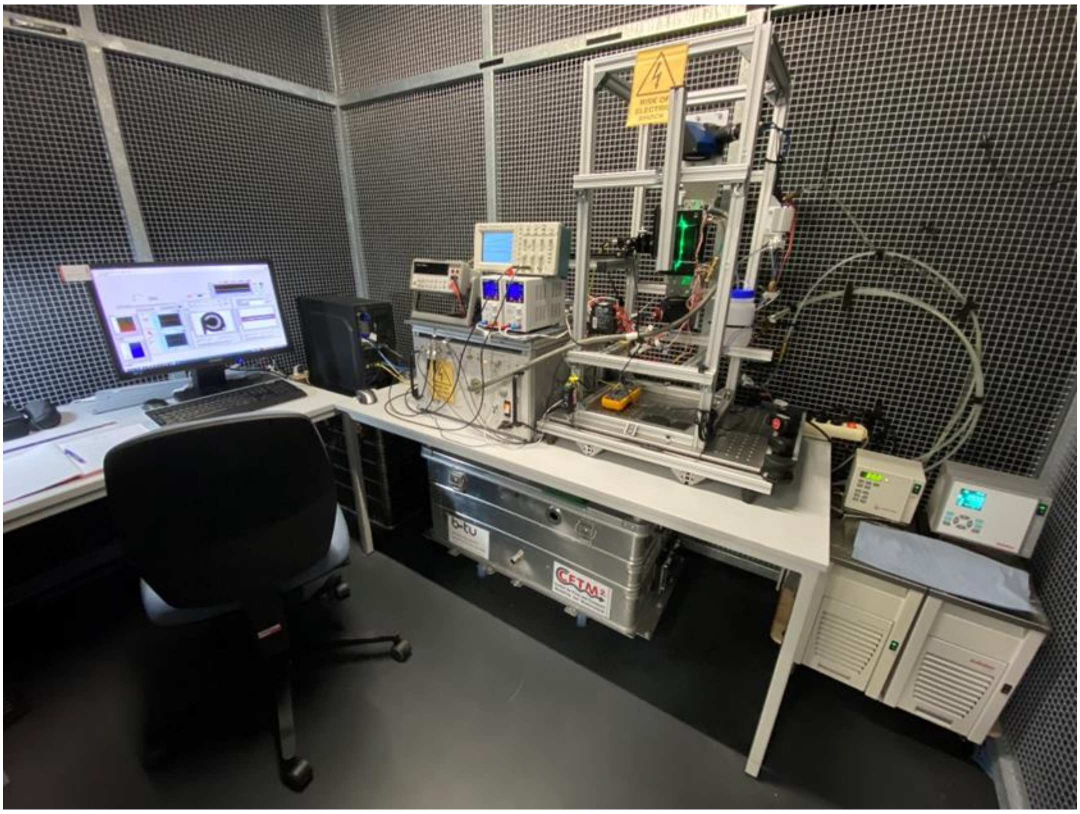

TEHD-Versuchsaufbau mit der Zylinderspaltzelle in vertikaler Ausrichtung im Faraday’schen Käfig des Hochspannungslabors des LAS

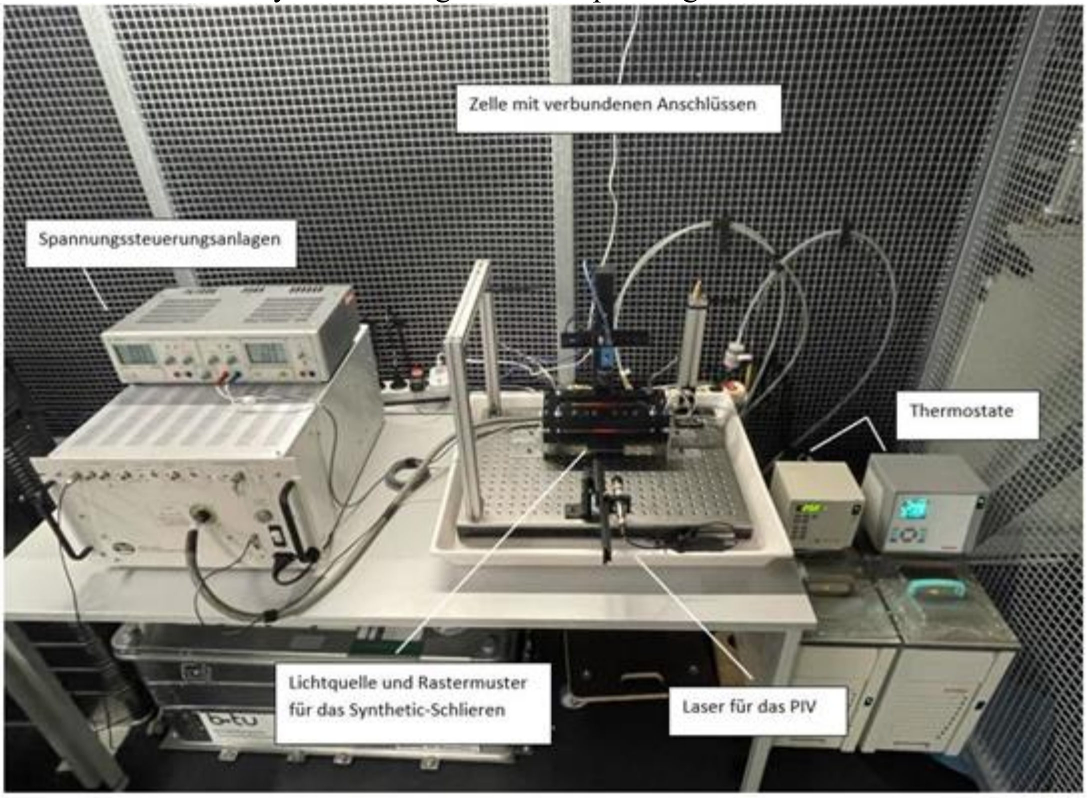

TEHD-Versuchsaufbau mit der Plattenspaltzelle in horizontaler Ausrichtung im Faraday’schen Käfig des Hochspannungslabors des LAS

Infrastruktur des Lehrstuhls / Laboratories and research facilities

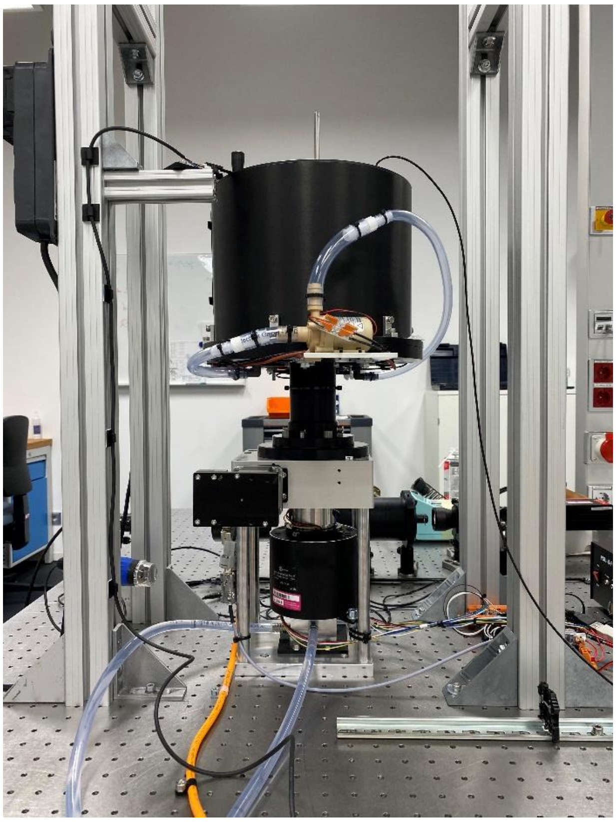

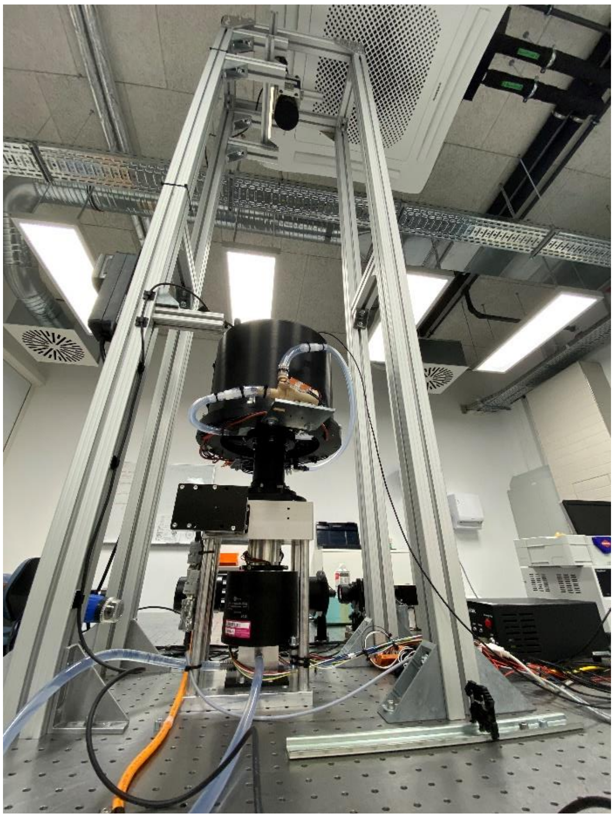

Der Barokline Wellentank für das Atmoflow-Experiment

Aktuelle Forschungsschwerpunkte / Current research topics

A Aerodynamics

A1 Some Features of Flow Statistics and Structures in CoLaPipe

E.-S. Zanoun, V. Motuz, and C. Egbers (DFG-SPP 1881, EG100/24-2)

Introduction

The experimental results reported here represent a continuation of contributions from the Cottbus large pipe facility to the priority program "Turbulent Super-Structures" DFG SPP (1881). The pipe flow is under intensive experimental and computational studies that are indeed well progressing over decades [1-3], providing considerable volume of data. Nevertheless, fundamental questions, recently, were raised regarding turbulence statistics and structures in fully developed turbulent pipe flows and are still under debate when compared with both the plane-channel and the flat-plate boundary layer flows, motivating our project. Obvious gaps in the present state of knowledge are still ill-understood in respect to aspects of the Reynolds number effects on the pipe flow turbulent statistics, scaling and structures that might be attributed to:

i. inadequate spatial and temporal resolutions where flow exhibits strong shear gradient [4].
ii. uncertainties introduced in velocity measurements due to temperature drift and calibration [5,6].
iii. improper selection of the inner and outer scaling parameters [1-3].

Experimental Setup

The large pipe facility at BTU C-S [7] is under intensive use to address the above issues. High-temporal resolution velocity data has been obtained using Dantec streamline hot-wire anemometer. In addition, the high-speed Particle Image Velocimetry (H-S PIV) was used to obtain high-spatial resolution velocity data, see [8] for more details. It is worth noting that the mean pressure gradient along the CoLaPipe test section was used to estimate the wall friction velocity u_τ [9].

Results

Visual examination of the turbulent pipe flow structures is one of the major aims of the running project to highlight the local flow organization as well as the large-scale structures in the CoLaPipe.

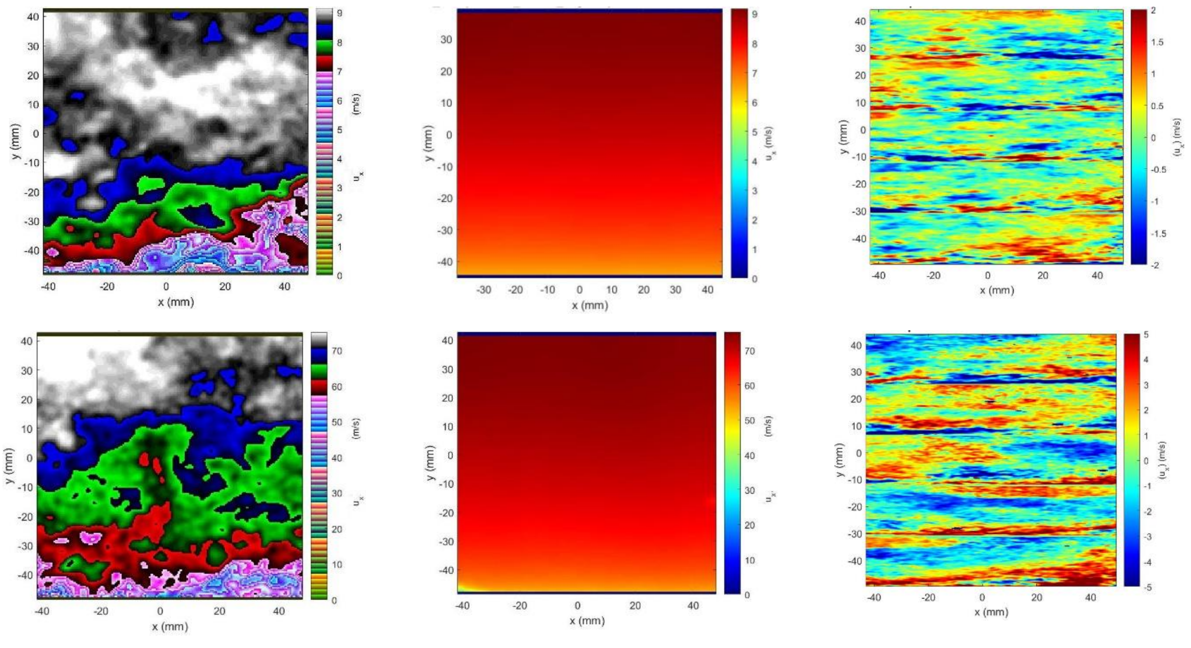

Figure 1: (left) instantaneous streamwise velocity field, (middle) streamwise average velocity field, and (right) contour plots of the streamwise velocity fluctuations for (top) $R^+ \approx 2200$ and (bottom) $R^+ \approx 17\,000$: x-streamwise, y-radial wise.

Aktuelle Forschungsschwerpunkte / Current research topics

Selected samples of the H-S PIV streamwise velocity data for a field of view limited to $R \times R$ in radial-streamwise directions, respectively is presented in Fig. 1 for Kármán numbers $R^+=2200$ & 17 000, where $R^+=R/\ell_c$, R the pipe radius, and $\ell_c=\nu/u_\tau$ the viscous length scale. Figure 1 (left) displays the instantaneous field for the streamwise velocity component, (middle) average velocity field, and (right) contour plots of the streamwise velocity fluctuations for (top) $R^+\approx 2200$ and (bottom) $R^+\approx 17\,000$. Regions of long meandering positive and negative velocity fluctuations are observable, revealing an evidence of the large scale motions/structures in the CoLaPipe flow. Two-point velocity-correlation analysis are under progress to quantify the strength, size, and frequency of various structures, examining the nature, and symmetry of hairpin-like vortices as well. Further analysis of the data using Proper Orthogonal Decomposition (POD) to identify the most energetic modes of such large scale motions are also progressing.

It is not surprising that the Reynolds number has a considerable effect on the mean velocity profile as well as on the higher order statisitics due to the dominance of either the viscous or inertia forces [1]. Figure 2 illustrates the inner scaling of the streamwise mean-velocity profiles from present experiments compared to simulations [10,11]. The figure shows satisfactory collapse of the present HWA and H-S PIV data, and good agreement with the DNS as well as with the logarithmic line [12]. An outstanding agreement between both the H-S PIV and the HWA profiles indicate the high spatial and temporal resolutions of both measuring techniques used, respectively.

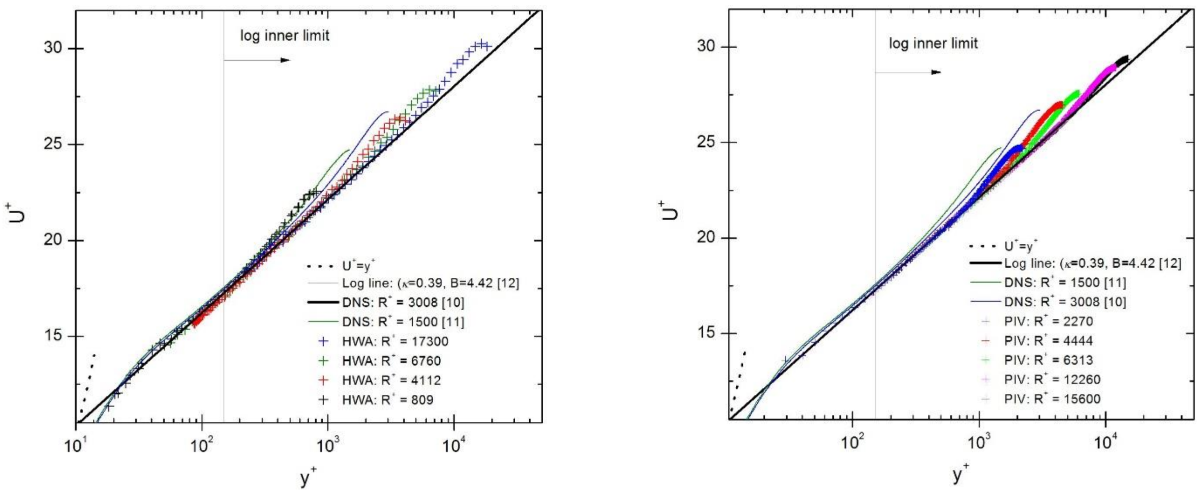

Figure 2: Inner scaling of the streamwise mean velocity (left) thermal hot-wire and (right) H-S PIV compared with the logarithmic velocity profile [12].

Interesting results concerning the effects of the Reynolds number on the turbulence higher order statistics (streamwise velocity fluctuations, flatness and skewness factors) are presented in [8].

References
[1] M. Gad-el Hak, Bandyopadhyay P. R. Appl. Mech. Rev. Rev. vol. 47, no. 8, pp. 307-365 (1994).
[2] A. J. Smits, B. J. McKeon, and I. Marusic. Annu. Rev. Fluid Mech., 43:353-375 (2011).
[3] I. Marusic, R. Mathis, and N. Hutchins, J. Heat Fluid Flow 1, p. 418428 (2010).
[4] P M Ligrani and P Bradshaw. J. Phys. E: Sci. Instrum. 20, 1987.
[5] E.-S. Zanoun, F. Durst, J. and Shi. Int. J. Heat Mass Transfer, Vol. 52, Issues 17–18, Aug. 2009.
[6] R. Örlü, J. H. M. FranssonJens, F.-H. Alfredsson. Nov. 2010, Progress in Aerospace Sciences 46(8):353-387.
[7] F. König, E.-S. Zanoun, E. Öngüner, and C. Egbers. In: Rev. Sci. Instrum. 85.7 (2014), p. 075115.
[8] E.-S. Zanoun and C. Egbers. under consideration for publication in Exp. in Fluids.
[9] E.-S. Zanoun, C. Egbers, H. Nagib, F. Durst, G. Bellani, A. Talamelli. European J. of Mech. / B Fluids 89 (2021).
[10] J. Ahn, J. H. Lee, J. Lee, J.-H. Kang and H. J. Sung. In: Phys. Fluids 27.6, p. 065110 (2015).
[11] D. Feldmann, C. Bauer, and C. Wagner. In: J Turbulence 19.3, pp. 274–295 (2018).
[12] A. E. Perry, S. M. Henbest, and M. S. Chong, J. Fluid Mech. 165, p. 163199 (2007).

Aktuelle Forschungsschwerpunkte / Current research topics

A Aerodynamics

A2 Two-Point Velocity Correlations for Fully Developed Turbulent Flow in CoLaPipe

E.-S. Zanoun, Y. Dewidar, and C. Egbers (DFG-SPP 1881, EG100/24-2)

Introduction

The experimental results reported here represent a continuation of contributions from the Cottbus large pipe facility to the priority program "Turbulent Super-Structures" DFG SPP (1881). The two-point correlations either space-time or two-point spatial correlations, and the cross correlations are of fundamental interest for the statistical data analysis of the turbulent pipe flow structures. It is thus worth reminding the readers here that flow structures were defined by Robinson (1991) as "three-dimensional region of the flow over which at least one fundamental flow variable (velocity component, density, temperature, etc.) exhibits significant correlation with itself or with another variable over a range of space and/or time that is significantly larger than the smallest local scales of the flow," motivating our pipe flow structure studies via the two-point velocity correlations of the streamwise velocity component. The aim of this short report is to summarize about the large-scale pipe flow structures using the two-point velocity correlations at various radial locations y/R=0.1-0.8 and 41 azimuthal positions for Kármán number $4040 \leq R^+ \leq 16\,000$, where $R^+ = R/\ell_c$, R the pipe radius, and $\ell_c = \nu/u_\tau$ the viscous length scale. Pre-multiplied energy spectra, two-point joint statistics, the cross-power spectral analysis for all the 41 measurement locations were adopted [2].

Experimental Setup

The large pipe facility at BTU C-S [3] is under intensive use to carry out study proposed, Fig. 1(left). Two hot-wire probe module was being utilized to measure the streamwise velocity component at different radial and azimuthal positions. One probe moves radially, while the other probe moves in radial and in azimuthal directions via a rotating pipe section, Fig. 1(right). 41 azimuthal positions were adopted between 10° and 210° minimum and maximum separation with 5° step with respect to the fixed probe. Measurements were performed using Dantec Streamline 9091N0102 Constant Temperature Anemometry (CTA) with commercial Dantec probes

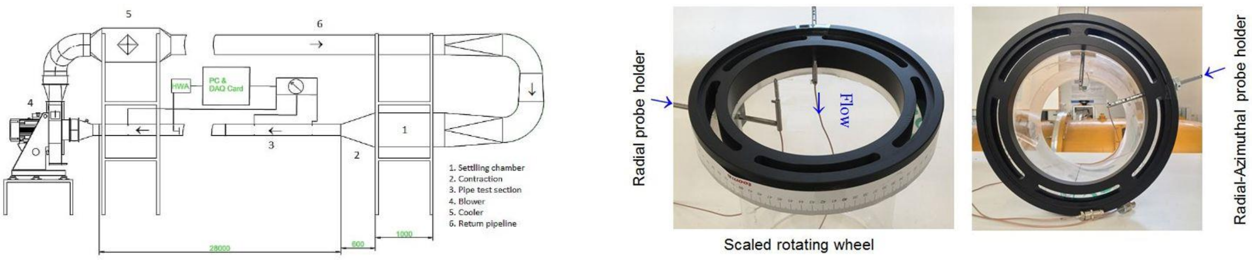

Figure 1: (left) The CoLa-Pipe facility and (right) the two hot-wire probes test module.

Results

The two-point velocity correlation coefficient, R_{uu}, is defined as follows:

$$R_{uu}(\Delta s) = \frac{\langle u'(s,t)u'(s+\Delta s,t)\rangle}{\sqrt{\langle u'^2(s,t)\rangle}\sqrt{\langle u'^2(s+\Delta s,t)\rangle}} \tag{1}$$

where <·> denotes the time averaging, Δs is the azimuthal space separation, and u' is the streamwise velocity fluctuations as a function of space (s) and time (t). The present work was undertaken with the aim to obtain consistent pipe flow turbulence data, utilizing the CoLa-Pipe under fully developed turbulent flow regime. Uncertainty introduced in the streamwise velocity component due to the blockage of the hot-wire holders and probable eccentricity of the hot-wire probes were estimated to be

Aktuelle Forschungsschwerpunkte / Current research topics

within. $\Delta U/U$=±0.5% of the local mean velocity and of ≈5.7% and ≈5.5% in turbulence intensity level $(u'^2)^{1/2}/U$ obtained either by the fixed or the movable probes, respectively. Figure 2 presents one azimuthal profile of the velocity correlation coefficient obtained from probes located at y/R=0.5 and 41 azimuthal positions for R^+≈4000. The profile shows clearly a region of negative correlation within the range $\Delta S/R$≈0.35 and 1.3 which is attributed to the contribution of the large-scale motions to the coherent structure in agreement with [3] for the pipe flow.

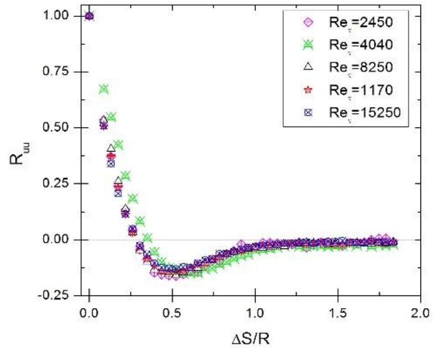

Fig. 2 The measured azimuthal velocity correlations of the streamwise velocity fluctuations at y/R=0.05 wall-normal location for various Reynolds numbers.

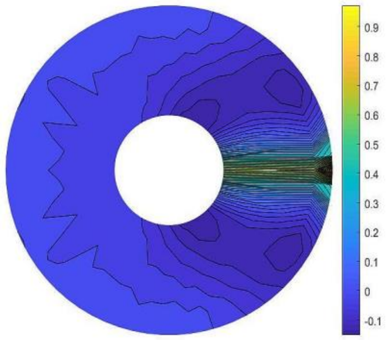

Fig. 3: Contours of the pre-multiplied cross-spectral density at y/R= 0:5 for R^+= 4000, the color bar represents $k_x R \psi^{++}$ and the contour levels are separated by 0.015.

The cross-spectral density $\psi(\Delta s, k_x)$ was being proposed by [4] to study the dependence of the two-point velocity correlations on the streamwise wavenumber k_x, and the azimuthal separation Δs:

$$\Psi(\Delta s, k_x) = \mathrm{Re}[G(\Delta s, k_x)]\sqrt{\langle u'^2(s,t)\rangle}\sqrt{\langle u'^2(s+\Delta s,t)\rangle} \quad (2)$$

To further quantify the differences in behavior of the azimuthal scales of the LSMs and VLSMs, the coherence function $\gamma(\Delta s, k)$ is introduced:

$$\gamma(\Delta s, k) = \frac{\Psi(\Delta s, k)}{\Psi^{1/2}(0,k))\Psi^{1/2}(\Delta s, k)} \quad (3)$$

Figure 5 illustrates the azimuthal distribution of $\gamma(\Delta s,k)$ at both the LSM and the VLSM peak wavenumbers. The overall appearance of $\gamma(\Delta s,k)$ distribution is similar to that of $R_{uu}(\Delta s)$ but the magnitude of $\gamma(\Delta s,k)$ was found to be greater than $R_{uu}(\Delta s)$ at the same azimuthal separation that reflects effect of averaging of the various scale motions on $R_{uu}(\Delta s)$.

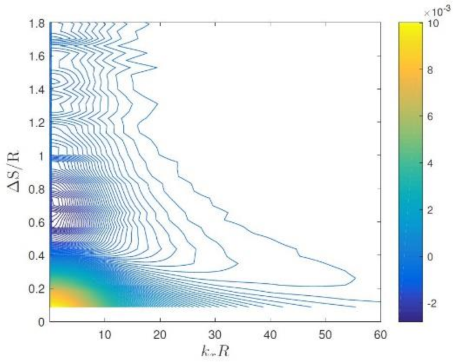

Fig. 4: Contours of the pre-multiplied cross-spectral density at y/R=0:5 for R^+≈4000, the color bar represents $k_x R \psi^{++}$ and the contour levels are separated by 0.015.

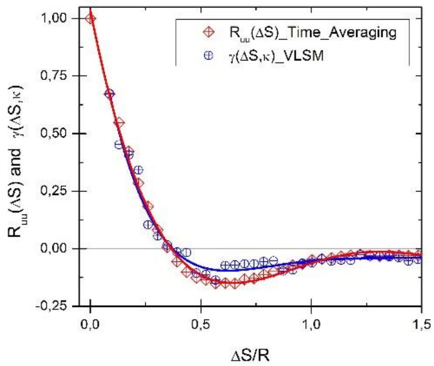

Fig. 5: Azimuthal coherence function based on wavenumbers of VLSMs at y/R=0.5

References

[1] S. K. Robinson, Annu. Rev. Fluid Mech. 23, p. 601-639 (1991).
[2].E.-S. Zanoun, Y. Dewidar, and C. Egbers. Under consideration for publication in J. Physics Fluids.
[3] F. König, E.-S. Zanoun, E. Öngüner, and C. Egbers. In: Rev. Sci. Instrum. 85.7, p. 075115 (2014).
[4] S. C. C. Bailey, M. Hultmark, A. J. Smits, and M. P. Schultz, J. Fluid Mech. 615, p. 121138 (2008).
[5].E.-S. Zanoun, C. Egbers, and Y. Dewidar. PAMM Proc. Appl. Math. Mech.; 20:1 e202000330 (2020).

Aktuelle Forschungsschwerpunkte / Current research topics

A Aerodynamics

A3 Cottbus Small Pipe: New Facility

S. Richter, E.-S. Zanoun, J. Peixinho, Ch. Egbers (DFG-SPP 1881, EG 100/24-2)

Pipe flow experiments showed flow transition over a wide range of the Re-number from $Re_{critical} \approx$ 2020 [1] to $Re_{critical} \approx 10^5$ [2], where Re = UR/ν with U the bulk velocity, D the pipe inner diameter and ν the kinematic fluid viscosity. Observations made by [3] and [4] showed a dependence of $Re_{critical}$ on inflows, outflows of pipes, pipe diameter and pipe length. The current work reports about the laminar pipe flow development and transition along the pipe test section of the Cottbus Small Pipe (CoSma-Pipe). Hot–wire anemometry and a pressure scanner were used to carry out measurements for $45.83 \leq x/D \leq 83.3$, where x is the streamwise distance along the pipe section. A disturbance bar of different heights was used to trigger the flow at the pipe inlet at Re values below the natural transition, see Fig.1. The general influence of the disturbance bar penetrating the flow can be seen in Fig. 2 (bottom) indicating a turbulent behavior whereas for the same Re without disturbance Fig. 2 (top) illustrates a laminar flow regime. Hence, it is desired to quantify the effect of the inlet flow disturbance on the critical Re and the transition length x/D, see Fig. 3 (a–k). The Figure shows the effect of the disturbance bar height on the pipe flow transition with respect to the critical Re. The turbulence intensity (I) u'_c/U_c implies the flow's state with u'_c the turbulent velocity component at centerline and U_c the bulk velocity at centerline. For low Re, I shows the characteristic decrease down to a level of ≈ 0.02 until a sudden peak at ≈ 0.1 is reached representing the transitional phase. This is followed by a second decrease heralding the turbulent state converging on an I level of 0.04. A laminar behavior was maintained up to $Re_{critical} \approx$ 12 000–14 000 and a transition phase within the range $6500 < Re_{critical} < 7500$ was observed for disturbance bar heights of 0.0mm and 5.0mm, respectively. The figure reveals that the critical Re for the laminar–to–turbulent pipe flow transition decreases with increasing disturbance bar height. This transition in flow condition is accompanied by puffs and slugs [3]. A puff is considered to be a low Re phenomenon and can be regarded as an isolated spot of turbulent flow travelling downstream with bulk velocity. With increasing the Re the puff develops into a slug having a different velocity at its front and back edges, resulting in an expanding size as it moves downstream [3]. Having detailed knowledge about the mentioned processes grant an opportunity for further transition studies under various controlled inlet/upstream flow conditions such as relaminarization efforts.

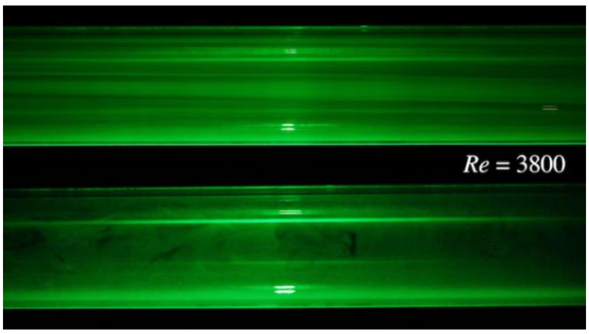

Figure 1: Disturbance bar at the pipe inlet Figure 2: Flow visualization at Re = 3,800

References

[1] O. Reynolds. 1883 *Proc. R. Soc. Lond.* 35 84
[2] W. Pfenninger. Ed. by G. V. Lachman. 1961.
[3] M. Nishi, B. Ünsal, F. Durst and G. Biswas. J. Fluid Mech. (2008), vol. 614, pp. 425–446.
[4] E.-S. Zanoun, M. Kito, and C. Egbers. In: J. Fluids Eng. 131 (2009), pp. 1–10

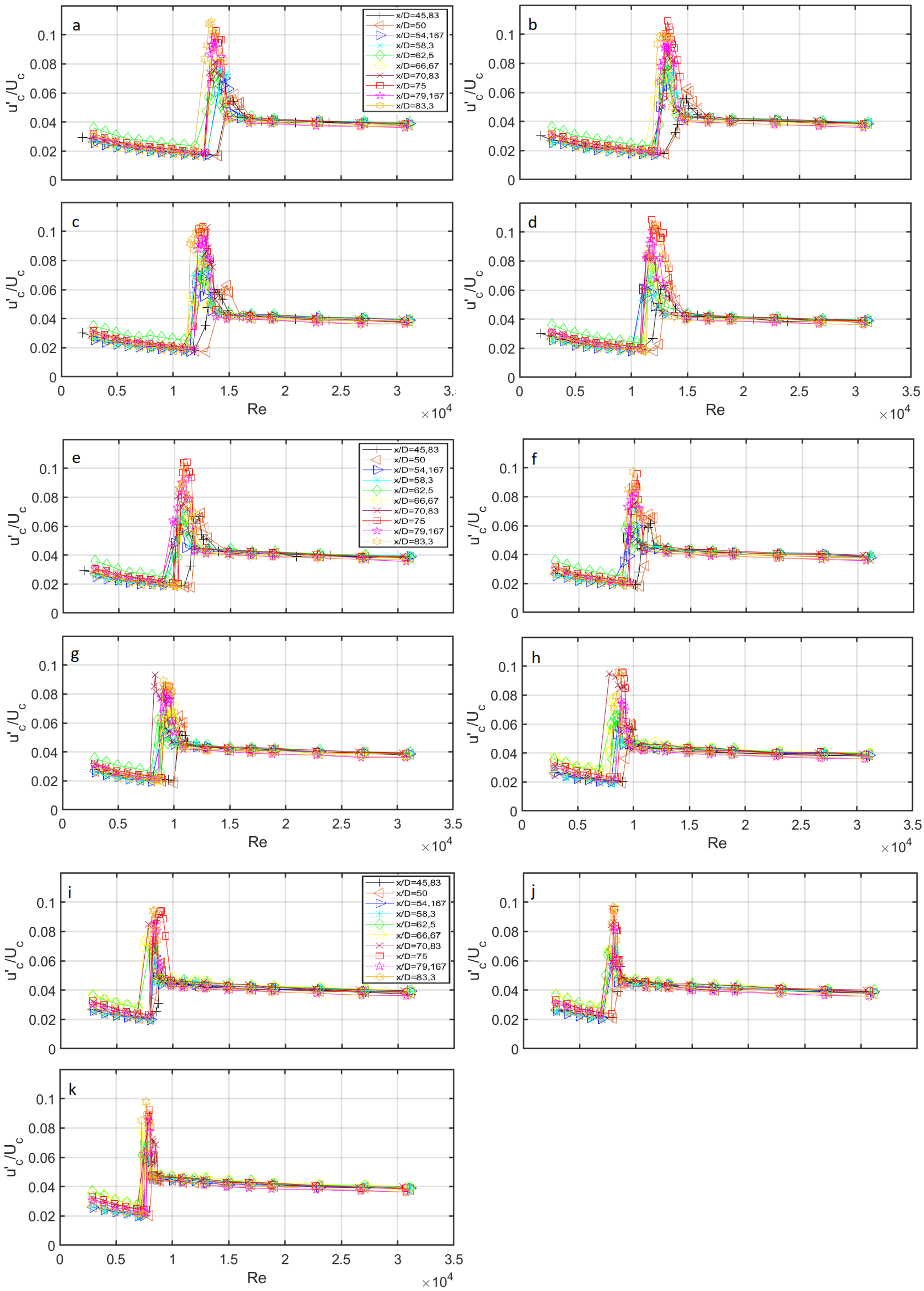

Figure 3: Present centerline–turbulence intensities u'_c/U_c versus Re at various streamwise positions, x/D, for 11 disturbance bar heights: (a) h=0mm, (b) h=0.5mm (c) h=1mm, (d) h=1.5mm, (e) h=2mm, (f) h=2.5mm, (f) h=3mm, (g) h=3.5mm, (h) h=4mm, (i) h=4.5mm, (h) h=5mm

Aktuelle Forschungsschwerpunkte / Current research topics

A Aerodynamics

A4 Analysis of turbulent coherent structures in turbulent pipe flow at high Reynolds numbers using time-resolved PIV

Z. Hallol*, S. Merbold, Ch. Egbers (*BTU- PhD Scholarship)

Experimental study of very large scale motions in fully developed turbulent pipe flow in the CoLaPipe test facility (König et al. 2014) has been quantified via turbulence statistics based on two-dimensional timeresolved particle image velocimetry. The experiment is carried out at high friction Reynolds numbers Re_τ=3200, 6605 and 10617 corresponding to bulk Reynolds numbers Re_D of 1.45 $\times 10^5$, 3.18 $\times 10^5$ and 5.33 $\times 10^5$, respectively. Based on the comparison of the present datasets with the reported experimental and numerical works of literature, the contour of stream-wise pre-multiplied spectra and Reynolds shear stress in u and v velocity components indicate good agreement. Pre-multiplied power spectra and co-spectra analysis combined with the scale separation are used to determine the contribution of VLSMs to the turbulent statistical quantities, including total kinetic energy and Reynolds shear stress. Major findings are summarized as follow:

Temporal-spatial analysis of time-resolved PIV datasets at Re_τ= 1667 and 3200 show a set of positive and negative stream-wise fluctuation velocities represented in the vertical lines across several short time intervals. These strains give evidence of the large coherent structures presence in turbulent pipe flow. The results support the conclusion of spectral analysis, which explain that VLSMs are initiated from the near-wall region and vanished at half the pipe axis y/R=0.5, while LSMs manifest to exist along the pipe axis. The pre-multiplied spectra results agree with the achieved results of one-dimensional spectral analysis for matched Reynolds number (Re_τ=6556) obtained from prior HWA measurements at high resolution, using 30 kHz sample rate. This agreement can be clearly shown by comparing the pre-multiplied spectra of stream-wise velocity fluctuation for the two implemented measurement techniques, HWA and PIV datasets. Although the small and large structures are not well resolved in the near-wall region using the PIV system representing in the partial disappearance of the inner peak as shown in Fig. 2. The selected pre-multiplied spectra show a significant agreement with HWA datasets. In addition, the detection of the outer spectral peak in identified the VLSMs that carry the same energy content at a similar selected Reynolds number (Re_τ=6556). The obtained results support the accuracy of the PIV measurement technique.

The obtained pre-multiplied spectra exhibit the presence of VLSMs and the footprint of LSMs, where the spectral content implies mainly the relationship between VLSMs and turbulent kinetic energy distribution phenomena. The VLSMs contribute about 55% to total kinetic energy at high Reynolds numbers of approximately equivalent association of small and large scale structures. The Reynolds number effects are assessed and found to have minimal influence on the VLSMs length scale, though the amplitudes of the pre-multiplied spectra and co-spectra demonstrate the dependence of Reynolds number. This is consistent with the turbulent boundary layer explanation (Balakumar and Adrian 2007; Hutchins and Marusic 2007a). The contribution of VLSMs is mainly apparent in the two-dimensional spectra (co-spectra uv), the VLSMs provide about 60% to Reynolds shear stress in the logarithmic region. This result shows the evidence of VLSMs presence and how they play an important role in the outer layer. It is also proved that VLSMs are the major contribution to total kinetic energy and Reynolds shear stress in the logarithmic and outer layer. A protracted flow field is required in future work to obtain sufficient spatial resolution over a longer stream-wise extent. However, large coherent structures (i.e. very large scale motions) are recognized to commonly persist with a length greater than 20 R (Adrian and Marusic 2012).

Aktuelle Forschungsschwerpunkte / Current research topics

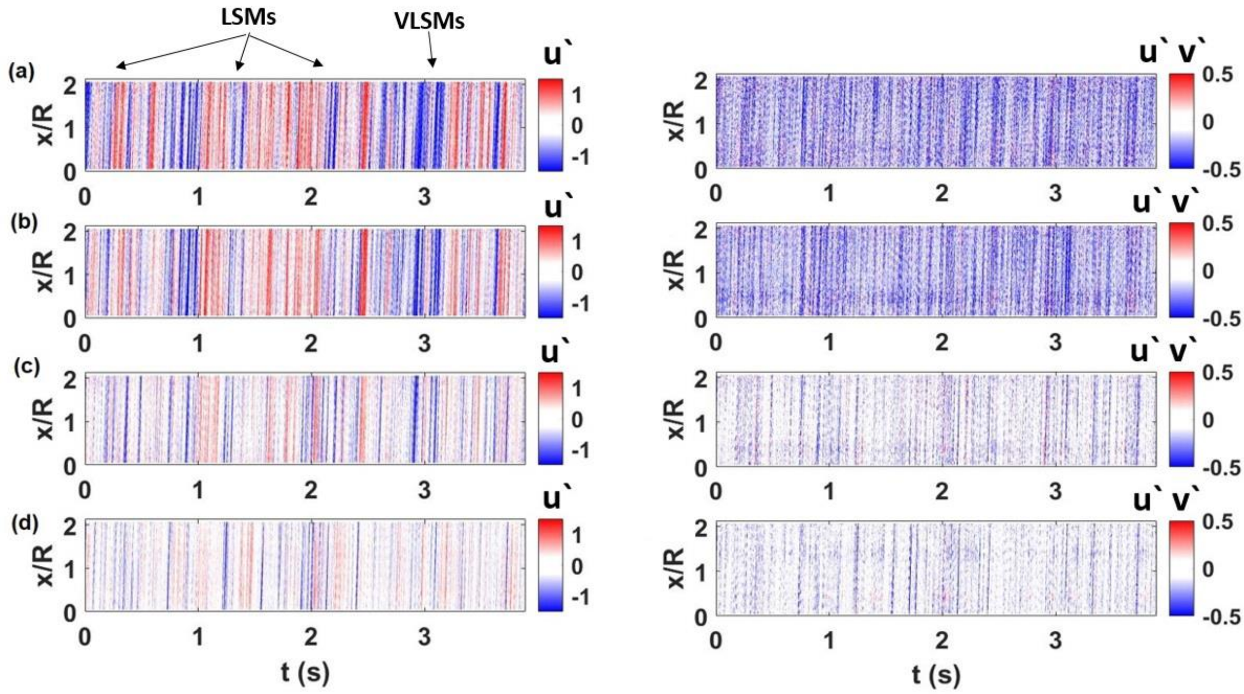

Figure 1 Temporal-spatial contour plots of the stream-wise fluctuation velocity u′ (left) and Reynolds shear stress u′v′ (right) for the PIV dataset Re_τ = 3200, measured with sample rate of 480 Hz, at different wall-normal locations. (a) y/R=0.1, (b) y/R=0.3, (c) y/R=0.5, and (d) y/R = 0.7.

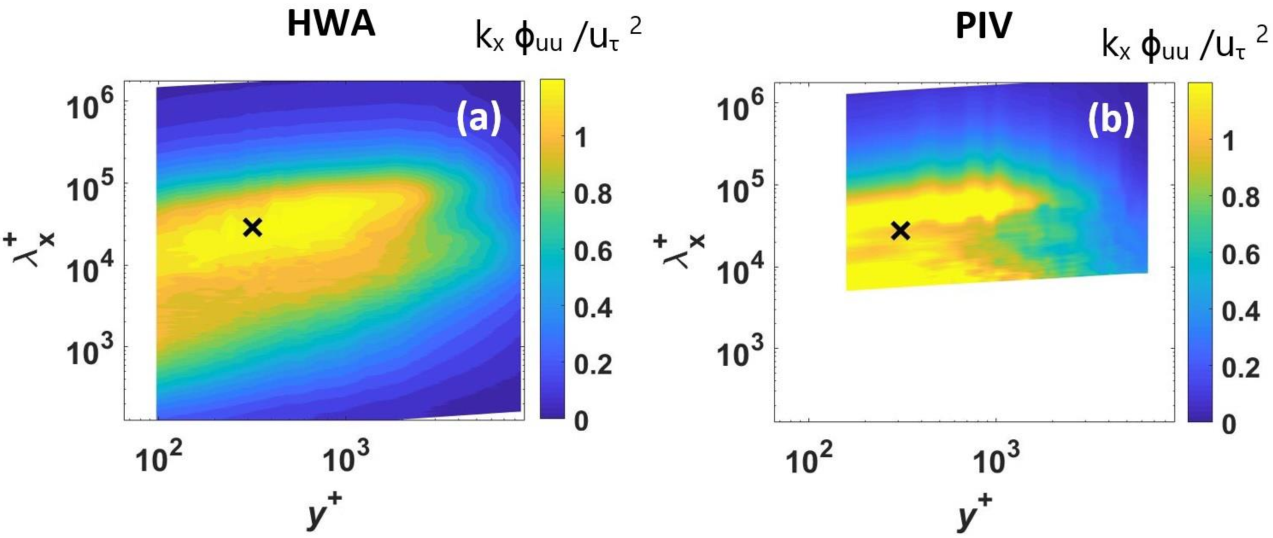

Figure 2 Contour of pre-multiplied spectra (inner scaled) of stream-wise velocity fluctuation for the two implemented measurement techniques, HWA (a) and PIV (b) datasets at $Re\tau$ = 6556.

Bibliography:

1. König F., Zanoun E.S., Öngüner E., and Egbers C. The CoLaPipe - the new Cottbus Large Pipe test facility at BTU Cottbus, Review Scientific Inst., Vol. 85, No. 7, pp. 075115-1075115-9, 2014
2. Balakumar B.J., Adrian R.J. Large and very large scale motions in channel and boundary layer flows, Philos. Trans. R. Soc. Lond. A, Vol. 365, pp. 665-681, 2007.
3. Adrian R.J. and Marusic I. Coherent structures in flow over hydraulic engineering surfaces, Journal of Hydraulic Research, Vol. 50, No. 5, pp. 451-464, 2012.

Aktuelle Forschungsschwerpunkte / Current research topics

A Aerodynamics

A5 Flow control in zero pressure gradient turbulent boundary layer (ZPGTBL)

Gazi Hasanuzzaman, Sebastian Merbold, Vasyl Motuz, Christoph Egbers

Experimental study of control experiments in wall-bounded turbulent flows such as ZPGTBL, has a long heritage at LAS. In order to reduce the friction drag, an optimized, open-loop control technique was used also known as uniform blowing [1]. The reference Ph.D thesis made an extensive experimental study for a wide range of Reynolds numbers at two different wind tunnel facilities namely, BTU and Le Laboratoire de Mécanique de Lille (LMFL) wind tunnel. Carefully measured data using Laser Doppler Anemometry (LDA) and Particle Image Velocimetry (PIV) were reported in the references [2] and [3] respectively. The complex interaction of coherent structures (CS) of different scales and their non-linear dynamics plays an important role establishing a robust control for drag reduction. A control technique such as uniform blowing is much suitable for aerospace, which also, can influence these CSs. Reference [1] presents a hypothesis that explains these CSs playing the most vital role within such drag reduction mechanism. Subsequently, reference [1] reported the statistical properties of the turbulent boundary layer at moderate Reynolds numbers under uniform blowing. Moreover, a novel approach was discussed in details to measure the near wall data when using LDA. However, the characteristics of a turbulent boundary layer at high Reynolds numbers were reported in reference [2] where, Figure 1 (a) legends introduces the different local Reynolds number based on momentum thickness. In addition, a suitable scaling to present statistical profiles was also proposed along with the statistical moments up to fourth order.

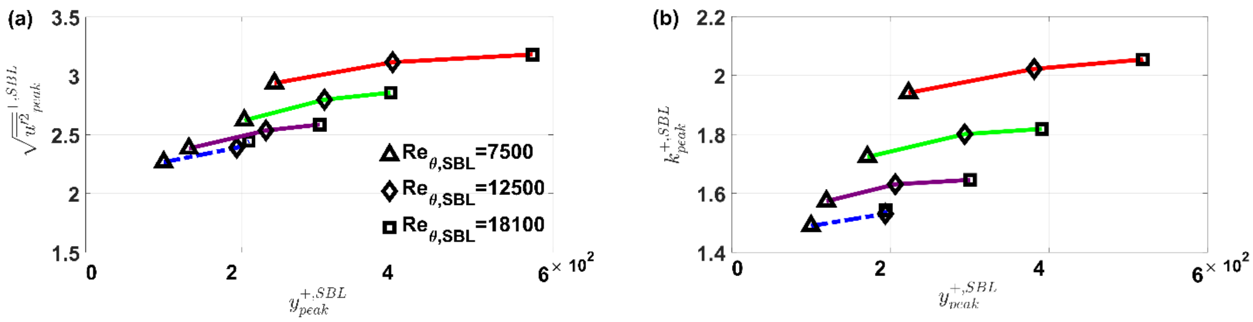

Figure 1. Outer peak values of $\sqrt{u'^2}^{+,SBL}_{peak}$ and their corresponding wall normal position $y^{+,SBL}_{peak}$ normalised with inner variables, (b) Peak of total kinetic energy ($k^{+,SBL}_{peak}$) along wall position $y^{+,SBL}_{peak}$ [2].

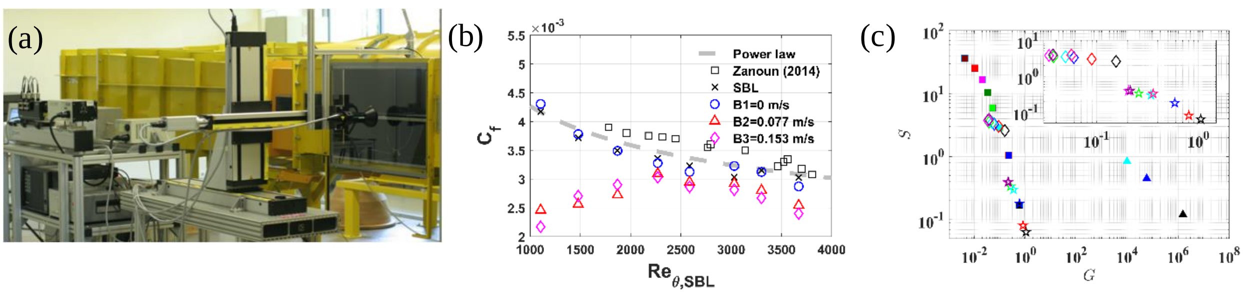

Figure 2. (a) LDA at BTU wind tunnel, (b) Friction drag co-efficient reduction at different blowing velocity and (c) Energy saving rate along different gain [3].

Aktuelle Forschungsschwerpunkte / Current research topics

As presented in Figure 1 (a) and (b), the outer statistical peak of streamwise velocity and total kinetic energy respectively are enhanced, their exact locations away from the wall are detected. The relative error of peak location determination remains very small, which varied between $y^+ = \pm 6.5 \sim \pm 18.2$ depending on the Reynolds number of the flow. In addition to high Reynolds number measurements, LDA data obtained at moderate Reynolds number measurement helped us look deeper into the friction parameters such as wall shear (τ_w), friction velocity (u_τ) and friction co-efficient (C_f). Direct measurements of these parameters at near-wall region were possible using an unique approach and correlation based wall distance correction. Figure 1 (b) shows the comparison of this new acquisition approach with other reference data including power law. Finally, Figure 2 (b) shows the friction drag reduction at different blowing velocities. For efficient control and energy optimization, there is a range of optimum blowing velocity that is shown here in Figure 2 (b). Now, we see the impact of blowing on drag reduction, turbulence statistics in a long spectrum of Reynolds numbers and last but not the least, their efficiency and potential to establish a robust control on the boundary layer flow. Later in reference [4], relationship of CSs morphology to the blowing control was presented through a number of Stereo PIV measurements at high Reynolds numbers, where Figure 2 (a), presents the experimental setup at LMFL wind tunnel in spanwise–wall normal orientation. The data is presented here after Taylor's frozen turbulence hypothesis in Figure (b) and (c), where large scale CSs at $y^+ = 36$ is visible. This indicates strong ejection events while blowing is applied. Our hypothesis is based on the wall normal blowing that effects the ZPGTBL similar to the one as adverse pressure gradient boundary layer. Therefore, blowing causes two effects, as such that the near-wall fluctuations get convected away from the wall, causing attenuation of near-wall turbulence. As reference [1] and [2] confirmed that the mean streamwise velocity and Reynolds stresses are modified with uniform blowing, subsequently, production or turbulent kinetic energy is also enhanced in logarithmic region. This leads to the second effect that a new, more energetic large scale CSs are formed in the outer region along with the small-scale turbulence which is now shifted within the outer region.

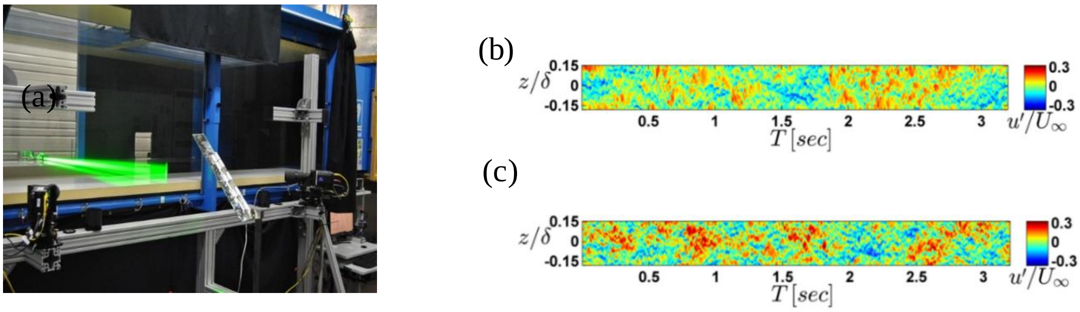

Figure 2. (a) Stereo PIV setup for YZ plane, free stream velocity normalized streamwise velocity fluctuation at $Re_\theta = 7500$; (a) blowing ratio at 0 and (c) blowing ratio at 6% of free stream velocity.

References

[1] Hasanuzzaman, G. (2022a). Experimental investigation of turbulent boundary layer with uniform blowing at moderate and high Reynolds numbers (1st ed.), Cuvillier Verlag, Göttingen, Germany, ISBN: 978-3-7369-7558-3, p. 1 - 152.
[2] Hasanuzzaman, G., Merbold, S., Motuz, V. and Egbers, Ch. (2022). Enhanced outer peaks in turbulent boundary layer using uniform blowing at moderate Reynolds number, Jour. Turb., DOI: 10.1080/14685248.2021.2014058, pp. 1 - 29.
[3] Hasanuzzaman, G., Merbold, S., Cuvier, C., Motuz, V., Foucaut, J.-M., and Egbers, Ch., (2020). Experimental investigation of turbulent boundary layers at high Reynolds number with uniform blowing, part I: statistics, Jour. Turb., DOI:10.1080/14685248.2020.1740239, 21(3), pp. 129 – 165.
[4] Hasanuzzaman, G., Merbold, S., Motuz, V., Egbers, Ch., Cuvier, C. and Foucaut, J-M. (2018). Experimental investigation of active control in turbulent boundary layer using uniform blowing, 5th International Conference on Experimental Fluid Mechanics (ICEFM), 2. - 4. July 2018, pp. 1 – 6.

Aktuelle Forschungsschwerpunkte / Current research topics

A Aerodynamics

A6 COVID-19 prevention through aerodynamic analysis of dynamic scenarios.

G. Hasanuzzaman, S. Merbold, Ch. Egbers, T. Buchwald, A. Schröder (DFG EG 100/36-1)

The pandemic COVID-19 started spreading at the end of year 2019. Since then, the world has already observed not only its devastating impact but also the weakness of available scientific information and evidences against an effective prevention. Although, vaccination has prevented its deadly impact on human health but what is still unknown is that how the transmission occurs in group dynamics such as in classrooms, briefing rooms (see Figure 1 (a) and (b)) or at the corridors. Aerosol particles are mainly responsible for the transmission of novel COVID-19 virus and their travel distance during different respiratory events such as breathing, coughing or sneezing depending on their sizes. Effect of preventive measures, for example different types of masks, air purifiers and air ventilation within group dynamic scenarios are scarcely investigated and needs proper attention.

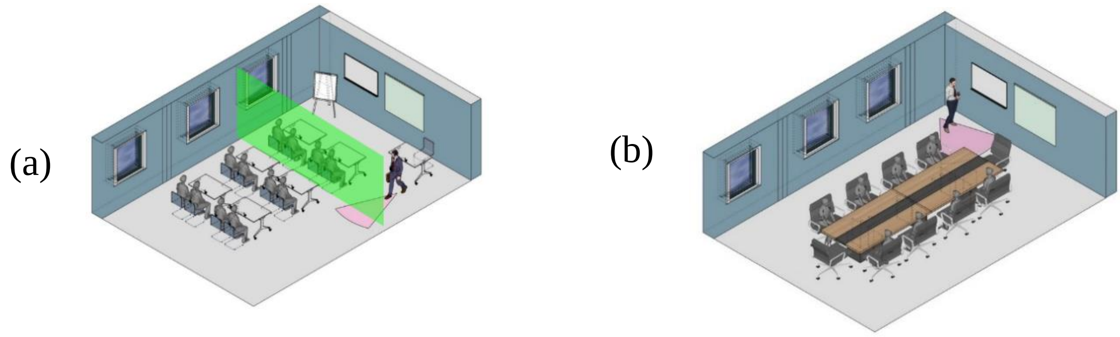

Figure 1. People gathering and group dynamics conceptual scenarios in (a) classroom and (b) briefing room.

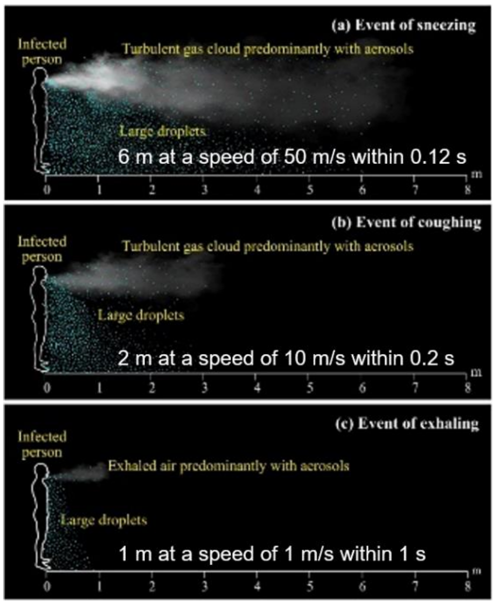

Figure 2. Aerosol particles travel distance during different respiratory events (a) sneezing, (b) coughing and (c) exhaling.

Reference [1] has reported on the travel distances of aerosol particles of different sizes. During these respiratory events, the large particles can travel as much as 7 meters (see Figure 2 (a), (b) and (c)). In particular, for particles with diameters less than 0.3 microns possess greater threat due to its longer life time and infiltration capacity, therefore, susceptible to the aerial transimission with sufficient viral loads.

Reference [2], conducted experimental study on different filtering elements such as masks and air purifiers in order to quantify their preventive impact on transmission. However, aerodynamic transmission experiments for group dynamic scenarios are not yet addressed. In addition, the static optical metrology such as conventional PIV or flow visualizations are not sufficient to assess group dynamic scenarios.

Figure 3 (a) to (d) exhibit the infiltration of such small particles penetrating through OP masks using flow visualization studies.

Aktuelle Forschungsschwerpunkte / Current research topics

Therefore, a new measurement approach with helmet mounted device was proposed which will be inexpensive, robust and possible to operate remotely. This device consists of a measuring head, LED light, camera optics and a RaspberryPi.

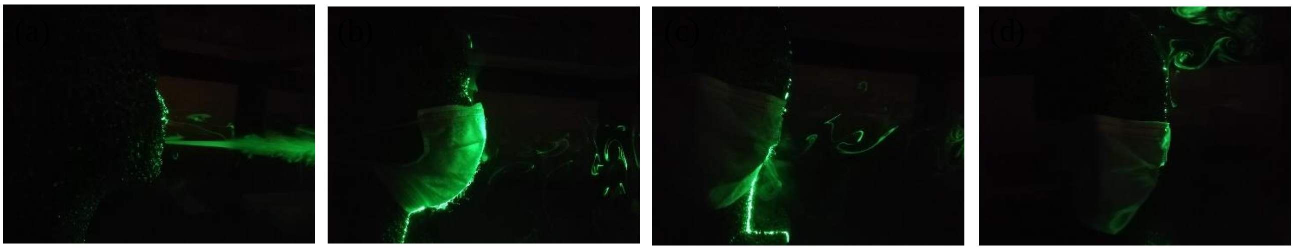

Figure 3. Flow visualization study of OP mask infiltration at BTU (a) without mask, (b), (c) and (d) with masks.

The project started at October 2021. Within the scope of this project, the transient and dynamic scenario is planned to be simulated in classroom (see Figure 1 (a)) arrangements, where closed and/or open windows in combination with air purifiers will also be tested. Proposed helmet mounted device and the measurement principle is presented here with Figure 4 (b) and (c) respectively.
In addition to the testing of the new measurement device, particle counting using DEHS particles will be perfomed. The aim is to investigate how aerosol particles exhaled from a model spreader are distributed in the room over time. Furthermore, conventional cross correlation based PIV software and the novel “Shake-The-Box (STB)” algorithm will be applied to get insight into the flow conditions of the room. This can be used to judge on the effectiveness of air purifiers and other strategies to avoid accumulation of aerosol particles. The findings from these experiments also provide information under which circumstances particularly high concentrations of aerosol particles can be found on which locations.
The aspect of ventilation systems installed in public spaces are still due with effective aerodynamic assessment. Therefore, the new device and approach will allow us to study such dynamic situations in public spaces and as a result, effectiveness of preventive measures such as masks, social distancing, air purifiers etc. in group dynamics are possible to assess. On the bright side, this approach will enable us to extend similar study of dynamic scenarios in other public spaces such as public transport, supermarket, cultural events, resturants etc.

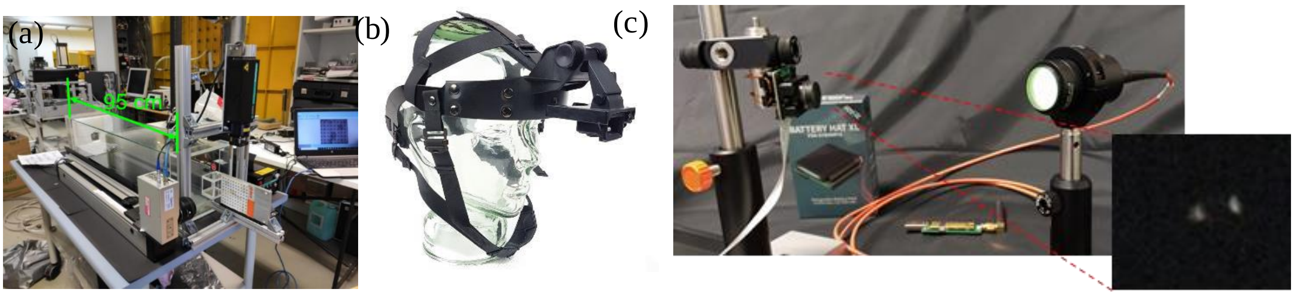

Figure 4. (a) PIV setup at particle counter, (b) proposed helmet mounted particle counter and (c) measurement principle for the new device.

References

[1] Jayaweeraa, M., Pererab, H., Gunawardanaa, B. and Manatunge, J., (2020), Transmission of COVID-19 virus by droplets and aerosols: A critical review on the unresolved dichotomy, Env. Res., 188, p. 1 -18.
[2] Kähler, C., J. and Hain, R., (2020), Fundamental protective mechanisms of face masks against droplet infections, Jour. Aerosol Sci., 148, p. 1-11.
[3] D. Schanz, S. Gesemann, A. Schröder (2018), Shake-The-Box: Lagrangian particle tracking at high particle image densities. Exp. Fl., 57, 70.

Aktuelle Forschungsschwerpunkte / Current research topics

B Fluid Mechanics

B1 DFG Core Facility Center "Physics of Rotating Fluids Lab" at BTU

S. Merbold, U. Harlander & Ch. Egbers (DFG EG100/23-1, HA 2932/9-1)

The present proposal aims to establish a new international research center in form of a core facility center for "Physics of Rotating Fluids (PRF)" with geo-/astrophysical, meteorological and technical applications located at BTU. The main goal is to integrate cutting-edge rotating and stratified fluid flow experiments across national boundaries in order to foster internationally competitive experimental research in the research field of rotating and stratified fluids by providing an easy access to outstanding experimental facilities (Fig. 1, left) equipped with state-of-the-art instrumentation. The research areas covered by the experimental facilities inside the new center are (Fig. 1, right):

- Planetary and astrophysical flows (with focus on disk formation, instabilities and mixing)
- Geophysical fluid dynamics (with focus on strato-rotational turbulence, mean flow generation and wave interaction)
- Rotating flows with technical applications (centrifuges, turbines, journal bearings and rotor/stator cavities)

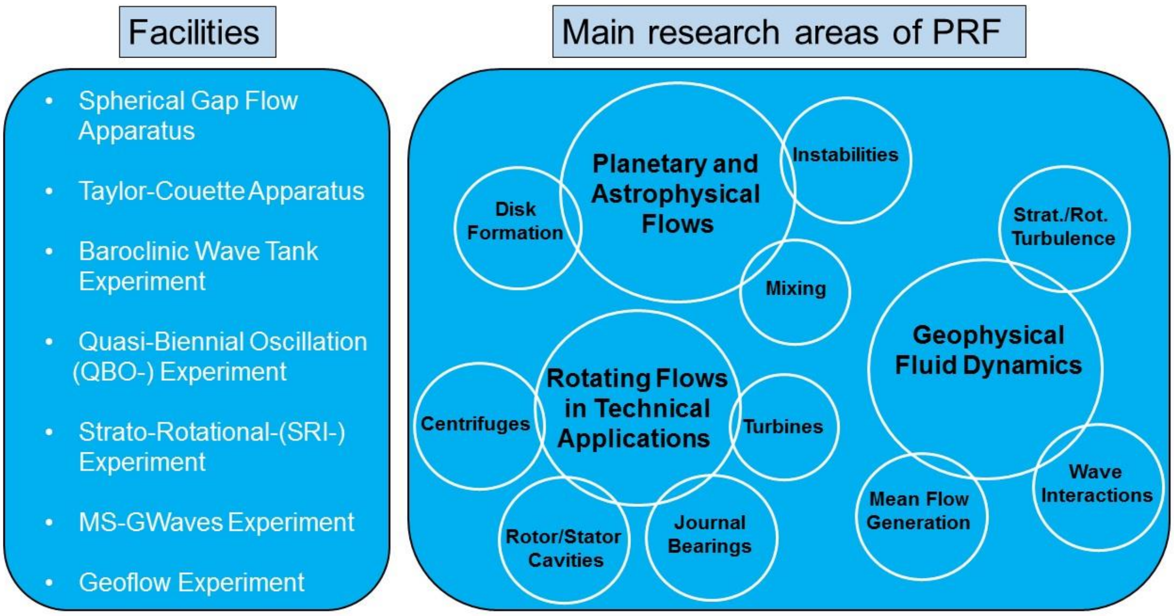

Figure 1: Summary of provided facilities and related and intended research areas of PRF

<u>Thus, the main goals of this proposal are to:</u>

- advertise and enforce the different research activities on rotating and stratified fluid flow experiments at BTU
- provide these outstanding research facilities at BTU to a larger national and international research community

Aktuelle Forschungsschwerpunkte / Current research topics

- bring together the recognized expertise of national and international working groups in the field of rotating and stratified fluids at BTU
- interconnect and help interested users by a networking program and joint research activities
- establish training groups for young researchers (Ph.D. students, Postdocs) in the field of rotating and stratified fluids
- organize exchange of scientific staff between the different research groups
- develop new experiments and models for a better insight into the dynamics and the role of these mean flows in geophysical, astrophysical, meteorological and technical flows at BTU
- deliver experimental data (including the use of modern experimental techniques like Thermography, Laser-Doppler-Anemometry, Particle Image Velocimetry (PIV), Laser Induced Fluorescence (LIF) techniques and Liquid Chrystal Tracer techniques, while the research approach as a whole is experimental, numerical and theoretical for the "PRF"
- organize and prepare collaborative applications to national and international calls for proposals (ANR, DFG, EU_FP8).
- collaborative data analysis of experimental, theoretical and numerical simulations.

<u>These goals will be achieved by</u>

- maintaining a suitable and safe physical environment with access to the required research services
- establishing a transparent and short review process for the external user community
- providing easy application forms for external scientific users, that ensures that proposals fit into the scientific frame of PRF research topics and are also compatible with the experiment facilities available
- sustaining a critical mass of scientific and technical expertise
- training and advising researchers as required
- providing appropriate and timely assistance
- enabling, advising and training on safe working practices
- ongoing research on new developments in instrumentation and responding to changes of experimental research; e.g. by designing, implementing or procuring appropriate mechanical, optical and electronic solutions to meet new experimental and diagnostic requirements
- documentation (user guides, safety-/laboratory manuals, annual reports, publications)
- public relations/ outreach (web-site, flyer, poster, presentations etc.)
- training / education (summer schools, workshops, young researcher meetings)
- continuation of core facility center activities after 3 years DFG funding through succeeding funding by BTU

<u>Organization and interfaces of the core facility center "Physics of Rotating Fluids (PRF)":</u>
The new core facility center for "Physics of Rotating Fluids (PRF)" will cover and focus all previous single research and guest scientist exchange activities like EuHIT, CNRS French/German-co-operation and ESA Topical Team with BTU/CFTM[2] in the field of rotating and stratified fluid flows as illustrated in Fig. 2. After funding from DFG via the present proposal, the core facility center for "Physics of Rotating Fluids (PRF) will be continued and financed sustainably by BTU.

Aktuelle Forschungsschwerpunkte / Current research topics

Services and joint research activities of the core facility center "Physics of Rotating Fluids (PRF)":
The actual status of the core facility center for "Physics of Rotating Fluids (PRF)" comprises all experimental facilities and measurement techniques located in the Fluid-Center-Building in different rooms next to each other.

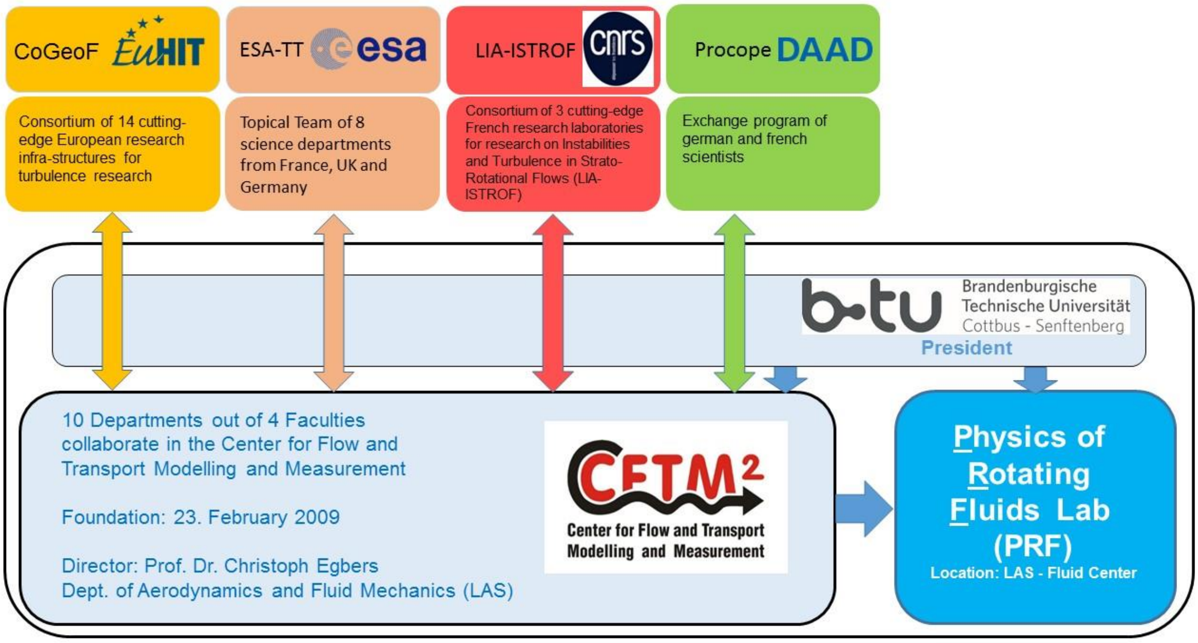

Figure 2: Organization structure and interfaces of core facility "Physics of Rotating Fluids (PRF)" Lab

The PRF is located in the Fluid-Center-building, on the campus of the Brandenburg University of Technology, Siemens-Halske-Ring 14, 03046 Cottbus, Germany. Responsible for the experiments is the Department of Aerodynamics and Fluid Mechanics. In this department about 30 technical & scientific employees work on experimental, theoretical and numerical questions of fluid mechanics. Generally we offer two types of services: i) in situ research with a direct access to the facility, and ii) commissioned research. In the first case i), the user in person will be conducting the research at our facility. To these researchers we offer practical guidance as well as technical assistance on the part of our scientific and/or technical staff, which is necessary due to the high complexity of the experimental installations. In preparation of such joint research project, the user will work with the facility lead scientist and the facility technician. The guesthouse of the BTU will minimize the organizational effort required for arranging the visits to the different facilities. In the second case ii), the commissioned research, the user can demand for certain measurements to be performed at our facility without being actually present in Cottbus. In this case our personnel will carry out the requested measurements and transmit the results to the user. This type of research is particularly appealing to users from the computational fluid dynamics community who are interested in validating their numerical data using experimental data.

Aktuelle Forschungsschwerpunkte / Current research topics

Scientific experimental equipment:

- Spherical gap flow apparatus (DFG EG 100/1-1, 1-2)
- Taylor-Couette apparatus (DFG EG 100/2, EG 100/7; EG 100/15-1, 15-2; FOR1182)
- Baroclinic wave tank experiment (DFG EG 100/3; EG 100/13-1, 13-2, 13-3; SPP 1276 “Metström”)
- Quasi-Biennial Oscillation (QBO-) experiment (DFG EG 100/14-1; HA2932/6-1)
- Strato-Rotational-experiment (DFG EG 100/18-1; HA2932/7-1)
- MS-GWaves experiment (HA2932/8-1,2; FOR 1898)
- Geoflow experiments (DLR, ESA)

Measurement equipment

- 2D-Particle Image Velocimetry (PIV) System, 15mJ Nd:YAG LASER, monochromatic CCD camera, resolution 1 megapixel (New Wave Research, TSI)
- Stereo-PIV system, 100mJ Nd:YAG LASER, 2 cameras with 2 MP resolution (Dantec Dynamics)
- Dantec Dyn. Laser Induced Fluorescence (LIF) system to measure concentration and temperature
- Volumetric Velocimetry, 100mJ Nd:YAG LASER, 3 cameras with a resolution of 2 megapixel, telecentric lenses for a measurement volume of 10 x 10 x 10 cm3 (Dantec Dynamics)
- Particle Tracking (2D, 3D) with the dantec system mentioned above
- 2x 1D (He-Ne LASER) and 2D Laser Doppler Anemometry (LDA), Ar-Ion-LASER
- Infrared-Thermography system

Bibliography:

1. Egbers, Ch., Pfister, G., (Eds), 2000, Physics of Rotating Fluids, **Lecture Notes in Physics 549**, Springer
2. Harlander, U., v. Larcher, T., Wang, Y., Egbers, Ch., 2011, PIV- and LDV-measurements of baroclinic wave interactions in a thermally driven rotating annulus, **Exp. Fluids,** 51**,** 37-49, DOI 10.1007/s00348-009-0792-5
3. Feudel, F., Bergemann, K. , Tuckerman, L., Egbers, Ch., Futterer, B., Gellert, M., Hollerbach, R., 2011, Convection patterns in a spherical fluid shell, **Phys. Rev. E**, 83 (2011), 046304
4. Harlander, U., Wenzel, J., Alexandrov, K., Wang, Y., Egbers, C., 2012, Simultaneous PIV- and thermography-measurements of partially blocked flow in a heated rotating annulus, **Exp. Fluids**, 52, 1077-1085
5. Koch, S., Harlander, U., Egbers, Ch., Hollerbach, R., 2013, Inertial waves in a spherical shell induced by librations of the inner sphere: experimental and numerical results, **Fluid Dyn. Res. 45**, Best paper 2013 Jap. Soc. Fluid Mech.
6. Merbold, S., Brauckmann, H.J., Egbers, Ch., 2013, Torque measurements and numerical determination in differentially rotating wide gap Taylor-Couette flow, **Phys. Rev. E** 87, 023014
7. Futterer, B., Krebs, A., Plesa, A.-C., Zaussinger, F., Hollerbach, R., Breuer, D., Egbers, Ch., 2013, Sheet-like and plume-like thermal flow in a spherical convection experiment performed under microgravity, **J. Fluid Mech., vol. 735,** 647-683 , Cambridge University Press 2013, doi:10.1017/jfm.2013.507,
8. Klein, M., Seelig, T., Kurgansky, M. V., Ghasemi V., A., Borcia, I.-D., Will, A., Schaller, E., Egbers, Ch., Harlander, U., 2014, Inertial wave excitation and focusing in a liquid bounded by a frustum and a cylinder, **J. Fluid Mech., vol. 751**, 255-297, doi:10.1017/jfm.2014.304, 2014
9. Vincze, M., Borchert, S., Achatz, U., von Larcher, Th., Baumann, M., Liersch, C., Remmler, S., Beck, T., Alexandrov, K.D., Egbers, Ch., Fröhlich, J., Heuveline, V., Hickel, S., Harlander, U., 2014, Benchmarking in a rotating annulus: a comparative experimental and numerical study of baroclinic wave dynamics, **Meteorolog. Zeitschrift**, 23, 611 - 635
10. Harlander, U., v. Larcher, Th., Wright, G.B., Hoff, M., Egbers, Ch., 2014, Orthogonal decomposition methods to analyze PIV, LDV and thermography data of a thermally driven rotating annulus laboratory experiment. AGU book: **Modelling Atmospheric and Oceanic flows:** insights from laboratory experiments and numerical simulations, Th. v. Larcher and P. Williams (ed.), Wiley

Aktuelle Forschungsschwerpunkte / Current research topics

B Fluid Mechanics

B2 Transport processes in the Turbulent Taylor-Couette Cottbus (T^2C^2) and Top-view Taylor-Couette Cottbus (TvTCC) facilities

S. Merbold, M. Hamede, A. Froitzheim, Ch. Egbers (DFG EG100/30-1)

The Taylor-Couette (TC) flow, which is the flow between independently rotating cylinders, is a model for general rotating shear flows with technical (turbines or compressors) as well as geo- and astrophysical applications (accretion discs, star formation). Within this geometry a rich variety of flow states can be adjusted by changing the control parameters, namely the ratio of angular velocities $\mu=\omega_2/\omega_1$, the radius ratio $\eta=r_1/r_2$, the aspect ratio $\Gamma=L/d$ with the gap width $d=r_2-r_1$ and the shear rate inside the gap in terms of the shear Reynolds number $Re_S=2r_1r_2d|\omega_2-\omega_1|/((r_1+r_2)\nu)$ with the kinematic viscosity ν of the fluid and the indices 1 for the inner and 2 for the outer cylinder. When only the inner cylinder is rotating, the flow is linear instable as the Rayleigh-Benard flow (flow heated from below and cooled from above), while for pure outer cylinder rotation, the flow is linearly stable as the pipe flow. Further, a close analogy between all three systems exists for the global transport properties, which shows the importance of understanding the Taylor-Couette flow.

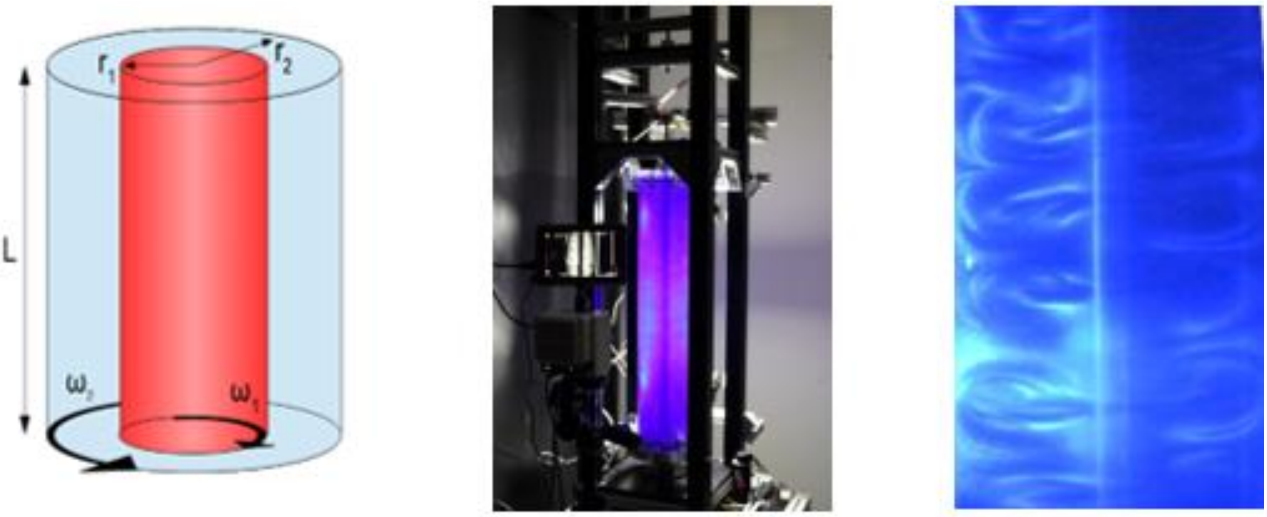

Figure 1: a) Sketch of Taylor-Couette geometry, b) Picture of the TC experiment with the visualization setup, c) the stable Taylor vortices inside the gap

A very important quantity for transport processes in Taylor-Couette flows is the angular momentum current $J_\omega=r^3(\langle u_r\omega\rangle_{t,\varphi,z}-\nu\partial_r\langle\omega\rangle_{t,\varphi,z})$, which can be directly measured by the torque T at the inner or outer cylinder. When J_ω is normalized by its corresponding laminar value $J_{\omega,lam}$, a quasi Nusselt number Nu_ω can be defined in analogy to heat transport problems [2].
For investigations of the TC flow, we have two facilities at the Department of the Aerodynamics and Fluid mechanics at the BTU-Cottbus, the Turbulent Taylor-Couette Cottbus (T^2C^2) facility and the Top-view-Taylor-Couette Cottbus (TvTCC) facility. The (T^2C^2) facility has a transparent outer cylinder, a precise torque measurement unit based on strain gauges inside the inner cylinder and is capable of controlling the angular velocities of the end plate. The (T^2C^2) facility has a radius ratio of (0.5) and it can go up to $Re_s = 10^6$. The TvTCC facility with its transparent top plate and outer cylinder give the advantage to use visualization and measurement techniques for the three flow component (radial, axial, and azimuthal).

Aktuelle Forschungsschwerpunkte / Current research topics

Another characteristic for the TvTCC facility is that it has a changeable inner cylinder, which gives the opportunity to study the flow for different radius ratios using one facility. The key parameters are summarized in table 1:

Table 1: Parameter for T^2C^2 and TvTCC facilities

	Gap width d (mm)	Radius ratio η	Aspect ratio Γ	Re_S
T^2C^2	35	0.5	20	10^3-10^6
TvTCC	35, 45, 56, 63	0.5, 0.357, 0.2, 0.1	20, 15.5, 12.5 11.1	10^3-$3\cdot10^5$

Previous works used this TC facility to study the flow and the angular momentum transport in the geometry of radius ratio 0.5 [1] and 0.357 [2]. Currently we are studying the flow in a very wide-gap configuration (η = 0.1). It's expected that the flow in this configuration shows different behavior compared to the flow in larger radius ratios facilities.
Figure (1b) shows the TC experiment with the visualization setup where the fluid was seeded with Kaliroscope particles and then lighted up using a LED light in order to observe the particles inside the gap. Deferent patterns were observed in the gap. Turbulent Taylor vortex (TV) and other oscillating patterns as well as stable Taylor vortices were observed too, as shown in figure (1c) at a very low counter-rotating ratio μ=-0.01, and for low shear Reynolds number $Re_s < 2500$.
In [2], the essential results of torque measurements in the T^2C^2 facility (η=0.5) are discussed. For pure inner cylinder rotation, the dimensionless torque scales as $G \sim Re_S^{\alpha}$ with two different regimes. For $3\cdot10^3 \leq Re_S \leq 8\cdot10^4$, the scaling is $\alpha=1.62\pm0.04$ and for $10^5 \leq Re_S \leq 10^6$, $\alpha=1.78\pm0.06$. In case of $Re_S > 6\cdot10^5$, the scaling exponent approaches against a constant value of $\alpha=1.75\pm0.03$. For small Reynolds numbers ($10^3 \leq Re_S \leq 2\cdot10^4$), the measured torques could be compared to direct numerical simulations with the same η and Γ=2, showing an excellent agreement with a relative deviation smaller than 4%. Further, in both studies the torque exhibits a maximum for μ=-0.2 independent of the shear Reynolds number for $Re_S < 7\cdot10^5$.
The underlying flow structures have been measured by the use of flow visualization technique [3] and sophisticated layered Particle Image Velocimetry. Herewith it was possible to determine the contribution of the large scale structures and the turbulent fluctuations onto the global transport of angular momentum [1].

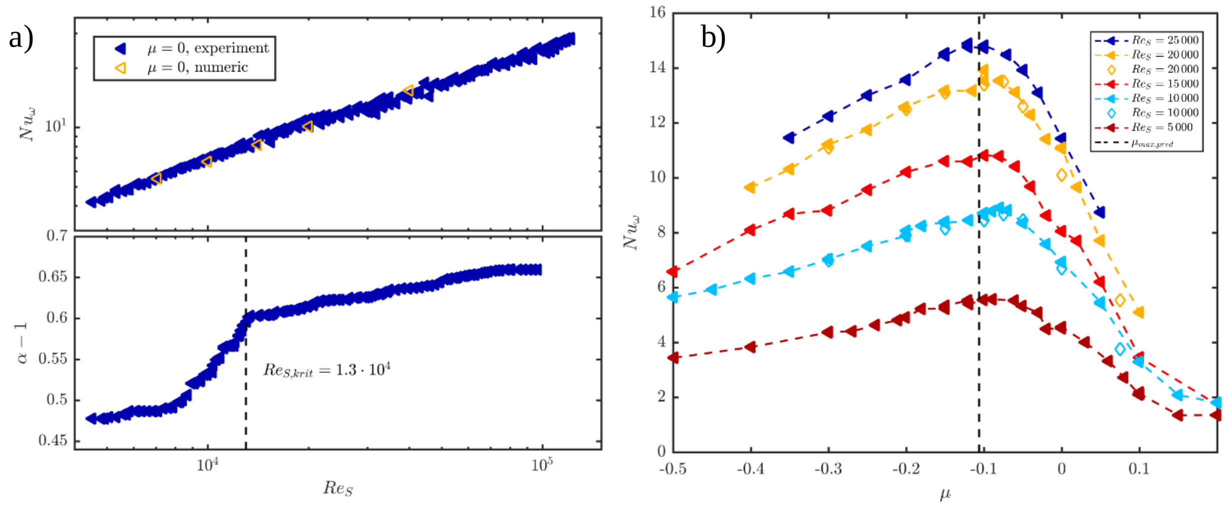

Figure 2: a) Torque data and local scaling exponent for pure inner cylinder rotation as function of the shear Reynolds number for η=0.357. b) Torque data for co- and counter rotation for various shear Reynolds numbers. The maximum of the Nu_ω curves is located at μ=-0.12. [4]

Aktuelle Forschungsschwerpunkte / Current research topics

These studies have been continued for very wide gaps (η=0.357) in the TvTCC experiment [4], depicted in Figure 2. For pure inner cylinder rotation we can again identify a power law scaling of the Nusselt number with the shear Reynolds number and the local exponent α shows a prominent change around $Re_S=1.3\cdot10^4$ much earlier than for η=0.5. Further, the torque maximum has been shifted to μ=-0.12 in good agreement with the predicted one ($\mu_{pred.}$=-0.106). These results are discussed in [4]

In [5], we experimentally studied the influence of large-scale Taylor rolls on the small-scale statistics and the flow organization in fully turbulent Taylor–Couette flow for Reynolds numbers up to $Re_S=3\cdot10^5$. The velocity field in the gap confined by coaxial and independently rotating cylinders at a radius ratio of η=0.71 is measured using planar particle image velocimetry in horizontal planes at different cylinder heights. Flow regions with and without prominent Taylor vortices are compared. We show that the local angular momentum transport (expressed in terms of a Nusselt number) mainly takes place in the regions of the vortex in- and outflow, where the radial and azimuthal velocity components are highly correlated. The efficient momentum transfer is reflected in intermittent bursts, which becomes visible in the exponential tails of the probability density functions of the local Nusselt number. In addition, by calculating azimuthal energy co-spectra, small-scale plumes are revealed to be the underlying structure of these bursts. These flow features are very similar to the one observed in Rayleigh–Bénard convection, which emphasizes the analogies of these systems. By performing a complex proper orthogonal decomposition, we remarkably detect azimuthally travelling waves superimposed on the turbulent Taylor vortices, not only in the classical but also in the ultimate regime. This very large-scale flow pattern, which is most pronounced at the axial location of the vortex centre, is similar to the well-known wavy Taylor vortex flow, which has comparable wave speeds, but much larger azimuthal wavenumbers.

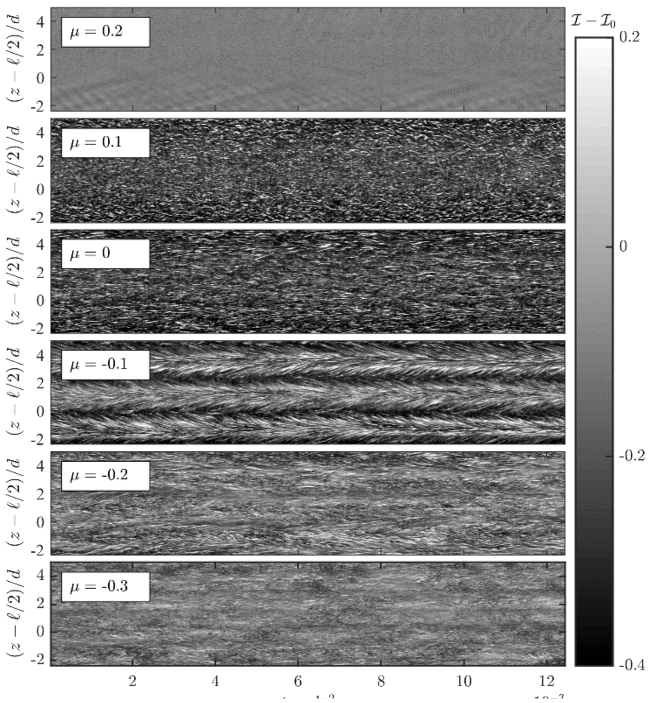

Figure 3: Space-time diagrams of the intensity distribution along an axial, central line over time for the shear Reynolds number $Re_S=2.5\cdot10^5$ and different μ. The time coordinate is normalized by the viscous time scale and the axial coordinate by the gap width d. All videos have been acquired at 60Hz [4].

Further a Particle Image Velocimetry is performed, using a Fast Speed PIV system. A Phantom VEO 640l (2560x1600 pixels) high speed camera was mounted in the top of the apparatus, and a LDY.300PIV laser (λ = 532nm,P0 = 15mJ) was placed beside the apparatus, by this it can generate a horizontal laser sheet inside the gap. The TvTCC apparatus used allow us to measure the azimuthal and the radial velocity component in the gap.

The radial and the azimuthal velocity component were obtained for different heights, and the angular velocity and angular momentum across the gap is calculated. The behavior of the angular momentum and angular velocity is compared for different μ and different Re_S were it shows a different behavior as the angular velocity profile for $\mu > 0$ where both inner and outer cylinder rotate in the same

direction follow the laminar profile of the angular velocity. Also for $\mu < 0$ and specially for $0.007 < \mu < 0.015$ velocity profiles shows a nearly linear shape in the bulk flow.
From the velocity fields measured using the PIV we can further investigate the angular momentum transport in the gap and how it is affected with the different control parameters.

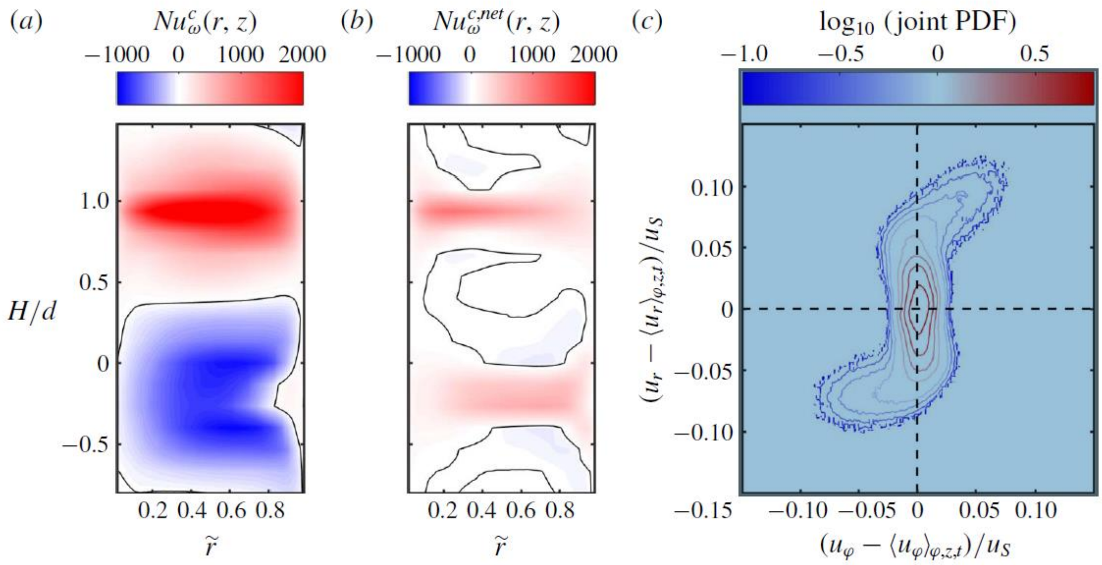

Figure 4: Contour plot of the dimensionless (a) convective and (b) net convective local angular momentum transport in a meridional plane for $Re_S=2.14\cdot10^5$ and $\mu=0.36$ (C_7). Black lines indicate the zero line of the depicted quantities. The colour codes are given in the legends. (c) Joint PDF of the radial and azimuthal velocity fluctuations for the same flow state at mid gap. The colours give the probability (in log scale), see [5]

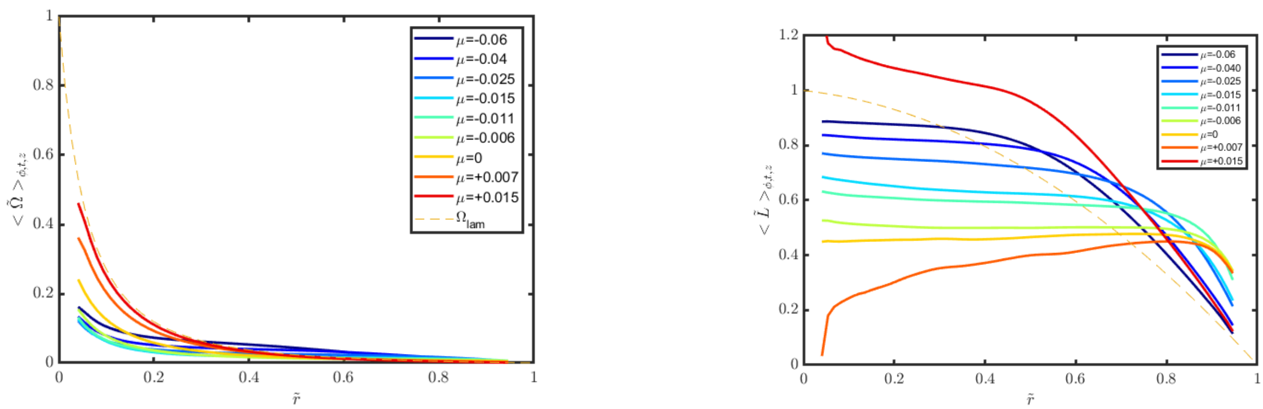

Figure 5: a) Averaged profile of angular velocity $\tilde{\Omega} = \Omega - \Omega_2/\Omega_1 - \Omega_2$, b) Averaged profile of angular momentum $\tilde{L} = L - L_2/L_1 - L_2$ as function of $\tilde{r} = r - r_2/r_1 - r_2$ for $Re_S=2.10^4$

Publication

[1] A. Froitzheim, S. Merbold, C. Egbers, Velocity profiles, Flow structures and scaling in a wide-gap turbulent Taylor-Couette flow, J. Fluid Mech., 831, 330-357, 2017
[2] S. Merbold, H. J. Brauckmann, C. Egbers, Torque measurements and numerical determination in differentially rotating wide gap Taylor-Couette flow, Phys. Rev. E, 87, 023014, 2013
[3] S. Merbold, A. Froitzheim, C. Egbers, Flow pattern and angular motion transport in a wide gap Taylor-Couette flow, TU Dresden, Strömungstechnische Tagung 2014, Schriftenreihe aus dem Institut für Strömungsmechanik Band 10, 2014
[4] A. Froitzheim, S. Merbold, R. Ostilla-Monico and C. Egbers, Angular momentum transport and flow organization in Taylor-Couette flow at radius ratio of η =0.357, Phys. Rev fluids 4 (2019), 084605.
[5] A. Froitzheim, R. Ezeta, S.G. Hisman, S. Merbold, C. Sun, D. Lohse, C. Egbers, Statistics, plume and azimuthally travelling wavs in ultimate Taylor-Couette turbulent vortices, J. Fluid Mech., 876, 733-765, 2019

Aktuelle Forschungsschwerpunkte / Current research topics

B Fluid Mechanics

B3 Nonlinear Surface Waves in a Circular Channel

U. Harlander, I.D. Borcia, R. Borcia, S. Richter, M. Bestehorn
(DFG: BO 3113/4-1, BO 3120/7-1, BE 1300/25-1, HA 2932/17-4)

Introduction

Due to their destructive power, the most prominent examples of nonlinear surface waves are Tsunamis. In December 2004, an earthquake in the Indian Ocean off the island of Sumatra caused one of the worst Tsunami disasters in history with at least 231,000 casualities in Asia. Some years later, in March 2011 a large Tsunami hit the eastern coast of Japan and triggered the Fukushima nuclear disaster. The latter marked the end of the nuclear facilities in Germany. Tsunamis are not only generated on the world's oceans, so-called inland tsunamis can also form on inland lakes. Tsunamis caused by landslides on Lake Geneva are known from historical records. Tsunamis also occurred at open-cast mining lakes, for example at Lake Concordia in Saxony-Anhalt in 2009 or at the Knappensee in Brandenburg in 2021.

Large amplitude nonlinear waves can also be triggered by tidal flows close to the estuariane zone of a river. Such waves are called tidal bores (Bestehorn and Tyvand, 2009). Observation of such waves have been made all around the world from Europe (Baie du Mont Saint Michel - France) to America (Colorado River -Mexico), Asia (Qiantang River - China) (see Chanson, 2011). Tidal bores manifest as a series of waves propagating upstream in the estuariane zone of a river. One of the most prominent tidal bore is Pororoca, at the entrance of the Amazon. Between February and March each year waves up to 4 meters high have been observed that travel more than 800 km inland upstream on the Amazon and adjacent rivers. In general, the wave height of a tidal bores can range from some tens of centimeters up to about 10 meters. In the latter case damages can be expected and also loss of human lives. Tidal bores are usually smaller and less dangerous than Tsunamis, but they can have an unpredictable development near the river bank. Moreover, they occur much more frequently (twice a day) and have a strong impact on sediment transfer and fishery in the river estuaries.

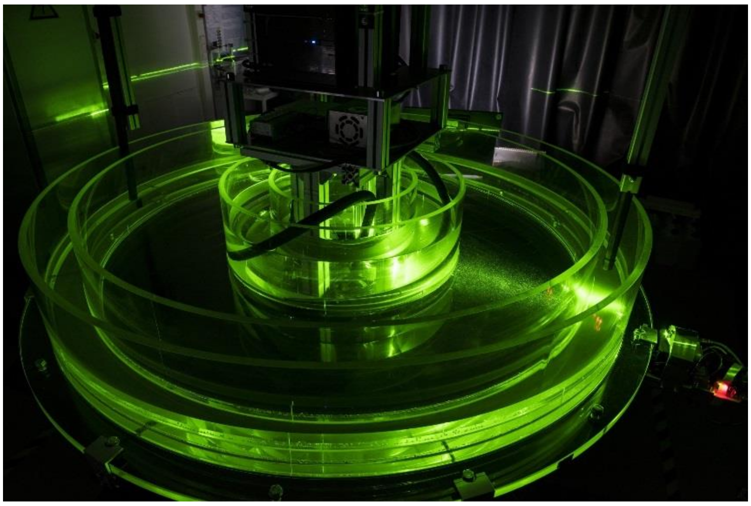

Figure 1: Experimental setup of the circular channel. The experiment consists of four cylinders. The two outer ones form a circular channel with a length of 4.76m and a width of 8.5cm. Water depth can be changed from millimeters to about 25cm. Surface waves can be triggered by movable barriers that separate regions of higher/lower water level or by fixed barriers and an oscillating tank. The former setup can be used to study freely propagating bores, the latter to investigate resonances due to bore reflections.

Experimental results

Many useful results on bore propagation have been obtained during a DFG Project “Experimental and Theoretical Study of Surface Waves Driven by Periodical Excitation" performed in the frame of the

Aktuelle Forschungsschwerpunkte / Current research topics

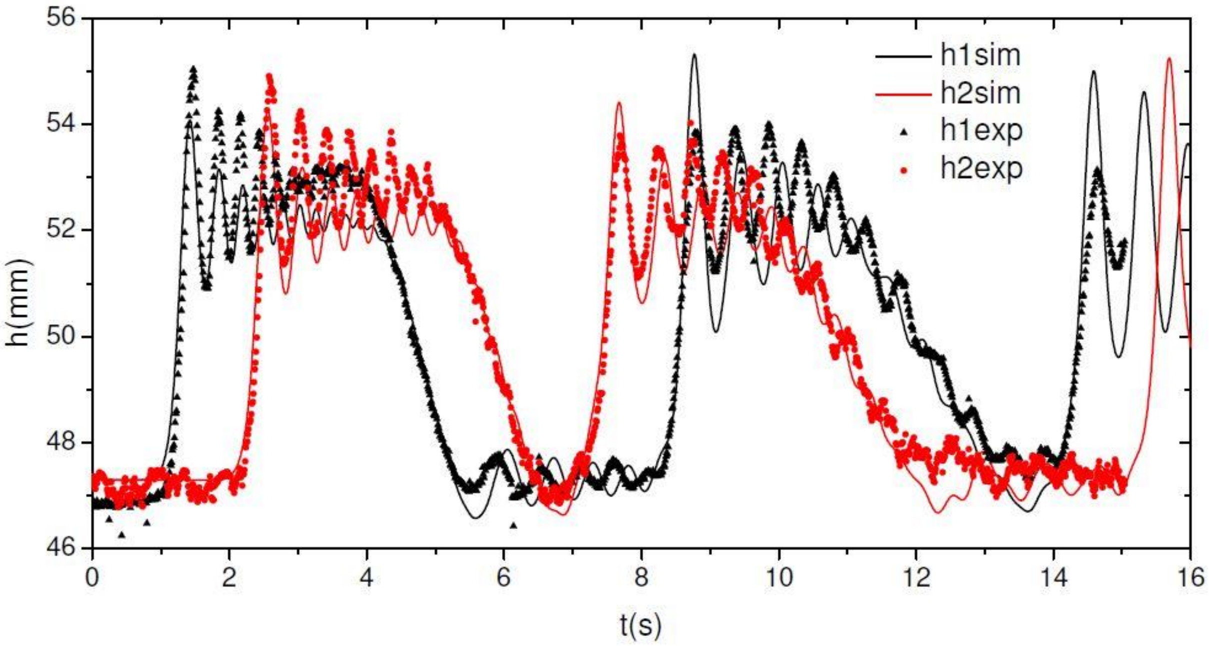

Figure 2: Comparison between experiment (black triangles, red dots) and simulation (black and red line) for a generated (first) and reflected (second) bore. See text for more information.

Core Facility Center "Physics of Rotating Fluids" that is located in the department of aerodynamics and fluid mechanics. In Fig.2 we display a comparison between numerical simulation and observationsof bores in the circular channel. The measurements have been done by using acoustic probes that measure the distance to the water surface via the propagation time of sound waves. Results from two neighboring probes are shown. Black triangles show a time-series from probe 1 and red dots a series from probe 2. Black and red solid lines show the results from corresponding 2D simulations. The agreement is very good and the characteristic shape of a bore with a large amplitude first peak and a following wave train with decreasing amplitude is visible. The first bore is the generated one whereas the second shows the structure after one reflection from a barrier. A weak decay in amplitude and a structural change can be found after reflection in good correspondence with simulations. It should be noted that bores belong to the class of solitons and are hence nonlinear waves. A more detailed analysis and more results can be found in Borcia et al. (2020).

In a follow up DFG project which is expected to start on March 2022 we will investigate issues not considered so far. The first one is fluid mixing due to bores in a two-layer setup with two different fluids. Such mixing processes can play an important role for many applications and might be relevant also for other nonlinear wave types. The second is the influence of asymmetric forcing and bottom topography on the bore properties relevant for applications in ocean flows.

I

Bibliography

[1] M. Bestehorn, and P.A. Tyvand, Merging and colliding bores", Physics of Fluids, 21(4),042107 (2009).
[2] I.D. Borcia, R. Borcia, W. Xu, M. Bestehorn, S. Richter, and U. Harlander, Undular bores in a large circular channel", European Journal of Mechanics - B/Fluids, 79, 67-73, (2020).
[3] H. Chanson, *Tidal bores, Aegir, Eagre, Mascaret, Pororoca: theory and observations*, World Scientific, pp. 220, 2011.

Aktuelle Forschungsschwerpunkte / Current research topics

B Fluid Mechanics

B4 Climate Change Scenarios in the Laboratory

U. Harlander, C. Rodda, M. Vincze (DFG research group FOR1898, HA2932/8-2)

Introduction

The climate on Earth shows a large variability. The evolution of life is tightly connected to this variability with a number of climate related collapses, which ultimately led to the development of *homo sapiens*. Nowadays, anthropogenic climate change is considered as one of the major threats of society and biodiversity. Although there is scientific consensus that the burning of fossil fuels leads to a CO_2 related greenhouse effect, heating up the biosphere, many aspects of local climate variability and the change of the frequency of extreme weather events are still poorly understood.

Numerical climate models are powerful tools to investigate climate change, however, they also have well-known weaknesses. These models are not well resolved and parameterizations are scale-dependent to name just a few problems. On the other hand, climate data series are rather short in particular in view of extreme events that are rare. To gain insight in certain aspects of climate dynamics it is hence worth to consider what can be learnt from laboratory experiments (Vincze et al., 2017).

Already in the 1950s, an elegant laboratory experiment, denoted as differentially heated rotating annulus (DHRA), had been designed to understand large-scale atmospheric motion. One pressing demand of the early experiments was to study how the atmospheric circulation transports heat from equatorial to polar latitudes and a large number of following investigations have revealed many different aspects of atmospheric flows (see e.g. the recent review by Read et al., 2014). All these studies have proven that the DHRA is a useful analog to atmospheric weather systems and recently even small-scale motions that are typically connected to Rossby waves and Rossby wave breaking have been successfully studied in the BTU lab (Rodda et al. 2019; Rodda and Harlander, 2020).

On 9 August 2021, the IPCC report AR6 Climate Change 2021 was released, the first time with a chapter devoted solely to extreme events, many of them connected to the large-scale circulation. The large-scale flow in the atmosphere is largely determined by the dynamics of Rossby waves. These Rossby waves are imbedded in the so called tropospheric polar vortex and they are responsible for a number of extreme weather events that have been intensively discussed in science but also in the public media. Rossby waves can also act as long-range precursors to extreme weather and might impact the predictability of midlatitude weather systems.

In the following section we will show some experimental results on the change of extreme events using the DHRA. In particular we focus on effects related to the so called *Arctic Amplification*. This denotes the fact that the Arctic heats up faster than the rest of the Northern Hemisphere which leads to a weakening of the North-South temperature contrast during a general heating of the atmosphere.

Experimental results

The DHRA consists of a cooled inner and heated outer cylinder mounted on a rotating platform, mimicking the heated tropical and cooled polar regions of the Earth's atmosphere. Depending on the strength of the heating and the rate of rotation, different flow regimes had been identified in the gap: the zonal flow regime, wave-regimes that can be classified by propagating waves of different wave numbers, and quasi-chaotic regimes where waves and small-scale vortices coexist. The radius of the inner (outer) and cooled (heated) cylinder is 4.5cm (12.0cm). The results presented originate from an experiment with 5cm fluid depth. The rotation speed of the tank was 8 rpm and the temperature gradient was varied in the range 3.0 < dT < 7.1 °C. For the largest (smallest) dT the flow is zonally symmetric (quasi-chaotic). The surface temperature of the fluid in the annulus between the inner and outer cylinder has been measured by using an infrared camera (InfraTec). This measurement gives the surface temperature field in high spatial and temporal resolution (640x480 pixel, dt=7.5s).

To detect extreme values, a number of techniques are in use. The *peaks over threshold* method collects values above a predefine threshold. The *block extreme* method collects extremes in a certain interval, e.g. highest temperature within a month. A simple measure is to collect values above the *standard deviation*. All the techniques suffer from a certain arbitrariness, i.e. the choices of the threshold, block length, and distance from the standard deviation. Here we define an extreme surface temperature value as a value above (hot event) or below (cold event) two times the standard deviation within a time series at a certain grid point. We collect the data in three rings, one close to heated wall (“equator”), one in the center of the gap (“midlatitude”), and one close to the cooled wall (“polar”). The results are shown in the figure below.

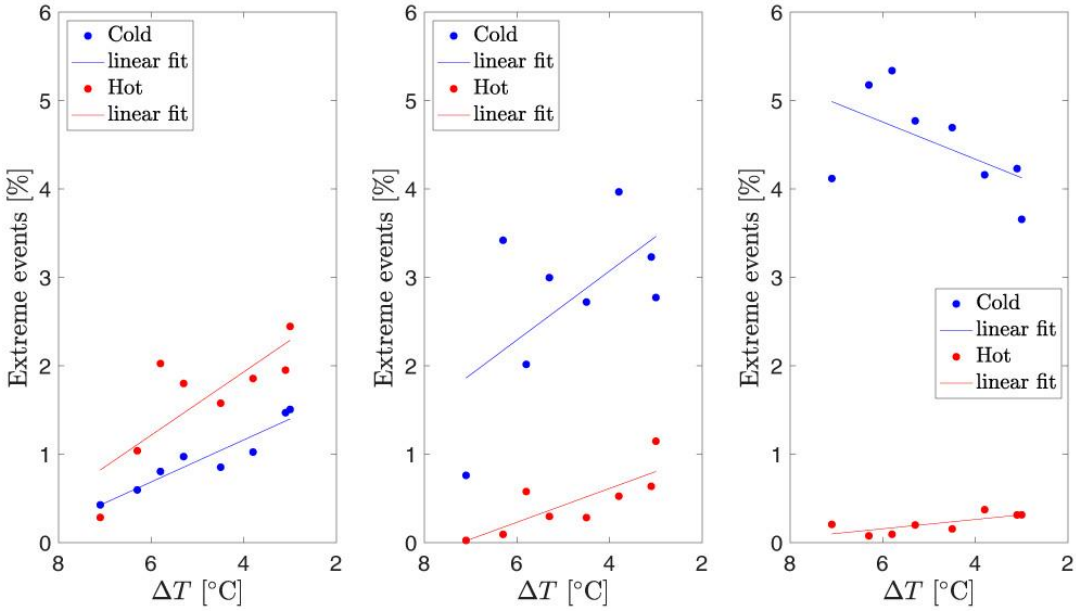

Figure 1: Frequency of occurrence (in %) of warm (red) and cold (blue) extreme events defined as events with deviations larger than 2 times the standard deviation. Left, region near the inner cold wall, center, region in the center of the annulus’ gap, right, region near the outer heated wall. (Rodda et al., 2021).

We find that under “Arctic Amplification”, i.e. a decrease in dT, extreme events become more frequent along the cold and central ring. For the warm ring the signal is less clear. More details can be found in Rodda et al. (2021). Finally we note that a bigger rotating tank has proven to be closer to the atmospheric case than the smaller system used here (Rodda et al., 2019). Hence, further experiments using this bigger DHRA and a deeper statistical analysis are planned for the future.

Bibliography

[1] P.L. Read, P.L., Edgar P. Pérez, Irene M. Moroz, and Roland M. B. Young. “Modeling Atmospheric and Oceanic Flows”, edited by Th. von Larcher and P. Williams, American Geophysical Union, 368pp, (2014).
[2] C. Rodda, S. Hien, U. Achatz, U. Harlander. Exp. Fluids, **61**, doi:10.1007/s00348-019-2825-z, (2019).
[3] C. Rodda and U. Harlander. J. Atmos. Sci., **77**(8), 2793-2806, (2020).
[4] C. Rodda, U., Harlander, M., Vincze. arXiv:2108.11865 [physics.ao-ph], (2021).
[5] M. Vincze, I.D. Borcia, U. Harlander. Scientific Reports, 7, **254**, (2017)

Aktuelle Forschungsschwerpunkte / Current research topics

B Fluid Mechanics

B5 TEHD in a cylindrical annulus: laboratory experiments

A. Meyer, M. Meier, Ch. Egbers (DFG EG 100/20-3)

The TEHD (Thermo-Electro-Hydro-Dynamics) project is concerned by the effect of the dielectrophoretic (DEP) force on a fluid confined in a cylindrical annulus. A dielectric fluid subjected to a temperature difference and a high frequency non-homogeneous electric field undergoes the DEP force that originates from the gradient of the square of the electric field. This force induced by the differential polarization of particles can be seen as the action of an electric gravity on the density stratification, and is therefore analogue to the Archimedean's buoyancy.

In a cylindrical geometry, the electric gravity is directed radially inward so that one can expect the destabilization of the flow if the inner cylinder is hotter than the outer one. To focus on that thermoelectric instability, many experiments have been performed during the microgravity conditions of parabolic flight campaigns and a TEXUS flight experiment is planned for the beginning of 2022 (see Section C dedicated to space researches). As the present project is concerned with laboratory experiments, the Earth gravity will also act on the fluid density stratification and will modify the stability conditions of the system. After the previous phase of the TEHD project which was concerned with a vertical cylindrical annulus[1,2], the new phase of this project aims to investigate two different systems.

First, the DEP force is investigated in a horizontal cylindrical annulus with hot inner cylinder and cold outer cylinder. The base state of the system then corresponds to two crescent shaped convective rolls symmetric with respect to the vertical plan containing the cylinders axis. The hot fluid rises up along the inner cylinder and rises down along the outer cylinder, resulting in an outward hot jet at the top and an inward cold jet at the bottom (see Figure B6-1). This base flow may destabilize for sufficiently large values of the electric Rayleigh number, which is sensitive to the temperature difference and to the square of the applied electric potential.

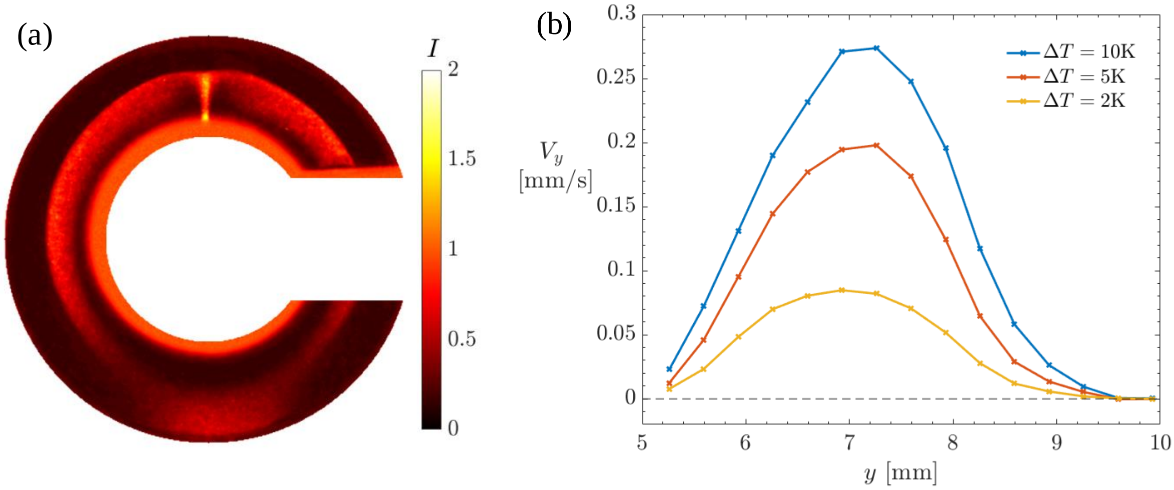

Figure 1: Experimental observation of the base flow of silicone oil B5 in a horizontal vertical annulus. The shadowgraph (a) results from a telecentric optical system observing the gap along the cylinders axis for $\Delta T = 5$K. The method highlights the second derivative of the oil refractive index. The average radial velocity profiles (b) for different ΔT are measured simultaneously to the shadowgraph techniques at the top of the cylinders.

Aktuelle Forschungsschwerpunkte / Current research topics

Second, the DEP force in a cylindrical annulus in vertical alignment is investigated by combining it with the rotation of the inner cylinder. In the isothermal case, the resulting stratification of angular momentum can destabilize the flow, leading to the well-known Taylor vortices. When a temperature difference is applied, the Earth's gravity, the centrifugal acceleration and the electric gravity act together on the density stratification. The three resulting thermal buoyancies play a role on the stability of the system and might change the special and temporal behavior of instabilities (see Figure B6-2). This experimental investigation, which finds its application in small sized heat exchangers should provide information about the transition from the base flow to the first instability, and its corresponding flow pattern and heat transfer enhancement.

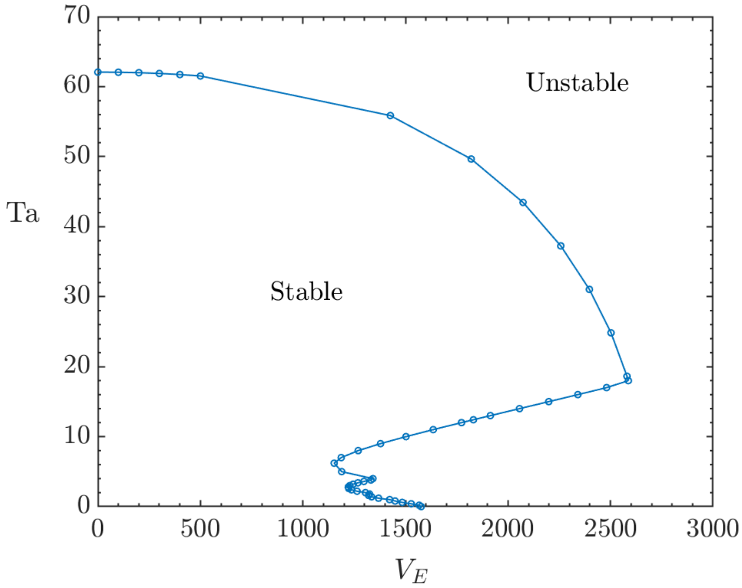

Figure 2: Stability diagram spanned by the dimensionless electric potential V_E and the Taylor number Ta for a silicone oil B5 confined in an infinite cylindrical annulus of radius ratio $\eta = 0.5$ in outward heating with a constant temperature difference of 1K. The diagram indicates the set of parameters for which the fluid bifurcates from a stationary, axisymmetric and axially invariant base flow to an unstable regime. For low Ta, the unstable modes are of electric nature and exhibit non-axisymmetric modes that are advected by the rotation of the inner cylinder. For larger Ta, the base flow destabilizes to the classical Taylor vortices to which the DEP force plays a destabilizing effect.

Bibliography

[1] Seelig, T., Meyer, A., Gerstner, P., Meier, M., Jongmanns, M., Baumann, M., Heuveline, V., Egbers, C., (2019) Dielectrophoretic force-driven convection in annular geometry under Earth's gravity, International Journal of Heat and Mass Transfer, 139, 386-398.

[2] Szabo, P., Meyer, A., Meier, M., Motuz, V., Sliavin, Y., Egbers, C., (2022) Simultaneous PIV and shadowgraph measurements of thermo-electrohydrodynamic convection in a radial electric force field, Technisches Messen, accepted paper on the 06.12.2021.

Aktuelle Forschungsschwerpunkte / Current research topics

B Fluid mechanics

B6 Baroclinic instability in a differentially heated rotating annulus – A new wave tank development for IR-thermography and Wollaston shearing interferometry

Y. Sliavin, P.S.B. Szabo, B. Schulze and C. Egbers (DLR 50WM2141)

Climate prediction and weather forecasting is a topic that has not lost its interest within thousands of years and are still of great interest among meteorologists and geophysicists. But even state-of-art numerical models possesses imperfections and drawbacks. While it is a difficult challenge to provide validation to experiments on the real atmosphere, models based on a simplified principle are commonly used. For large-scale flows it is important to carry out systematic and reproducible studies under controlled circumstances in order to capture their nature of complexities. Experimental setups could provide scientists with a well-controlled test system for geophysical flow fields for their numerical validation; one is the differentially heated rotating annulus, which was firstly introduced by Hide [1] and Futz et al. [2]. A schematics of the baroclinic wave tank and principle is shown in Figure 1.

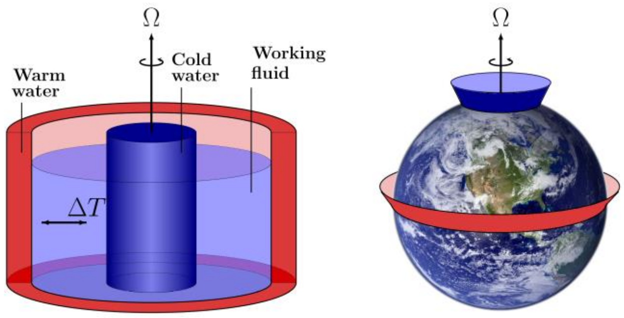

Figure 1: Schematic diagram of a rotating annulus left panel; schematic equivalent configuration in a spherical fluid shell (cf. an atmosphere) in right panel found in Rodda [3].

The baroclinic wave tank has been used for several years [2,4,5] to study the main features of the large- and mesoscale flows, like baroclinic waves or circulations. In analogy to the Earth, it provides the framework to study heat transport from equatorial to polar latitudes.

Here, we present the lasted development at our institute and a new wave tank that has been constructed with three concentric thermal conductive cylinders creating three containments one for the experiment fluid and the other two for heating and cooling the boundaries of the experiment gap. The outer and inner containments are filled with water whereas the experiment gap can be filled with different working fluids. The system is heated at the outer containment and cooled at inner containment that reflect the equatorial and polar regions of a planet. A more details overview of the system is given by a technical drawing on the left panel of Figure 2 whereas the physical built tank is given on the right panel.

The temperature at the inner boundary is maintained by a copper heat exchanger with a thermostat water bath whereas the outer boundary is heated by a heating wire that is fixed inside the outer containment. The temperature of both boundaries is maintained by PT 100 temperature sensors that use a self-developed control feedback loop via a PID-controller to establish a set temperature across the experiment gap. The rotation of the tank is performed by a stepper motor in combination with a turntable having a 1:48 revolution ratio. The motor is controlled by using SSR-relays and the preprogrammed motor controller in manufacturer software BAC-CFG. The system is connected to a LabView program that is to control the overall system.

Aktuelle Forschungsschwerpunkte / Current research topics

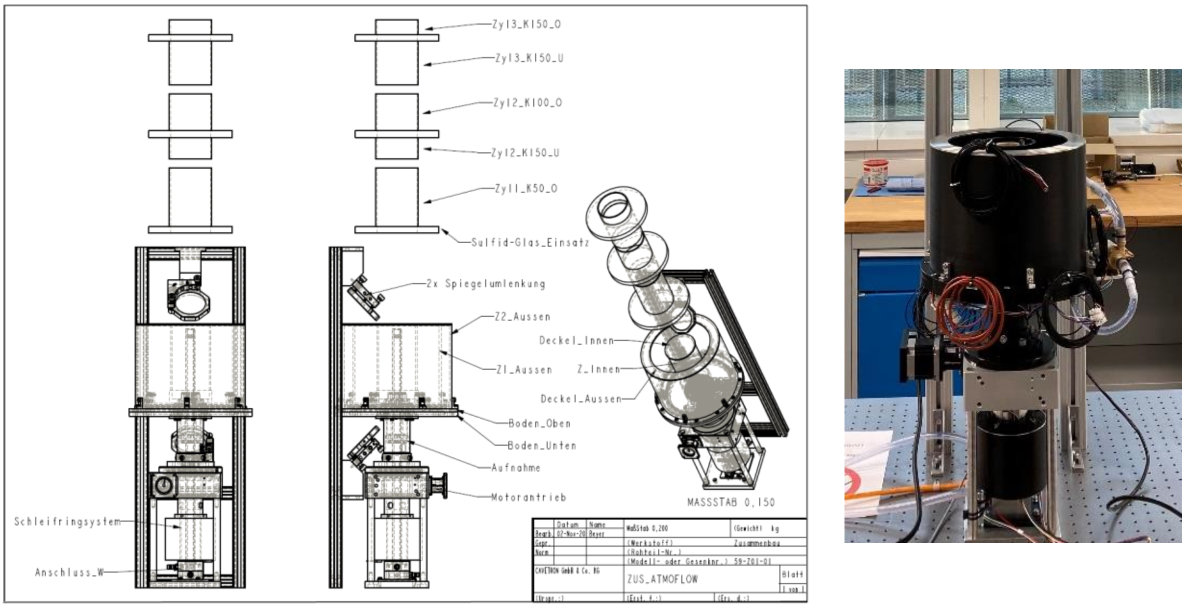

Figure 2: Technical drawing of wave tanks (left panel) physical built wave tank (right panel).

To record the evolving baroclinic instabilities IR-thermography is used in combination of a Wollaston shearing interferometry (WSI). While the IR-thermography records the surface temperature of the baroclinic instability the laser beam of the WSI system is passed through the tank from top to bottom and interfered on two Wollaston prism that provide a 2-dimensional picture of the 3-dimensional vertical temperature field. The results are used to validate and compare both techniques to be able to reconstruct the 3-dimensional temperature field within the baroclinic tank. For this purpose, a parameter space is defined by non-dimensional parameters one the Taylor number (Ta) that counts rotation relative to viscous dissipation and the thermal Rossby number (Ro) that counts for the strength of buoyancy forces relative to rotation in correspondence to the defined fluid's Prandtl number (Pr) to be able to classify the wave development.

References

[1] R. Hide, An experimental study of thermal convection in a rotating fluid, Phil. Trans. Roy. Soc. Lond. A, 250, 441–478, (1958).
[2] D. Fultz, R.R. Long, G.V. Owens, W. Bohan, R. Kaylor, J. Weil, Studies of thermal convection in a rotating cylinder with some implications for large-scale atmospheric motions, Meteor. Soc., (1959).
[3] R. Rodda, Gravity wave emission from jet systems in the differentially heated rotating annulus experiment. Cuvillier Verlag, (2019).
[4] F Vettin, Über den aufsteigen Luftström, die Entstehung des Hagels und der Wirbel-Stürme, Ann. Physik Chemie, 102, 246–255, (1857).
[5] F. Vettin, Experimentale Darstellung von Luftbewegungen unter dem Einfluss von Temperatur-unterschieden und Rotations-impulsen, Meteorolol. Z., 1, 227–230, 271– 276, (1884).

B Fluid mechanics

B7 Experimental investigation of baroclinic instability in a differentially heated rotating annulus – A combined measurement technique utilizing IR-thermography and Wollaston shearing interferometry

Y. Sliavin, P.S.B. Szabo, A.O. Erdogdu, B. Schulze and C. Egbers (DLR 50WM2141)

The motivation of combining IR-thermography and Wollaston Shearing Interferometry (WSI) arises out of the AtmoFlow project. The AtmoFlow experiment deals with a spherical shell that mimics a planet at a small scale where terrestrial gravity is artificially induced by an equivalent electric central force field. The measurement system used is a WSI-system that is to be benchmark via ground experiments carried out in a terrestrial lab in the rotating baroclinic wave tank. The wave tank considers a very simple system with thermally heated boundaries at the outer and inner cylinder as seen in the schematic design in Figure 1. This system is rotated and convective patterns may develop depending on the rotation rate and thermal forcing. The evolving pattern can be referred to atmospheric flow fields and are recorded via the WSI-system.

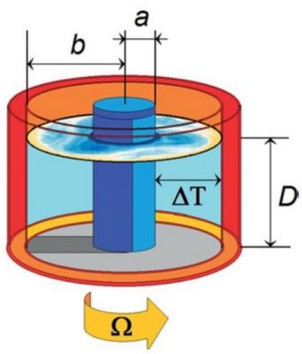

Figure 1: Schematics of a differentially heated rotating annulus with a given temperature difference.

A sketch of the WSI system and the Wollaston prism is given in Figure 2. The system is based on a plane polarised laser with 532nm with a beam diameter of 2 mm at the aperture produces a Gaussian laser beam that is expanded via a beam expander. A mirror system directs the beam further into a polarised beam splitter where the plane polarized beam is transmitted and passed through a quarter wave plate that is rotated 45°. Thus, the linear polarised beam becomes circular polarised and is expanded via two lenses into the test section

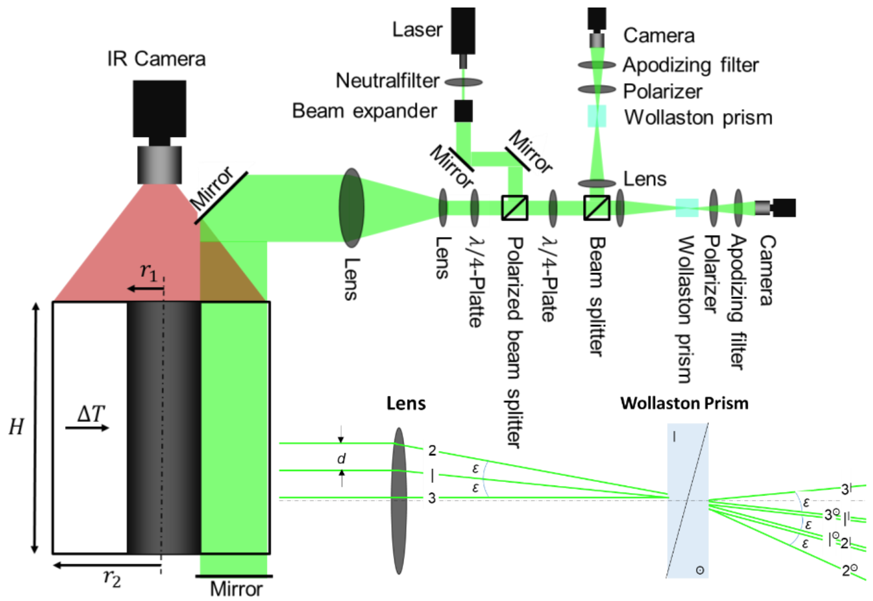

Figure 2: Schematics of the WSI setup in measurement configuration.

of the baroclinic wave tank. The circular polarised beam is than reflected via a mirror at the bottom of the tank. Hence, the reflected beam with circular polarisation is passed back through the two lenses and the quarter wave plate such that the beam converts back to plane polarisation orthogonal to the initial polarisation state (as the beam passed twice the 45° rotated quarter wave plate).

The beam is now able to reflect through the polarised beam splitter into another quarter wave plate to convert the plane polarised beam into circular polarisation. A beam splitter splits the beam into two with a 50:50 ratio where each beam is focussed via a lens into a Wollaston prism. The Wollaston prism will split the two components of the circularly polarised beam by deflecting (and expanding) one of the states along one coordinate axis. After passing through a linear polariser (rotated at 45°) these two beams will interfere on a camera. Variations in the optical path length (e.g., due to refractive index changes in the water tank) will then be visible over the area the two beams overlap and are displaced. Therefore, each prism will only measure the refractive index changes in the coordinate direction it has split the beams. Each camera provides than the images that represents the information only in one gradient direction. More details about the WSI system can be found in [1].

The IR-thermography uses an InfraTec infrared camera VarioCAM®HD to record the temperature fields in the baroclinic annulus. An example of the systems capability is the recorded temperature distribution of the EuHit project conducted by Früh et al. [2]. Figure 3 left panel shows a recorded thermography image of a baroclinic instability with a wave number four. This thermography image post-processed to produce an artificial interferogram that is to be expected to be recorded by the WSI seen in the right panel of Figure 3.

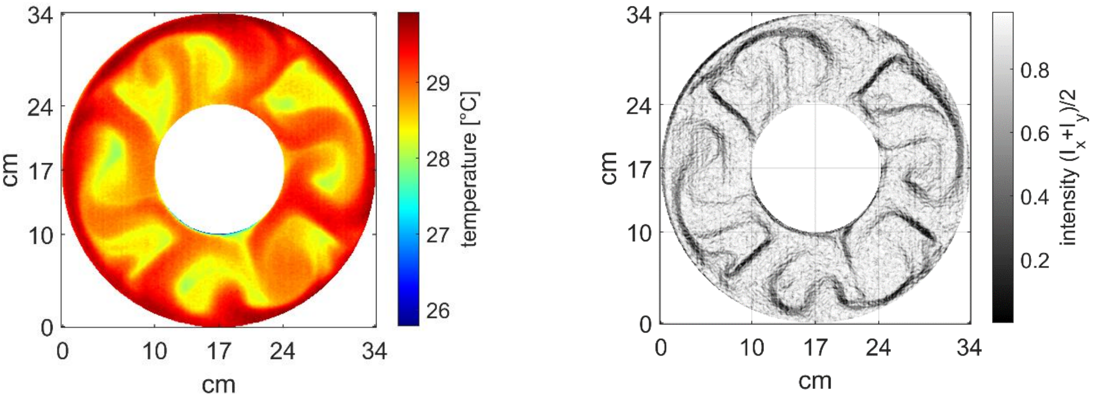

Figure 3: Recorded IR-thermography pictures (left panel) and artificial numerically developed WSI-interference (right panel) of a temperature difference of 9 Kelvin and a rotation rate of 21.4 rpm. Data extracted from [2].

The overall aim of this project is to record baroclinic waves simultaneously by IR-thermography and the WSI system to reconstruct the temperature profile only by the WSI interferograms. These can then be compared with the thermography images to develop an algorithm for the AtmoFlow space experiment that utilises the same WSI-system to support and improve the data post-processing.

References

[1] A. O. Erdogdu, P.S.B. Szabo, R. Carter, M.-E. Gevrek, P. Haun, F. Zaussinger, B. Schulze, M. Meier, C. Egbers, Utilizing Wollaston Shearing Interferometry to investigate the double component density gradient in a differentially heated annulus, in: Experimentelle Strömungsmechanik: 28. Fachtagung, German Association for Laser Anemometry GALA e.V., Bremen, 7–9 September, 19.1–19.8 (2021)
[2] W.-G. Früh, P.S.B. Szabo, U. Harlander, T. Seelig, M. Hoff, C. Egbers, Turbase, URL https://turbase.cineca.it/init/routes/#/logging/ view_dataset/14/tabfile, accessed: (2018)

Aktuelle Forschungsschwerpunkte / Current research topics

C Space Research

C1 Project TEKUS – Thermoelectric convection in parabolic flight conditions I

M. Meier, V. Motuz, P. Szabo, A. Meyer, Y. Sliavin, T.R. Bista, C. Egbers (DLR FKZ 50WM1944)

One of the most common heat exchangers is the thermally heated annulus, a system consisting of a working fluid confined between two concentric cylinders where the inner cylinder is heated and the outer cooled. Large heat transfer rates are in general achieved with forced convection, however it requires fans or pumps whereas passive convection, e.g. natural convention, requires a body force with a temperature-dependant fluid property. Dielectric fluids exhibit a different type of passive convection in addition to natural convection, by which the fluid is not only driven by density changes alone but also by permittivity variations in the presence of a non-isothermal fluid and an alternating electric field. This type of convection is called thermo-electrohydrodynamic (TEHD) convection. As buoyancy is able to induce natural convection in a vertical or horizontal aligned annulus by the thermal expansion of the working fluid, we study convection induced by the temperature-dependant electrical permittivity of a dielectric fluid experimentally. To observe the evolving convective flow fields PIV and shadowgraph recordings are utilised during a parabolic flight campaign (PFC) reaching gravity levels of about 0.1 to 17.7 m/s² ($\sim 10^{-2}g$ to $\sim 1.8g$), where gravity, g, is defined as the magnitude of the earth gravity and equals to 9.81 m/s². Beside laboratory investigations we performed 3 parabolic flight campaigns (PFC) within the TEKUS-project; one of them with a combined cylindrical annulus and rectangular cavity-experiment set-up. For these experiments, the control parameters are the temperature difference ΔT and the alternating high voltage V_0 applied between the two cylinders or plates. The dimensionless form of these parameters are the thermoelectric parameter $\gamma_e = e\Delta T$ and the dimensionless electric potential $V_E = V_0/\sqrt{\rho\nu\kappa/\varepsilon}$, where e is the coefficient of thermal variation of the permittivity ε of a dielectric fluid with density ρ, kinematic viscosity ν and thermal conductivity κ.

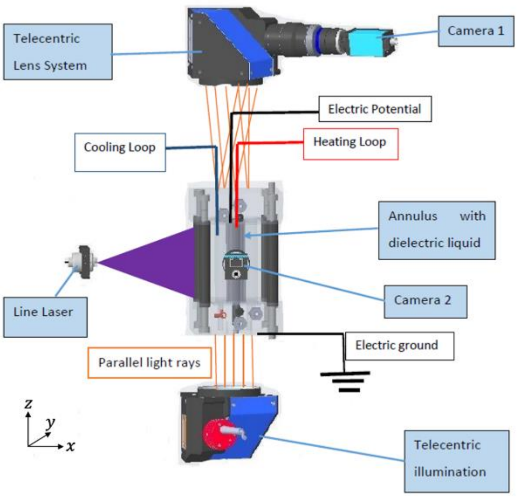

Figure C1-1, Simultaneous measurement of flow structure with a combined SG- and PIV-technique

Aktuelle Forschungsschwerpunkte / Current research topics

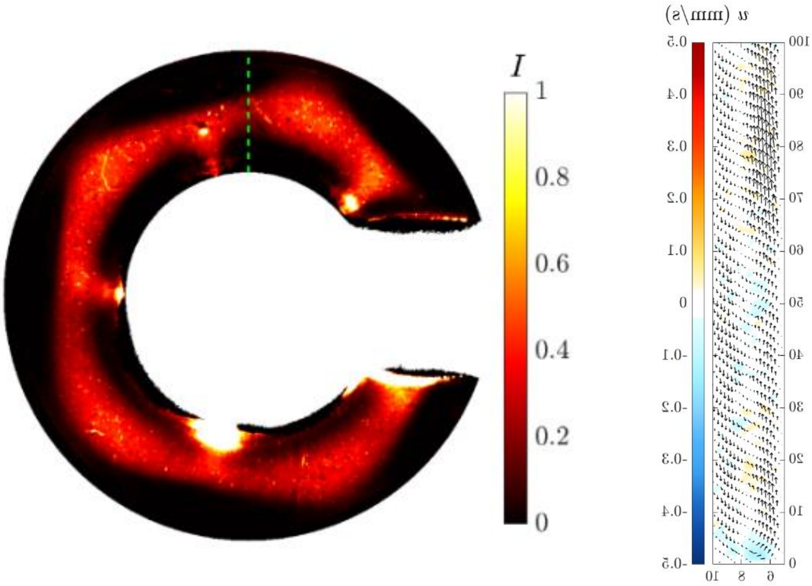

Figure C1-2: Shadowgraph (left) and PIV-image at the final time of the microgravity phase for $\Delta T = 2\ K$ and $V_0 = 7\ kV$.

We use two different measurement methods, which are combined in our new set-up, and are working simultaneously, see Figure C1-1, to visualize the structure of the flow. The first one is the Shadowgraph technique. For that method, the cylindrical annulus is illuminated from the bottom to the top with a telecentric light source producing rays parallel to the axis of the cylinder. The light intensity, initially homogeneous, is modified because of optical index variations due to temperature perturbations. The light intensity profile at the top of the cell is captured by a camera with telecentric lens and compared with a reference profile. The second method, now applied simultaneously, is the particle image velocimetry (PIV), which provides the 2-dimensional velocity field. Figure C1-2 shows the results from both combined two methods. The experimental threshold for convective motion in microgravity conditions qualitatively follows the theoretical one. But, one important reason remains the too short duration of the microgravity phases to obtain an established unstable flow. Therefore, we prepared a sounding rocket flight experiment, which will be launched in February 2022 with a µg-time of about 6min.

References

[1] Meyer, A., Jongmanns, M., Meier, M., Egbers, C., Mutabazi, I. (2017) Thermal convection in a cylindrical annulus under a combined effect of the radial and vertical gravity, *C. R. Mécanique* 345, 11–20

[2] Meyer, A., Crumeyrolle, O., Mutabazi, I., Meier, M., Jongmanns, M., Renoult, M.-C., Seelig, T., Egbers, C. (2018) Flow Patterns and Heat Transfer in a Cylindrical Annulus under 1g and low-g Conditions: Theory and Simulation, Microgravity Sci. Technol. 30, 653–662, DOI: 10.1007/s12217-018-9636-3

[3] Meier, M., Jongmanns, M., Meyer, A., Seelig, T., Egbers, C., Mutabazi, I. (2018) Flow pattern and heat transfer in a cylindrical annulus under 1g and low-g conditions: Experiments, Microgravity Sci. Technol. 30, 699-712, DOI 10.1007/s12217-018-9649-y

[4] Meier, M., Szabo, P., Motuz, V., Egbers, C. (2021) Strömungsfeldvisualisierung von thermo-elektro-dynamischer Konvektion mit einer kombinierten PIV- und Schattentechnik” 27. GALA - Fachtagung Experimentelle Strömungsmechanik, 7. - 9. Sept. 2021, Bremen

[5] Szabo, P. S. B., Meier, M., Meyer, A., Barry, E. B., Mutabazi, I., Egbers, C. (2021) PIV and Shadowgraph measurements of thermo-electrohydrodynamic convection in a horizontal aligned thermally heated annulus at different gravity conditions”, Experimental Thermal and Fluid Sc. **129**, 110470

C Space Research

C2 Project TEKUS – Thermoelectric convection in parabolic flight conditions II

V. Motuz, M. Meier, A. Meyer, Y. Sliavin, P. Szabo, T. Bista, E.B. Barry, O. Crumeyrolle, I. Mutabazi, C. Egbers (DLR FKZ 50WM1944, CNES)

In our last parabolic flight campaign in Bordeaux (CNES VP 161th, Sept./Oct. 2021), we investigated the effect of the dielectrophoretic force on thermally induced convection in the dielectric silicone oils B3 and B5 (Böwing GmbH, B3 and B5 have kinematic viscosities of 3 mPas and 5 mPas, resp.) in two different geometries. The first experiment geometry was a rectangular cavity (RC) and the experiments are presented in part C4 of this report. The second experiment geometry was a cylindrical annulus. Both parts of the experiment were focussed on the investigation of thermal convection in a dielectric liquid inside a cavity under the influence of a superimposed electric force field. In this report, we present the investigation of the thermo-electrohydrodynamic convection in the B5 silicone oil in a cylindrical annulus under microgravity during that parabolic flight campaign.
Convective heat transfer plays an important role in many processes especially in cooling or heating applications. In weightlessness where natural buoyancy convection induced by gravity does not exist, convection may be induced by other means e.g. by electric fields. Through a control of electric field parameters, it is possible to control heat exchange processes efficiently by increasing, suppressing or switching on or off the convective transport. Theoretical and numerical investigations carried out by Yoshikawa et al. [1] and Malik et al. [2] resulted in helical structures as a general shape of the evolving structures in the fluid under microgravity (μg) - conditions.

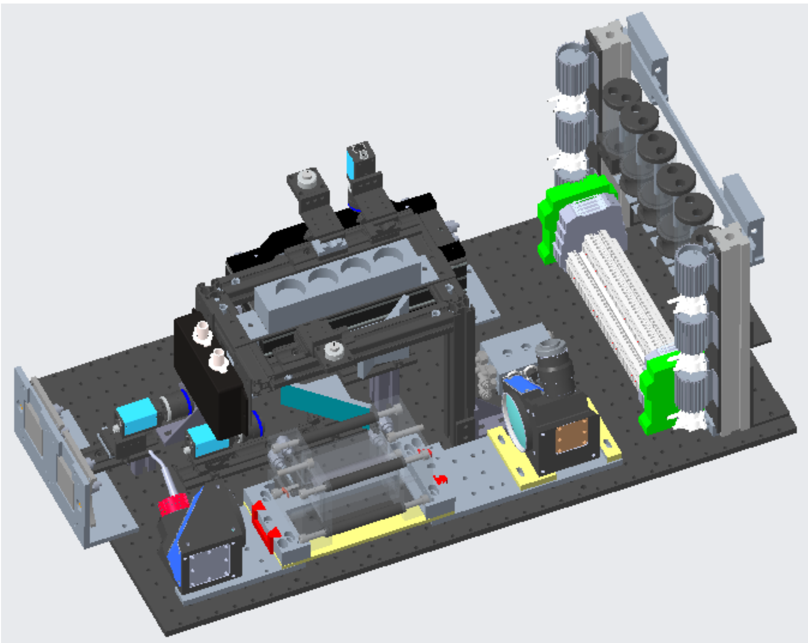

Figure C2-1: Schematic representation of the experimental setup for the investigation of thermal convection in a dielectric liquid inside the two different cavities under the influence of a superimposed electric force. On the anterior is an experimental cell with a cylindrical annulus; in the background is the rectangular cavity cell.

In our experimental setup (Figure C2-1), the dielectrophoretic (DEP) force is produced by means of a high voltage a.c. electric field. In a cylindrical geometry, the electric gravity is directed radially inward so that one can expect the destabilization of the flow if the inner cylinder is hotter than the outer one. The used measurement techniques shadowgraph and particle image velocimetry (PIV) provide an indication of the temperature and velocity distribution of the convective flow inside the cylindrical experiment cell as given by Meier et al. [3]

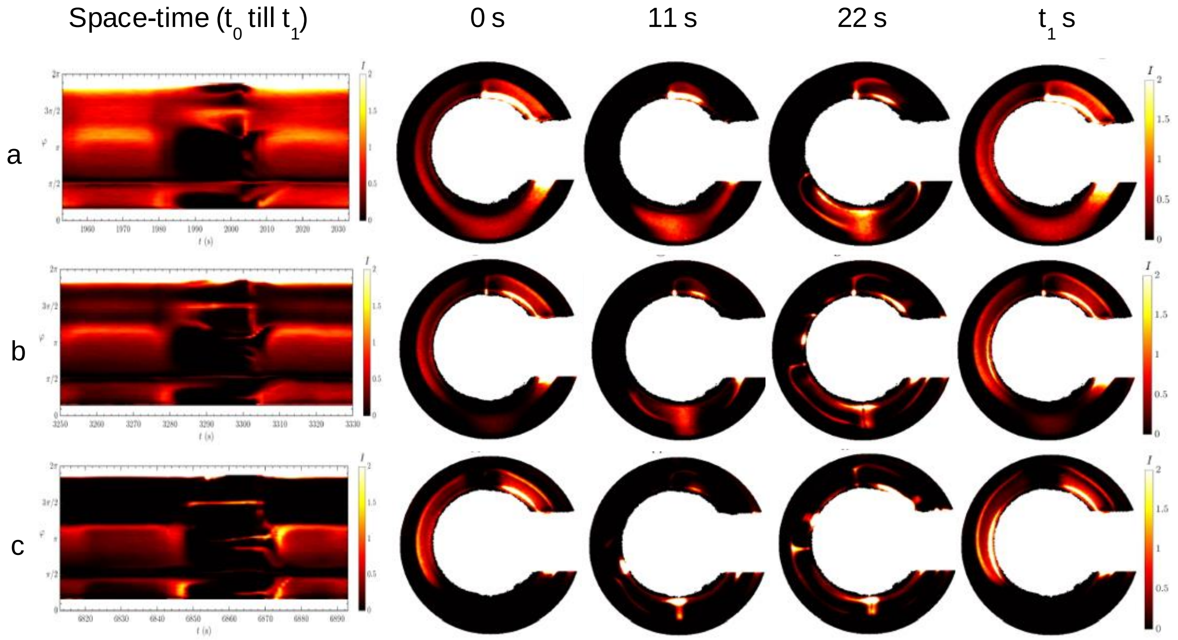

Figure C2-2: Experimental observation of the flow of silicone oil B5 in a cylindrical annulus. The shadowgraph pictures (right) result from a telecentric optical system observing the gap along the cylinders axis by 10 kV a.c. peak voltage at different times during the parabola flight for three different temperature gradients a) $\Delta T = 5K$, b) $\Delta T = 7K$, c) $\Delta T = 11K$. Time t_0 is the time of parabola start at about 20 sek before the start of the microgravity phase and t_1 is the time of parabola end, about 20 sek after the end of the µg-phase. The space-time diagrams (left) represent the reconstructed state of the studied system during specific time, which include the time before µg (about 20 s at 1.8g), 22 seconds µg-phase and time after µg (about 20 s at 1.8g). This diagram consists of narrow strips in the middle of the gap (2.5 mm to the walls) between the inner aluminium and outer glass cylinders during the specified time for one particular parabola.

Under conditions of weightlessness, the higher the temperature difference between the inner and outer parts of the cylindrical annulus, the faster stable convective structures are formed (Figure C2-2). The obtained results correspond well to the theoretical simulations made within the framework of the same project and also presented in this volume. As part of the TEXUS 57 campaign in February 2022, it is planned to investigate the formation of convective patterns at lower electric field strengths and a much longer time of weightlessness as in the parabolic flights.

References

[1] H. Yoshikawa, O. Crumeyrolle, I. Mutabazi (2013) Dielectrophoretic force-driven thermal convection in annular geometry. Phys. Fluids, 25, 024106-0214120

[2] S.V. Malik, H.N. Yoshikawa, O. Crumeyrolle, I. Mutabazi (2012) Thermo-electro-hydrodynamic instabilities in a dielectric liquid under microgravity, Acta Astronautica 81, 563 –569

[3] M. Meier, P. S. B. Szabo, V. Motuz, C. Egbers (2021) Flow field visualisation of thermo-electrodynamic convection utilising a combined PIV and Shadowgraph technique, in: Experimentelle Strömungsmechanik: 28. Fachtagung, German Association for Laser Anemometry GALA e.V., Bremen, 7–9 September, 6.1–6.7

Aktuelle Forschungsschwerpunkte / Current research topics

C Space Research

C3 Thermo-electrohydrodynamic convection in annular geometry under microgravity utilizing sounding rocket experiment – A numerical FEM approach

P.S.B. Szabo, M. Meier, A. Meyer, C. Egbers (DLR 50WM1944)

Convection in weightlessness is investigated in a differentially heated annular geometry by a numerical model using the finite element method (FEM). While buoyancy flow of free fluids is usually induced by gravity in a terrestrial environment, it is not possible to induce convection in free space where gravity is almost always close to zero. Thus, convection may be induced by other means e.g. by electric fields. Here, we investigate thermo-electrohydrodynamic convection (TEHD), a convective flow that is produced by a non-isothermal dielectric fluid in the presence of an alternating electric potential. While terrestrial buoyancy would cause natural convection that may overpower TEHD convection, both convection phenomena have to be separated to be able to investigate the means of thermal transport related only to one physical phenomena. In this particular case the focus is on the experimental investigation of TEHD convection within an annular geometry that is placed in a sounding rocked. This rocket is part of the TEXUS 57 mission to obtain a research environment in free space for about 6 minutes. TEHD convection can therefore arise where natural convection is absent and thus induce a thermal flow. However, due to viscous and thermal dissipation that inhibit fluid motion a critical threshold has to be exceeded before convection sets in. This threshold is referred to a critical electric Rayleigh number and is crucial for the investigation as the microgravity period of the sounding rocket is limited.

The conducted parametric study investigated the critical threshold by utilizing a numerical FEM model to get an indication at what time frame TEHD convection sets in for two different silicone oils (B3 and B5). For this purpose, a set of four different voltages are applied between the inner and outer cylinder which are thermally forced to maintain a temperature difference either 5 or 10 Kelvin. Here, we show in Figure C3-1 the evolving thermal structures as a function of radial distance expressed in a grey level for the fluid B3. As can be seen at 4 kV peak convective structures evolve at about 90 s after the voltage was applied. This suggest a much larger period as is the case for the 5 kV peak before convection is obtained. The structures observed may be described by the detachment of convective plumes at the tangent cylinder. In fact, cold fluid is attracted to higher electric fields strength while hotter fluid is displaced and thus a thermal flow is developed between both cylinders that is purely driven by the electric field intensity in presence of a non-isothermal fluid.

The general shape of the evolving structures can be referred to Yoshikawa et al. [1] and Malik [2] who found their helical nature by utilizing a linear stability analysis. While the numerical FEM results provide in general such helical structures, their appearance may not only result in one single direction of right or left turning helical appearance within the geometry. In fact, the numerical simulations suggest that both right and left turning helical structures co-exist and compete with each other providing a more complex flow and heat transfer between both cylinders.

Aktuelle Forschungsschwerpunkte / Current research topics

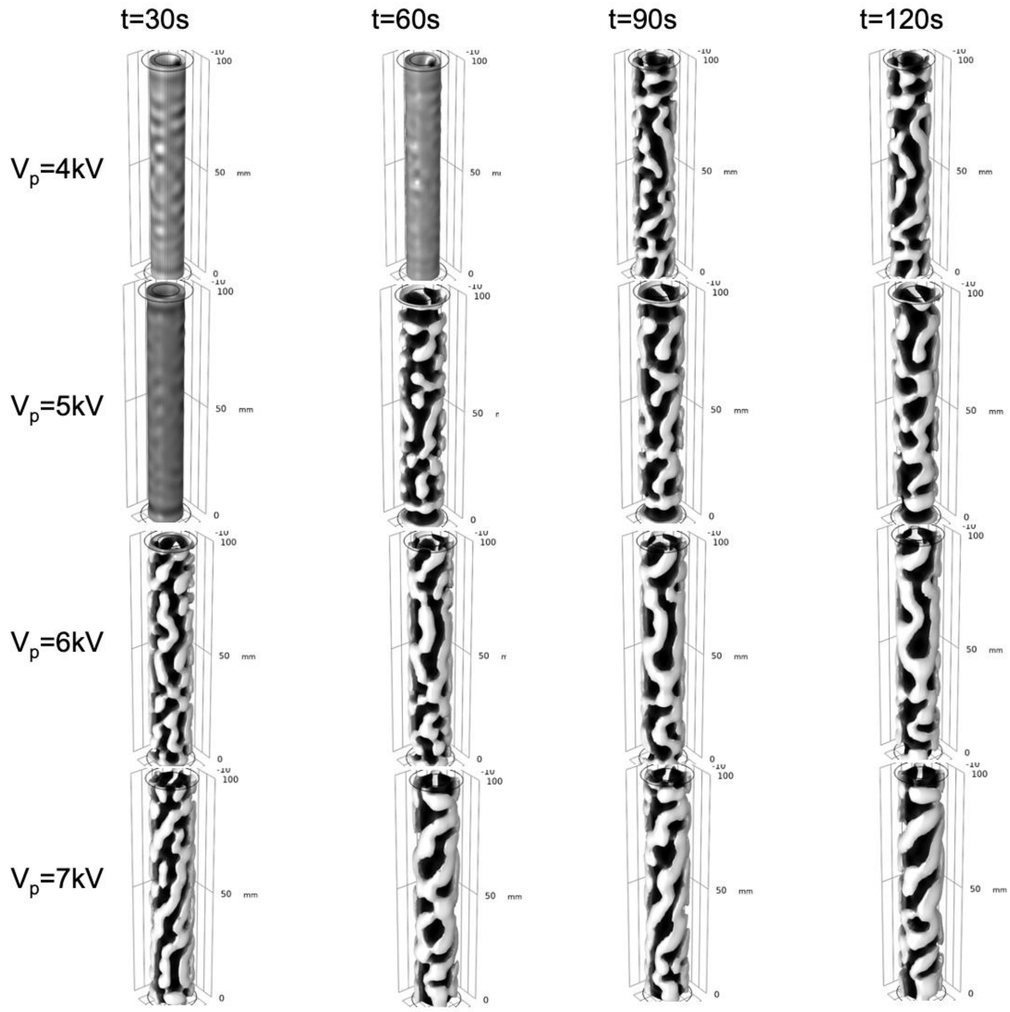

Figure C3-1: Isothermal plot in radial distance in grey scale. The parametric study induced a set of electric peak potentials applied at the tangent cylinder for a given temperature difference of 10 Kelvin at different periods after the electric voltage was applied. The working fluid is a silicone oil B3.

How such structures can co-exist will be investigated by experimental investigations via particle image velocimetry and shadowgraph measurements planned to be conducted during the TEXUS 57 campaign planned in February 2022. This combination of both measurement techniques is found in Meier et al. [3] and Szabo et al. [4] and will provide simultaneous measurements of fluid velocity and the refractive in index of the fluid to get an indication of the temperate distribution inside the cavity.

References

[1] H. Yoshikawa, O. Crumeyrolle, I. Mutabazi (2013) Dielectrophoretic force-driven thermal convection in annular geometry. Phys. Fluids, 25, 024106-0214120

[2] S.V. Malik, H.N. Yoshikawa, O. Crumeyrolle, I. Mutabazi (2012) Thermo-electro-hydrodynamic instabilities in a dielectric liquid under microgravity, Acta Astronautica 81, 563 –569

[3] M. Meier, P. S. B. Szabo, V. Motuz, C. Egbers (2021) Flow field visualisation of thermo-electrodynamic convection utilising a combined PIV and Shadowgraph technique, in: Experimentelle Strömungsmechanik: 28. Fachtagung, German Association for Laser Anemometry GALA e.V., Bremen, 7–9 September, 6.1–6.7

[4] P. S. B. Szabo, A. Meyer M. Meier, V. Motuz, Y. Sliavin, C. Egbers (2022) Simultaneous PIV and shadowgraph measurements of thermo-electrohydrodynamic convection in a differentially heated annulus, Technisches Messen, accepted Dec. 2021.

C Space Research

C4 Project TEKUS – Thermoelectric convection in parabolic flight conditions with rectangular cavities

M. Meier, A. Meyer, V. Motuz, Y. Sliavin, E.B. Barry, O. Crumeyrolle, I. Mutabazi, C. Egbers (DLR FKZ 50WM1944, CNES)

For our latest parabolic flight campaign (CNES VP 161th, Sept./Oct. 2021), we investigated the effect of the dielectrophoretic force also in a rectangular cavity (RC), similar to our experiments 3 years before, performed during the CNES-PFC VP139 in autumn 2018. Compared to the cylindrical annulus case, the RC case needs a fluid with low viscosity and/or a large permittivity to fulfil the conditions of the available parameter range of our experimental set-up. Indeed, for a given fluid, the electric gravity in a plane cavity is weakened since the curvature plays an important role for the non-homogeneity of the electric field (figure C4-1). Under microgravity conditions, theoretical and numerical investigations carried out by Yoshikawa et al. [1] and Tadie Fogaing et al. [2] showed the increase of the heat transport in the RC, as well as the important feedback effect of the perturbation electric gravity in this configuration. Because of this last point, it is known that the critical electric Rayleigh number ($L_c = 2128$) is larger than that of the classical Rayleigh-Bénard problem ($Ra_c = 1708$).

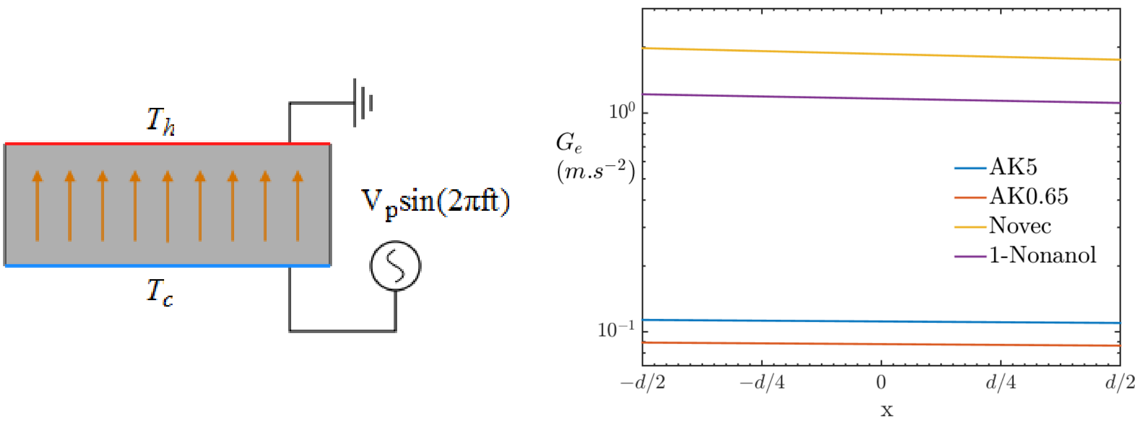

Figure C4-1: Schematic representation of the rectangular cavity (left) and electric gravity as function of the distance between the two plates for a gap of d = 5 mm and for various fluids.

Modular experiment cells have been designed and constructed in our department [3]. The gap between the two TCO-coated plates has a length of 200 mm, a width of 40 mm and a depth of 5 or 10mm. The Synthetic Schlieren technique is used to visualize the density variations and the PIV technique allows to measure a 2D velocity field. For the Synthetic Schlieren technique the gap is illuminated from one side of the rectangular cavity by an LED panel to which is directly placed a foil with black dots randomly distributed. A camera placed on the other side of the rectangular cavity captures the dot pattern and its displacement with respect to a reference image, which is taken as the image of the dot pattern when no temperature gradient and no high voltage are applied. For the PIV technique, a LASER light sheet illuminates the gap along the length of the cavity. Particles prior dispersed in the fluid reflects the light of the sheet and a camera looking at this sheet captures the particle motions. The velocity is then calculated through the displacement of the particles during a given time.

High voltage is applied only during microgravity conditions. The horizontal plate is heated from the top and cooled from the bottom so that there is no flow due to the previous gravity phases of the parabolic flight when the high voltage is applied. In the CNES VP 161th campaign, the chosen fluid was 1-Nonanol for its quite high electric permittivity.

Aktuelle Forschungsschwerpunkte / Current research topics

However the liquid we used has been found to be contaminated, and its dielectric property could not be ensured. Our experience from the-PFC VP139 in 2018 indicates that only Novec 7200 fluid has shown a destabilization during the microgravity phases of the CNES-PFC VP139.

Figure C4-2 show the Synthetic Schlieren result obtained for Novec 7200 at the end of the microgravity phase of two different parabolas. For $V_p = 1\text{kV}$, the displacement field of the pattern shows no particular divergence, indicating a homogeneous temperature field along the x and y directions. For $V_p = 2\text{kV}$, a disturbance of the displacement field is measured and its divergence highlights a modal structure of the perturbation with a certain wavelength of the order of twice the gap size ($d = 5\text{mm}$). The Novec 7200 fluid has then destabilized to a Rayleigh-Bénard like instability induced by the electric gravity.

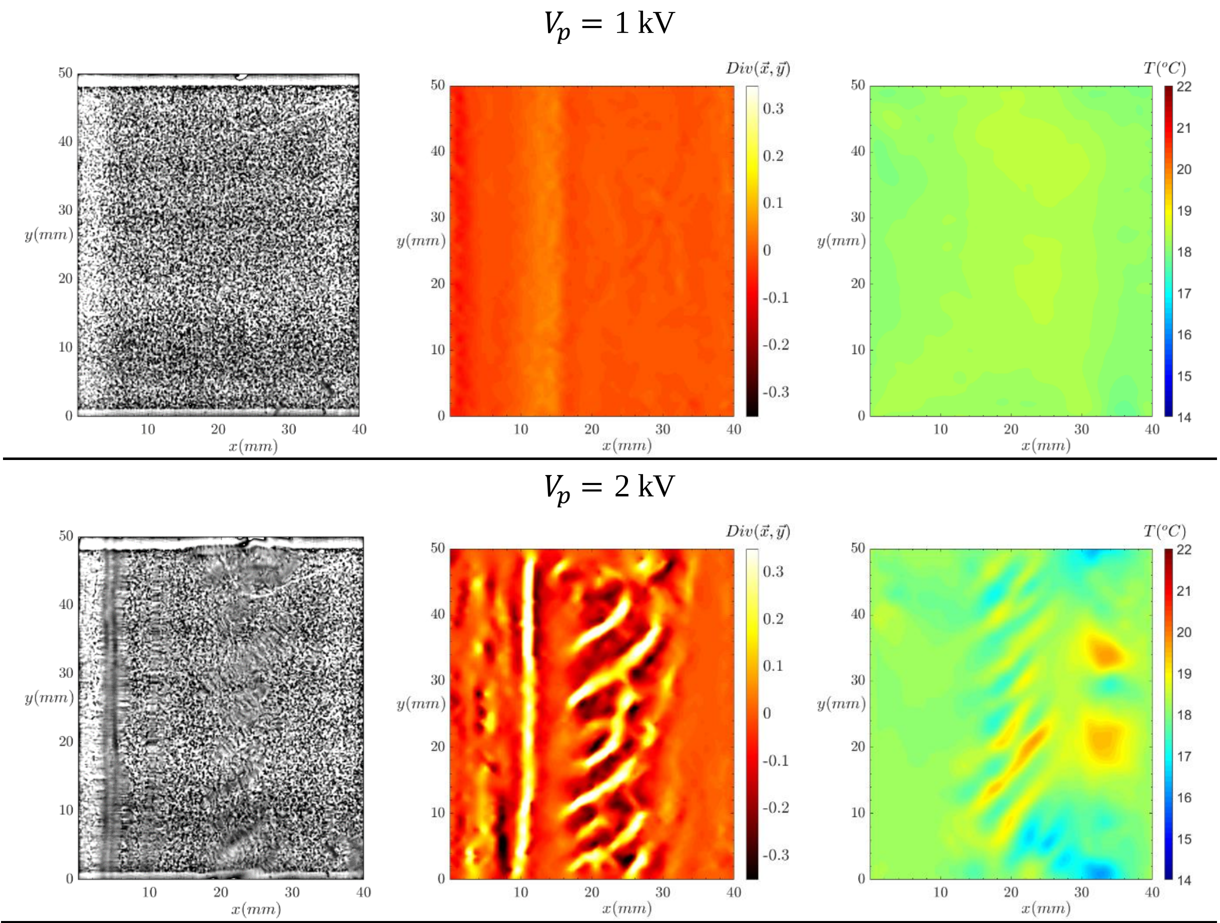

Figure C4-2: Synthetic Schlieren technique and its post-treatment for Novec in a 5mm gap with $\Delta T = 6.5K$ at the end of the microgravity phase of two parabolas corresponding to two different tensions applied. Direct visualization of the background (left), resulting divergence of the displacement field of the random pattern (middle) and simulation of the temperature field resulting from the divergence of the displacement field (right).

References

[1] Yoshikawa, H. N., Tadie Fogaing, M., Crumeyrolle, O., Mutabazi, I. (2013) Dielectrophoretic Rayleigh-Bénard convection under microgravity conditions. Phys. Rev. E, vol. 87, 043003.

[2] Tadie Fogaing, M., Yoshikawa, H. N., Crumeyrolle, O., Mutabazi, I. (2014) Heat transfer in the thermo-electro-hydrodynamic convection under microgravity conditions. Eur. Phys. J. E, vol. 37, pp. 35-40

[3] Ostmann, V. (2018) Planning and construction of a modular experimental cell for the investigation of a thermal electro hydrodynamic convection in a rectangular cavity, MSc-Thesis, BTU Cottbus-Senftenberg

Aktuelle Forschungsschwerpunkte / Current research topics

C Space Research

C5 Project TEKUS – Thermal convection in a sounding rocket flight

M. Meier, V. Motuz, A. Meyer, Y. Sliavin, T.R. Bista, P. Szabo, C. Egbers (DLR FKZ 50WM1944)

The parabolic flight campaigns with the ZERO-G-airplane of NOVESPACE, which we did quite regularly during the last 10 years deliver a short duration of the microgravity phases -about 20s. This is too short to obtain a fully established stable flow in a large part of our experimental parameter field. Therefore, over 6 years, we prepared a sounding rocket flight experiment, which will be conducted in February 2022 as part of the TEXUS 57 campaign. These TEXUS-(**T**echnologische **Ex**perimente **u**nter **S**chwerelosigkeit) flights have a much larger µg-phase -about 6min- as parabolic flights with an airplane.

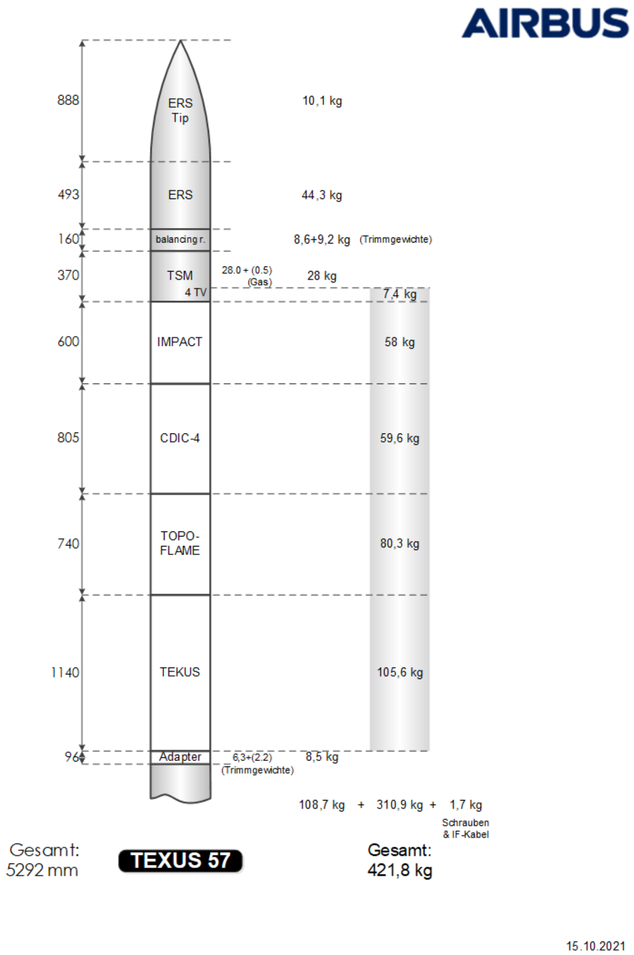

Figure 5-1, The scientific payload of TEXUS 57 with its 4 experiment modules of the projects, IMPACT, CDIC, TOPOFLAME and TEKUS.

Beside our Experiment “TEKUS (TEM06-42)”, 3 other experimental set-ups will be part of the TEXUS 57-campaign: “CDIC-4, Chemo-Hydrodynamic Patterns and Instabilities - Flow-Driven Reaction Patterns" as a cooperational ESA-project; “TOPOFLAME, Wirkung der Topographie auf die Flammenausbreitung längs fester Brennstoffe" from ZARM, University of Bremen and “IMPACT, Untersuchung mikrogravitationsinduzierter Phosphorylierungs- und Kalziumänderungen” from J. W. Goethe-Universität Frankfurt. DLR commissioned Airbus Defense and Space (ADS), TEXUS engineering, in Bremen for the design and manufacturing, the launch preparations and implementation of our TEKUS-module for the TEXUS 57 campaign.

Aktuelle Forschungsschwerpunkte / Current research topics

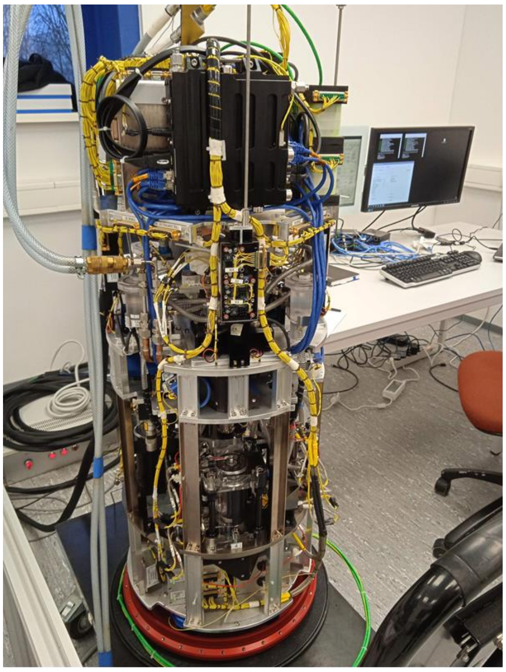

Figure C5-2, Final set-up of the TEKUS-module TEM06-42. Drawing (Airbus DS) and photo (M. Meier).

The German TEXUS program begun in 1976 through DLR's Space Agency and uses sounding rockets to achieve microgravity experimental conditions. Following a parabolic trajectory, the payload can reach an altitude of up to 270 km (TEXUS57: about 240km) before parachuting back to Earth and being recovered by helicopter. During the flights, experiments are performed in separate, autonomous modules within the launcher. Data is acquired using telemetry during the flight and upon recovery of the scientific payloads. The tests can be directly controlled and monitored via telecommanding and video transmissions.

After the flight the experiment data will be evaluated. Based on these results it is planned to make a reflight of the TEKUS-module with new parameter settings within a follow-up project to TEKUS.

References

[1] Schütte, A., Wilde, D., Joop, O. (2018) "The TEXUS/MAXUS Transformation - How to Keep Sounding Rockets Versatile and Cost Effective" 69th International Astronautical Congress, 1.-5. Oktober, Bremen (IAC-18.A2.5.5x45013)

[2] Meier, M., Zaussinger, F. (2020) Abschlußbericht Projekt „Konvektion im konzentrischen Spalt (KIKS), 50WM1644, 12. Oktober 2020, TIB Hannover

[3] Meier, M., Szabo, P., Motuz, V., Egbers, C. (2021) Strömungsfeldvisualisierung von thermo-elektro-dynamischer Konvektion mit einer kombinierten PIV- und Schattentechnik" 27. GALA - Fachtagung Experimentelle Strömungsmechanik, 7. - 9. September 2021, Bremen

Aktuelle Forschungsschwerpunkte / Current research topics

C Space Research

C6 Unifying approach for Thermo-Electro-Hydrodynamic in various geometries under microgravity conditions

P. Haun, F. Zaussinger, Ch. Egbers (DLR 50WM2141)

Experiments in Thermo-Electro-Hydrodynamics (TEHD) experiments have long tradition at the LAS. In the last decade more effort to numerical investigations was spend. Since the laboratory experiments are focused on cylindrical geometry and plate capacitors, stability analysis and numerical investigations are made for complex experiments in spherical geometry under microgravity conditions, namely GeoFlow and AtmoFlow [1].

Recently OpenFOAM is utilized for modelling TEHD with the advantage of adaptability to various Geometries. Simulations in 2D meshes with heated Plate and Cylindrical Capacitors showed convection patterns comparable to patterns observed in a cross-section of 3D-GeoFlow Simulations, some examples are given in Figure 1. The key to categorize and parametrize the occurrence of these structures are appropriate dimensionless numbers. But the electrical counterpart of the well-known Rayleigh-Number has no uniform definition. The definition of electric Rayleigh-Number is always specific to the geometry and differs between authors [2] [3].

A new approach tends to lead to more suitable reference values and more general definition of the electric Rayleigh-Number. There are two innovations in making Navier-Stokes equations dimensionless.
First is to consistently distinguish between the reference length d for the flow properties, and the reference length for the electric field d_E. While d can be set as distance between the anode and cathode, d_E. is specific to the electric field, thus specific to the geometry.

Plate	Cylinder	Sphere
$d_E = d;$	$d_E = ln(R_2/R_1)R_2;$	$d_E = \frac{R_2 - R_1}{R_1 R_2} R_1^2$

(a)

(b)

(c)

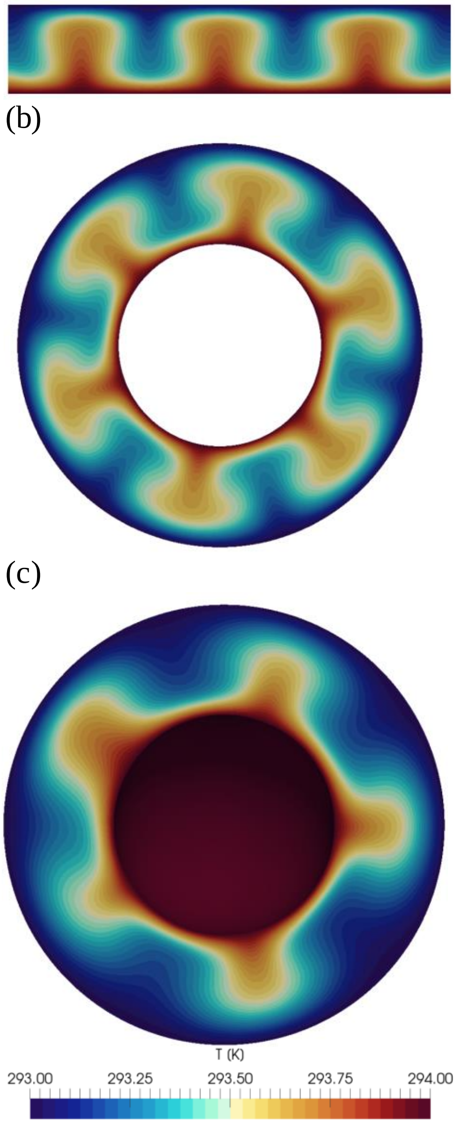

Figure 1 Temperature field of a heated (a) plate capacitor (b) cylindrical Capacitor and (c) cross-section of spherical capacitor (GeoFlow)

This enables the possibility to theoretical investigate boundary quantities. For instance, a boundary layer Rayleigh-number with boundary layer thickness as characteristic length d can be defined, while the characteristic length for the electric field d_E remains the same.
Second, the reference velocity of κ/d does not seems to be characteristic for a developed flow. In boundary layer theory for classical Rayleigh-Benard the characteristic velocity is connected to the fluid motion [4] while κ/d represents a fluid parameter only.
The dimensionless set of equations is:

Aktuelle Forschungsschwerpunkte / Current research topics

$$\rho^*\frac{\partial\vec{u}^*}{\partial t^*} + \rho(\vec{u}^*\cdot\nabla\vec{u}^*) = -\nabla p^* + \frac{\nu}{u_{ref}d}\nabla^2\vec{u}^* + \frac{\nu^2}{u^2{}_{ref}\,d^2}\frac{1}{2}\frac{\epsilon_0\epsilon_r}{\rho_0\nu^2}\frac{d^2}{d_E^2}V_{rms}^2\vec{E}^{2*}\nabla\epsilon_r^*,$$
$$\frac{\partial T^*}{\partial t^*} + (\vec{u}^*\cdot\nabla T^*) = \frac{\kappa}{u_{ref}d}\nabla^2 T^* + \frac{\kappa^2}{u^2{}_{ref}\,d^2}\frac{2\pi f\,\epsilon_0\epsilon_r\,tan\delta\,d^2}{\rho_0 c_p\kappa\Delta T}\frac{d^2}{d_E^2}V_{rms}^2\vec{E}^{2*},$$
$$\nabla\cdot\left(\vec{E}\epsilon\right) = 0,$$

with the electrical Grashof-Number $Gr_E = \frac{1}{2}\frac{\epsilon_0\epsilon_r}{\rho_0\nu^2}\frac{d^2}{d_E^2}V_{rms}^2$ and its critical value Gr_{crit} describing the onset of electrical convection.
The asterisks marking dimensionless quantities e.g., the electric permittivity follows $\epsilon = \epsilon_0\epsilon_r\epsilon_r^*$.

So, direct numerical simulations (DNS) are utilized to calculate the boundary-layer velocity which is the maximum velocity parallel to the anode or cathode respectively. This also defines the boundary layer thickness. Doing this for various applied voltages and temperature differences for bespoken geometries shows a dependence on the experimental parameter (Figure 2) from which a physical relationship can derived, and finally a characteristic velocity u_{ref} can be defined. This will help to estimate the order of magnitude of the individual terms in Momentum and Energy equation in the limit of very high electrical Grashof-Numbers.

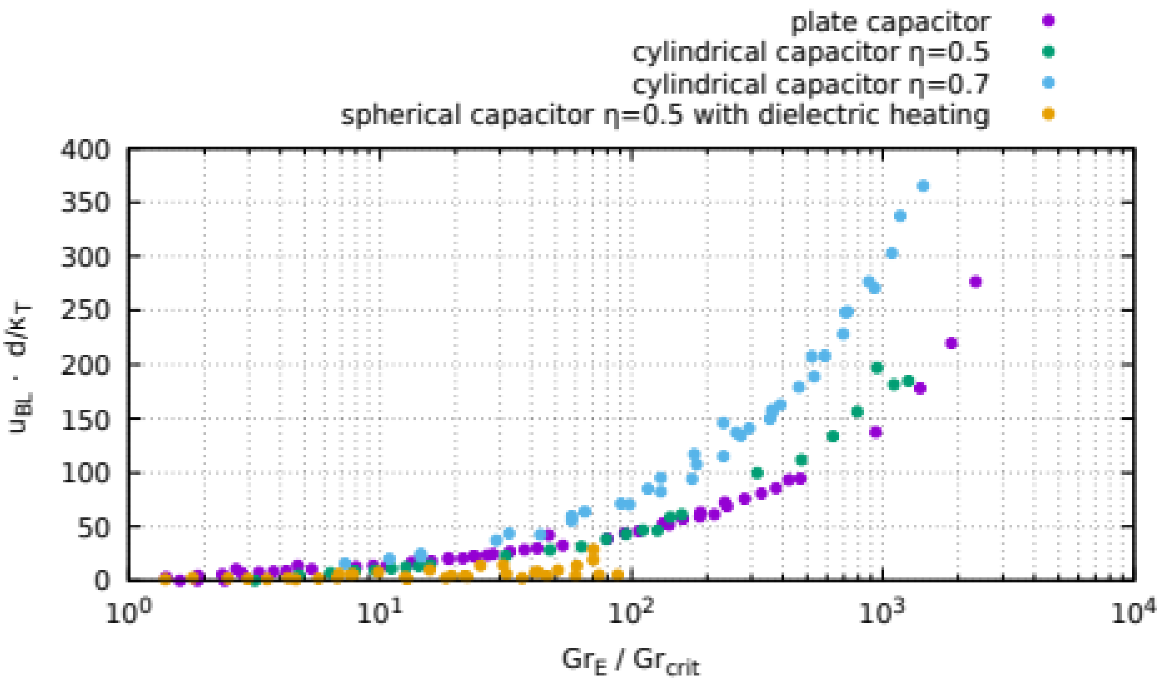

Figure 2 Reference velocity from CFD-data in various geometries plotted over dimensionless electric buoyancy parameter by its critical value concerning the onset of convection.

Aktuelle Forschungsschwerpunkte / Current research topics

C Space Research

C7 AtmoFlow Breadboard experiments under terrestrial gravity (Laboratory) conditions

P. Haun, M. Strangfeld,Y. Gaillard and C. Egbers (DLR 50WM2141)

The AtmoFlow space experiment [1] is making good progress. The partner of technical realization Airbus Defense and Space (ADS) has built the thermal and optical breadboard for testing individual parts of the space experiment under laboratory conditions.
For further testing the thermal breadboard and optical breadboard was made available for the scientists. The combination of these two test facilities leads to a novel experiment with an extraordinary measuring method.
The purpose of this experiment is to calibrate the beam path of a Wollaston shearing interferometry system (WSI) to the spherical shells of AtmoFlow (the thermal breadboard) and its operating temperature ranges. Thus, numerical investigations are made to find a suitable set of parameters, namely applied voltage and temperature difference in which the observable flow structures are made visible and distinguishable. For limiting the parameter space for numerical investigation, non-dimensional numbers were identified. While previous simulations modelled the experiment under microgravity conditions, this study must take the terrestrial gravitational acceleration into account as main contributor to the buoyancy forces. The non-dimensional set of governing equation can be written as

$$\rho^*\frac{\partial \vec{u}^*}{\partial t^*} + \rho^*(\vec{u}^*\cdot\nabla\vec{u}^*) = -\nabla p^* + \frac{1}{\sqrt{Ra\,Pr}}\nabla^2\vec{u}^* + \frac{\Pi_1}{Ra\,Pr}\vec{E}^{2*}\nabla\epsilon_r^* + \frac{1-\rho^*}{\beta\Delta T},$$

$$\frac{\partial \mathrm{T}^*}{\partial t^*} + (\vec{u}^*\cdot\nabla\mathrm{T}^*) = \frac{1}{\sqrt{Ra\,Pr}}\nabla^2 T^* + \frac{\Pi_2}{\sqrt{Ra\,Pr}}\vec{E}^{2*},$$

and the Gauss equation

$$\nabla\cdot\left(\vec{E}\epsilon\right) = 0.$$

The non-dimensional numbers, describing the problem are:

$$\Pi_1 = \frac{1}{2}\frac{\epsilon_0\epsilon_r}{\rho_0\kappa^2}\frac{R_2^2}{R_1^2}V_{rms}^2,$$

$$\Pi_2 = \frac{2\pi \mathrm{f}\,\epsilon_0\epsilon_r\,tan\delta}{\rho_0\kappa\,c_p\,\Delta T}\frac{R_2^2}{R_1^2}V_{rms}^2$$

as electrical parameters and

$$Ra = \frac{\mathrm{g}\beta\Delta\mathrm{T}(\mathrm{R}_2 - \mathrm{R1})^3}{\kappa\nu}$$

for natural convection buoyancy and the Prandtl-Number

$$Pr = \frac{\nu}{\kappa}.$$

The Scope of interest is on the ratios of non-dimensional numbers, scaling the term of the dielectrophoretical acceleration $\vec{f}_{DEP}^* = \vec{E}^{2*}\nabla\epsilon_r^*$. It can be interpreted as a ratio between electrical buoyancy and terrestrial buoyancy. With these ratios of non-dimensional numbers, a first guess of an appropriate parameter space for the laboratory experiments was build.

In the next step a grid study was made for a 3D-CFD with the extension made for OpenFOAM which is also used for the investigations of the AtmoFlow space experiments, including gravitational acceleration. The grid study showed that the computational effort of is huge. Nevertheless, Simulations with reduced resolutions where made, in order to get an indication of the expected flow structures. This should be sufficient because only global structures are of interest for this study.
First runs show very promising results. At least three different regimes can be identified.

Aktuelle Forschungsschwerpunkte / Current research topics

(a)
$$\Pi_1 = 1.3 \times 10^8$$
$$\Pi_2 = 111$$
$$\frac{\Pi_1}{Ra\,Pr} = 2$$

(b)
$$\Pi_1 = 3 \times 10^8$$
$$\Pi_2 = 11$$
$$\frac{\Pi_1}{Ra\,Pr} = 52$$

(c)
$$\Pi_1 = 8 \times 10^8$$
$$\Pi_2 = 43$$
$$\frac{\Pi_1}{Ra\,Pr} = 20$$

Figure 1 radially averaged magnitude of temperature gradient for three different regimes in 3D spherical shell CFD.

Figure 1 is showing the radial averaged temperature gradient projected on the outer spherical shell. The vector of terrestrial gravity is pointing downwards, the dark spot in the middle of the upper sphere is the result of the cooled copper insert in the boundary of the outer shell, representing the north pole. This representation is meant to be comparable with pictures captured by the WSI-system. An optimal calibrated WSI-system is expected to deliver similar pictures. In Figure 1 (a) the influence of the electric force is not high enough to disturb the basic flow within the field of view. There are waves travelling upwards to the pole region but they are hardly visible in this presentation, that means they will not likely to be observable within the laboratory experiment or hardly distinguishable from distortions in the optical path. Due to the gravitational acceleration the observed structures are chaotic, turbulent in all cases, but their density of occurrence rises with the dimensionless Parameter Π_1. The small dots in Figure 1 (c) and more clearly visible in Figure 1 (b) corresponding to streams of cold fluid moving from the outer shell to the heated inner sphere. In addition to that they are moving down, towards the equatorial zone of the sphere. The speed of these falling plumes also increases with rising electrical parameter Π_1.

All in all, we have shown, that there are at least three completely different regimes to be expected within the adjustable parameter range, which can be clearly distinguished from possible artefacts. We are looking forward to comparing the results with the experiment in 2022.

References

[1] Zaussinger, F., Canfield, P., Froitzheim, A., Travnikov, V., Haun, P., Meier, M., Meyer, A., Heintzmann, P., Driebe, T., Egbers, Ch., 2019. AtmoFlow - Investigation of Atmospheric-Like Fluid Flows Under Microgravity Conditions. Microgravity Sci. Technol. 31, 569–587. https://doi.org/10.1007/s12217-019-09717-7

Aktuelle Forschungsschwerpunkte / Current research topics

C Space Research

C8 AtmoFlow – Numerical investigation of convective flow in the atmosphere utilizing thermo-electrohydrodynamics – A comparison between linear stability and FEM analysis.

P.S.B. Szabo, C. Egbers (DLR 50WM2141)

Model of our atmosphere become more and more important not only form a metrological or climate point of view but also from a global perspective to understand the fundamentals of large-scale motion of planetary waves. These waves transport a large amount of energy and are crucial for a planet's atmosphere. This study investigates such large-scale motions in a militarized model that is aligned to the AtmoFlow experiment. The AtmoFlow experiment is a spherical shell that mimics a planet at a small scale where terrestrial gravity is artificially induced by an equivalent electric central force field. A description of the boundary system is given in Figure 1. As can be seen this small model can rotate synchronized or differentially by moving the inner and outer boundaries to simulated planetary rotation. Analogous to a real planet the poles are cooled and the equator heated. A dielectric fluid is used that is sensitive to electric fields and temperature to induce convection similar to a terrestrial buoyancy. As the fluid is sensitive to the temperate-dependent density, the spherical shell experiments are performed in free space and thus the experiment is planned to be operated on the Inter- national Space Station (ISS) after 2024.

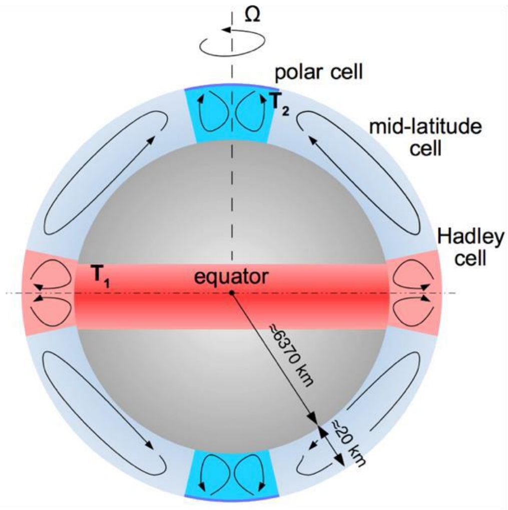

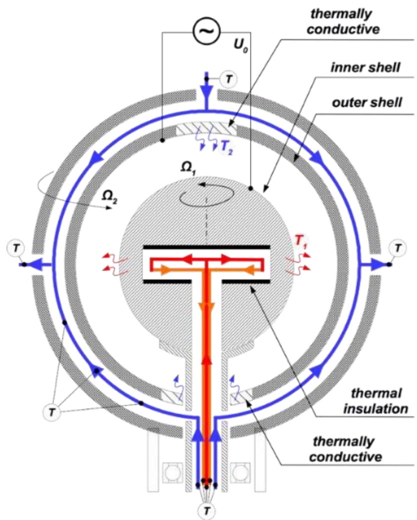

Figure 1: (left) simplified planetary atmosphere as found on the Earth. Not to scale. (right) vertical cut through the AtmoFlow experiment. Blue lines depict the cooling loop, red lines show the heating circuit. Inner and outer rotation is labeled by Ω_1 and Ω_2, respectively. The maximum temperature is found at the equator, the minimum temperature at the poles.

To investigate the ability of the experiment model a stability analysis was performed by Travnikov and Egbers [1] to locate the stability curve that separates the axisymmetric basic flow from more complex three-dimensional flow. This study aimed to provide a suitable parameter space that is used for the experiment model. To provide a comparable benchmark the experiment system is modeled with different codes based on the finite volume method (FVM) and finite element method (FEM). While the FEM model currently focuses on the experimental model, the FEM model uses the ideal boundary conditions suggested in [1].

In the FEM study we show in Figure 2 temperature and velocity fields for two cases studied by which corresponds to the expected physical model in Figure 1.

Aktuelle Forschungsschwerpunkte / Current research topics

In addition, a comparison of the linear stability analysis is possible with the conduced numerical investigation which shows corresponding results that are in qualitative agreement.

$Ta = 10^3$ $Ra_E = 38000$ | $Ta = 10^3$ $Ra_E = 2 \cdot 10^5$

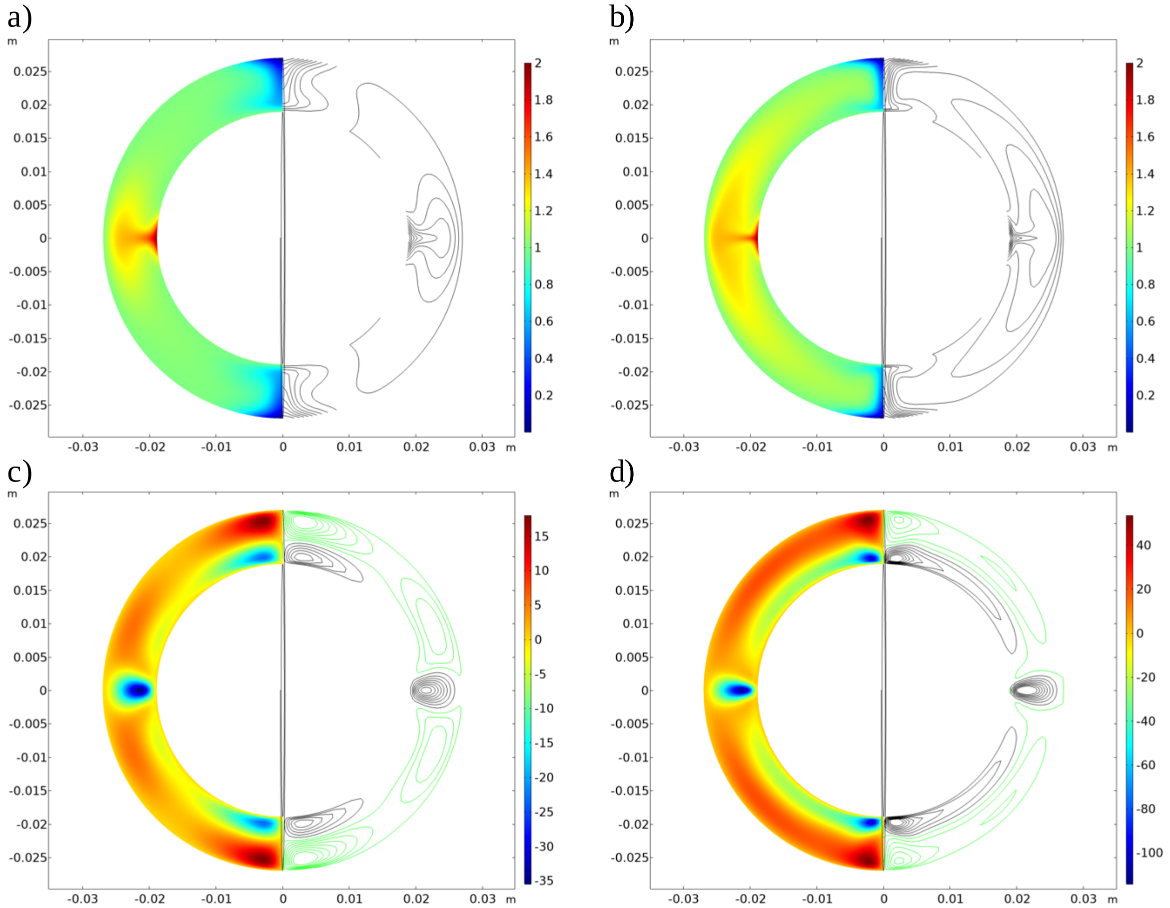

Figure 2: Basic flow for two different electric Rayleigh numbers at a fixed Taylor number. The top panel shows the temperature distribution whereas the velocity in azimuthal direction is shown bottom panel. The temperature counters are for (a) and (b) T_2 (20) and the velocity counters are (c) 14 (2) -35 (5) and (d) 50 (5), -80 (10).

The results reveal flow structures from equatorial region to poleward regions that are axisymmetric presenting the basic flow for two different Rayleigh numbers at a fixed Taylor number of 10^3.
The FEM results may be utilized as a benchmark to compare both numerical models the FVM and linear stability analysis and the experiment itself. For this purpose, further studies are computed in the non-axisymmetric regime to be able investigate a simplified atmospheric model rather than thermo-electrohydrodynamic convection in a spherical shell. The aim is to investigate higher electric Raileigh numbers to observe the desired mid-latitude cells or polar cells that transport a large amount of energy on planetary atmospheres e.g., on Earth.

References

[1] V. Travnikov and C. Egbers, Numerical investigation of atmospherelike flows in a spherical geometry, Physical Review E, 104, 065110 (2021).

C Space Research

C9 AtmoFlow – Numerical investigation of convective flow in the atmosphere utilizing thermo-electrohydrodynamic – A 2D FVM analysis.

Y. Gaillard, P.S.B. Szabo, P. Haun, C. Egbers (DLR 50WM2141)

The AtmoFlow project deals with a spherical gap geometry that aims to investigate fluid flow of atmospheric systems such as planetary atmospheres or interiors by utilizing thermo-electrohydrodynamics (TEHD). The experiment is built by Airbus Defense and Space and placed on the ISS after 2024. Here, we numerically investigate this particular experimental setup via computational simulations. These simulations consider the complex geometry around the shaft and the combination of fluid and solid regions to enable non-ideal boundary conditions that are present in the physical system [1]. To solve the numerical system and to include the necessary physical environments that must be couple such as fluid flow, heat transfer, electromagnetic fields and rotation the OpenFOAM platform is used to implement customized solvers for the TEHD equations. All the simulations are performed in the absence of turbulent models resulting in direct numerical simulation that increase the computational effort [2, 3].
For a first iteration the complex geometry of AtmoFlow is simplified in a 2-dimensiaonal (2D) simulation. For this the spherical structure of the AtmoFlow experiment is sliced at the equator resulting in a 2D cylinder as shown in Figure 1. The boundary conditions of the fluid are set as ideal constant Dirichlet boundary condition, where the hotter temperature is at the tangent cylinder and the cooler temperature at the outer cylinder, see right panel of Figure 1. For the simulation campaign the rotation is restricted to solid body rotation. To ensure accurate result a grid study was performed that is also used as an indication of how may cells are of need for a 3-dimensional consideration in future studies.

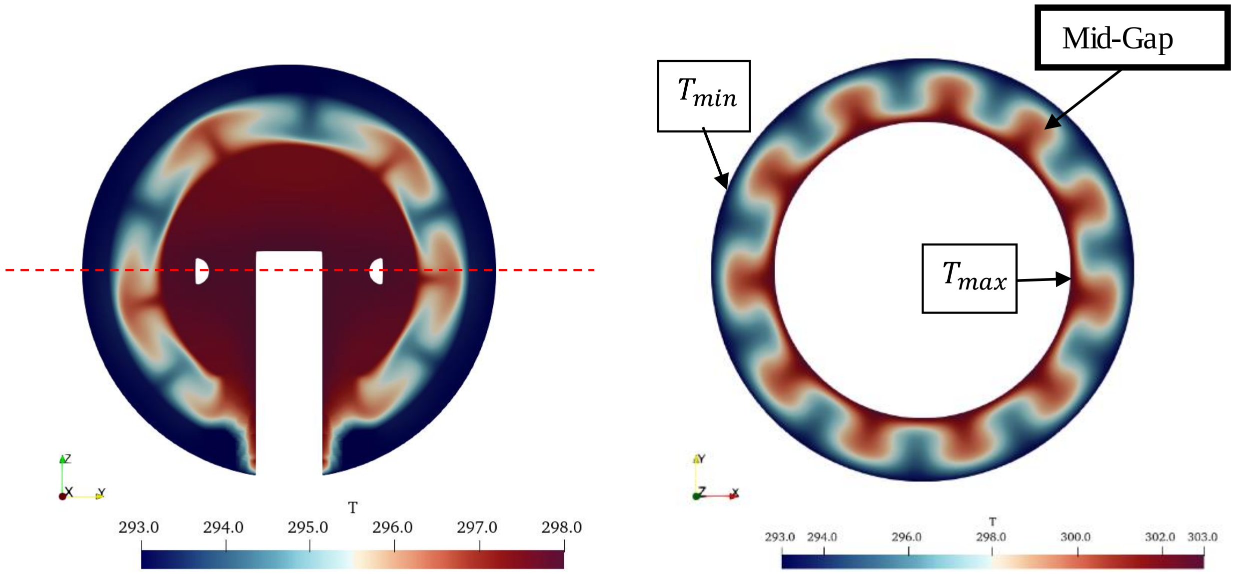

Figure 1: Temperature contour of the AtmoFlow numerical twin simulation including solid and fluid regions (left panel). The red dotted line marks the slice for the resulting 2D cylinder cut that is investigated in this study. Temperature contour of the 2D cylinder at T=10[K] V=600.8[V] and ω=0.1[Hz] (right panel).

Aktuelle Forschungsschwerpunkte / Current research topics

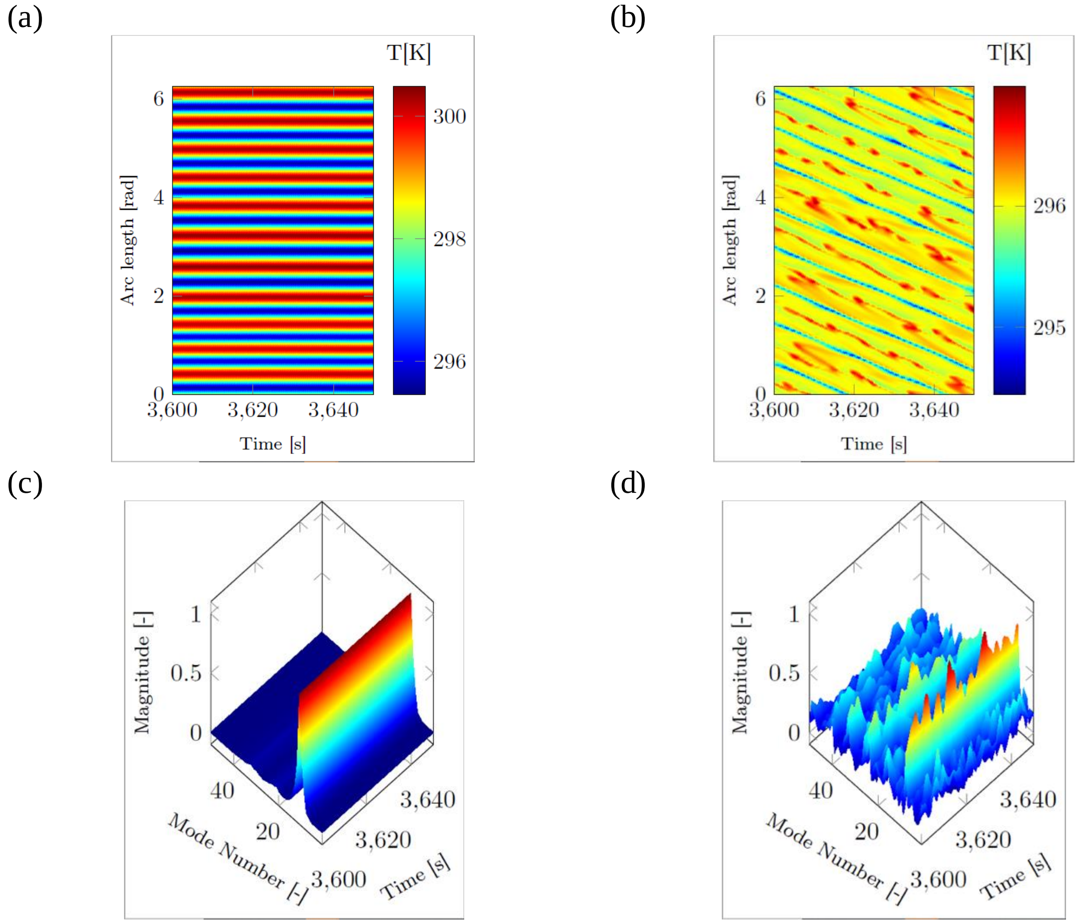

Figure 2: (top) contours of Hovmöller diagrams along the mid-gap of the 2D cylinder for two set of parameter. (bottom) surface of normalized spatial FFT along the mid-gap of the 2D cylinder taking in account the evolution over time.

By varying the temperature, voltage and rotation speed one obtains different flow regimes, see Figure 1 right panel that can be classified usually at the mid-gap of the system. Figure 2 (a) and (b) show a time resolved temperature of the modes observed by using a Hovmöller diagram. The cases presented are for temperature differences $\Delta T = 10$ K and 5 K, voltage V=600.8 V and 6008 V with a rotation of frequency $\omega = 0.1$ Hz and 1 Hz, respectively. Both temperature plots show a certain mode distribution that varies form stationary modes to irregular modes when the Rayleigh number is increased. To classify the mode number a spatial fast Fourier transformation is used. The FFT is processed for several timesteps to ensure a time independent investigation as shown in Figure 2 (c) and (d).
The results suggest further investigations of the stability of the modes and their nature to generate a regime diagram for the AtmoFlow project.

References

[1] F. Zaussinger, Florian, P. Canfield, A. Froitzheim, V. Travnikov, P. Haun, M. Meier, A. Meyer, A. P. Heintzmann,, T. Driebe, C. Egbers, AtmoFlow - Investigation of Atmospheric-Like Fluid Flows Under Microgravity Conditions. Microgravity Science and Technology. 31. (2019).
[2] V. Travnikov and C. Egbers, Numerical investigation of atmosphere like flows in a spherical geometry, Physical Review E, 104, 065110 (2021).
[3] F. Zaussinger, P. Haun, P.S.B. Szabo, V. Travnikov, M. Al. Kawwas, C. Egbers, Rotating spherical gap convection in the GeoFlow International Space Station (ISS) experiment Physical Review Fluids 5 (6), 063502 (2021)

Aktuelle Forschungsschwerpunkte / Current research topics

C Space Research

C10 Numerical investigation of the atmosphere-like flows in the spherical geometry

V. Travnikov, C. Egbers (DFG, 439798763)

Buoyancy-driven convective flows play a crucial role in geophysics and meteorology for global heat and momentum transport. Simplified planetary and stellar atmospheres (Figure 1 left) can be described by a spherical gap geometry with special boundary conditions (Figure 1 right).

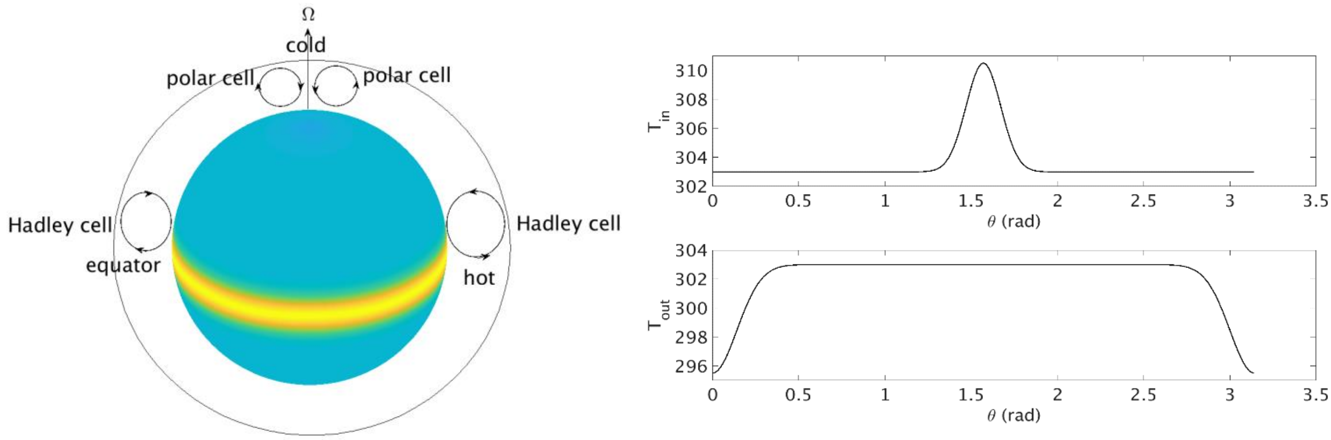

Figure 1: (left) simplified planetary atmosphere as found on the Earth. Not to scale. (right) Boundary conditions for the temperature on the inner and outer surfaces. The maximum temperature is found at the equator, the minimum temperature at the poles.

Besides, radial gravitational acceleration and rotational effects have to be taken into account. The dielectrophoretic effect is used in the spherical gap to synthesize the radial gravity field and causes a convective flow described due to the electrical Rayleigh number $\mathrm{Ra_E} = \frac{2\varepsilon_0\varepsilon_r\gamma}{\rho\upsilon k}\mathrm{V_{rms}^2}\Delta\mathrm{T}$, where $\Delta\mathrm{T} = (\mathrm{T_{equator}} - \mathrm{T_{pole}})/2, \mathrm{V_{rms}}$ is the applied voltage between surfaces.

The influence of the Coriolis and centrifugal forces should be taken into account in terms of the Taylor number $Ta = \left(\frac{2\Omega d^2}{\upsilon}\right)^2$, d is the gap width. Additionally, lateral thermal boundary conditions are used to model the solar radiation at the equator and the poles. The temperature has a maximum value on the equator and becomes colder near the poles. Due to the temperature dependence on the polar angle θ, the basic flow occurs that has to be calculated. First, we performed the classification of the two-dimensional axisymmetric basic flow [1]. Secondly, linear stability theory is used in investigating the stability of the basic flow (Figures 2 and 3). The main results of this investigation are:

- The range in which the flow is stable to infinitesimal perturbations, bounded by the intervals $(0, \mathrm{Ta_c})$, $(0, \mathrm{Ra_{Ec}})$ and the stability curve.
- The basic flow becomes unstable regarding non-axisymmetric perturbations.
- Equatorially symmetric and equatorially antisymmetric perturbations are responsible for the instability.
- In all cases considered, the instability sets in as an oscillating bifurcation.

Aktuelle Forschungsschwerpunkte / Current research topics

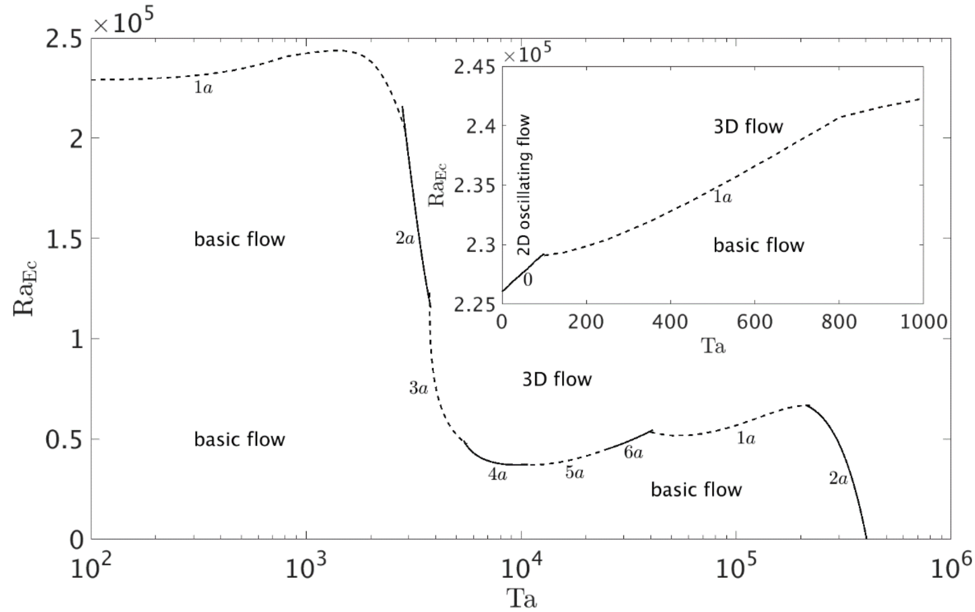

Figure 2: Ra_{Ec} vs. Ta for $\eta = 0.7$. The numbers in the vicinity of the stability curves are the critical azimuthal wave numbers m_c.

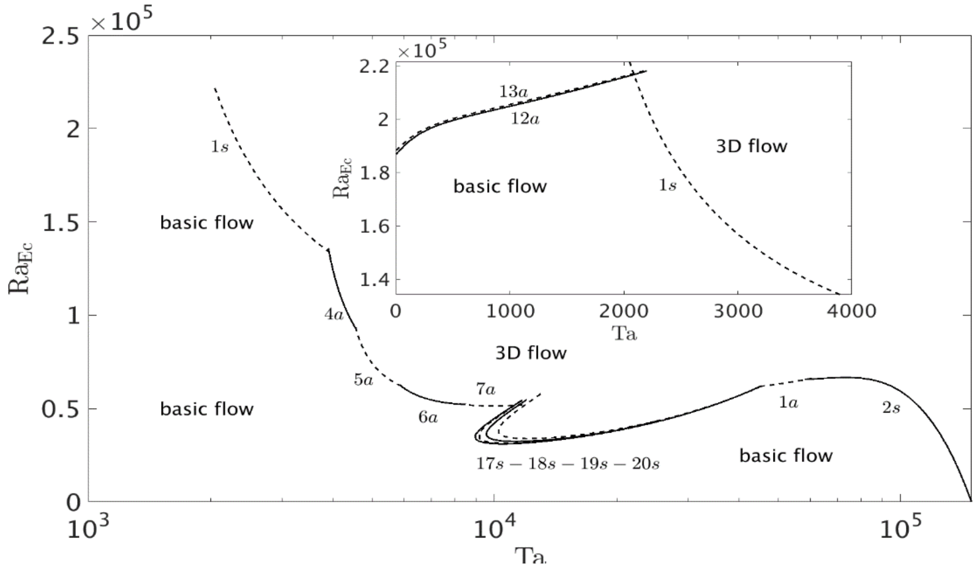

Figure 3: Ra_{Ec} vs. Ta for $\eta = 0.8$. The numbers in the vicinity of the stability curves are the critical azimuthal wave numbers m_c.

The three-dimensional flows were calculated using a 3D pseudo-spectral numerical code developed by R. Hollerbach [4]. Some examples of these flows can be found in [1, 2, 3].

References

[1] V. Travnikov, C. Egbers, Numerical investigation of atmosphere-like flows in a spherical geometry, Phys. Rev. E 104, 065110 (2021)
[2.] V. Travnikov, F. Zaussinger, P. Haun, and C. Egbers, Influence of dielectrical heating on convective flow in a radial force field, Phys. Rev. E 101, 053106 (2020)
[3] F. Zaussinger, P. Haun, P. Szabo, V. Travnikov, M. Kawwas, and C. Egbers, Rotating spherical gap convection in the GeoFlow International Space Station (ISS) experiment, Phys. Rev. Fluids 5, 063502 (2020)
[4] R. Hollerbach, A spectral solution of the magneto-convection equations in spherical geometry, Int. J. Num. Met. Fluids, 32, 773-797 (2000)

C Space Research

C11 Using Wollaston shearing interferometry to investigate convective pattern in an electrical central force field of a differentially heated annulus.

P.S.B. Szabo, A.O. Erdogdu, R. Carter, B. Schulze, M.-E. Gevrek, M. Meier, C. Egbers (DLR 50WM2141)

Convection in dielectric fluids exhibit a novel possibility as such fluids are not only sensitive to temperature differences in the density but also possess a large temperate variation in the electric permittivity. Thus, convection may also be induced in a non-isothermal dielectric fluid in the presence of an electric field. The arising convection is known as thermo-electrohydrodynamic (TEHD) convection. Here, we investigate TEHD convection in a differentially heated annulus with boundary conditions shown in Figure 1. The annulus is heated at the inner cylinder and cooled at the outer cylinder whereas all remaining boundaries are thermally insulated but kept optical accessible to be able to recorded evolving convective patterns. The measurement technique used is an interferometry system based on a Wollaston prism. The principle of the measurement technique is based on interfering conjugated light beams that also pass the test section beam. Thus, the system is referred to a shearing interferometry the so-called Wollaston shearing interferometry (WSI). The particular setup of the interferometry unit is given in Figure 2 and full description of the WSI system and operation ability is found in [1].

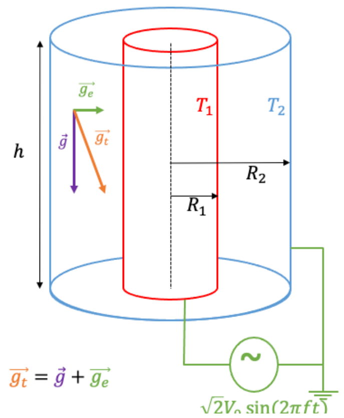

Figure 1: Boundary conditions of experiment system.

With the particular setup the configuration is similar to Seelig et al. [2] that investigated the same experiment cell with a height of 100 mm using particle image velocimetry and a shadowgraph system. The purpose of the system was to investigate convective pattern formation in a radial electric force field and their structure development when the fluid was

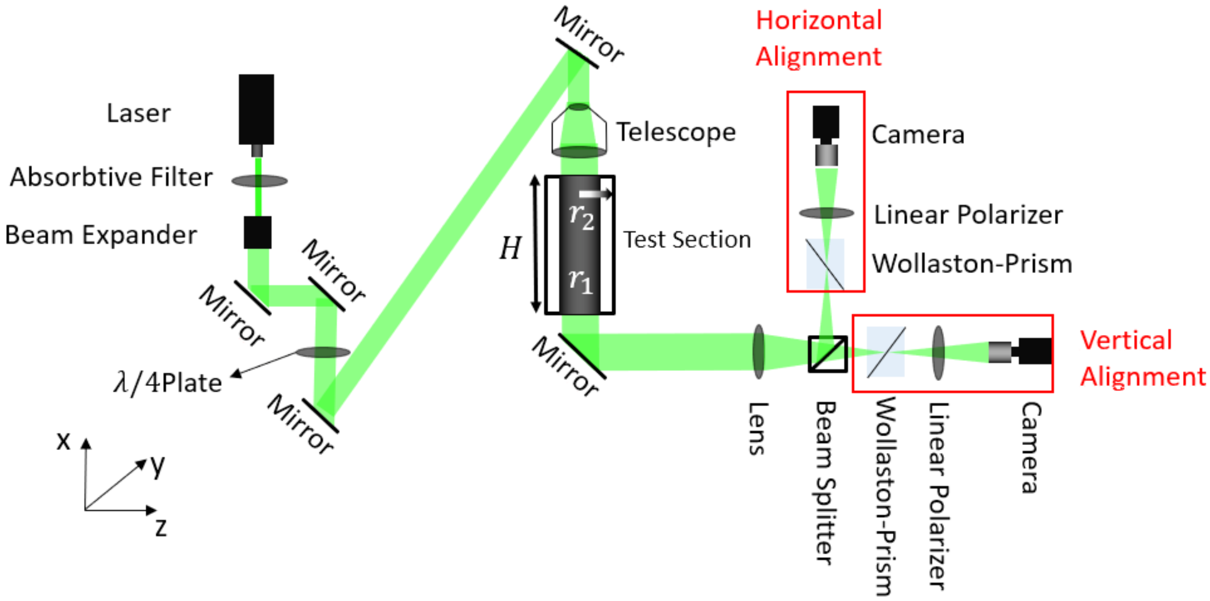

Figure 2: Schematics of the Wollaston shearing interferometry and setup of the test section.

Aktuelle Forschungsschwerpunkte / Current research topics

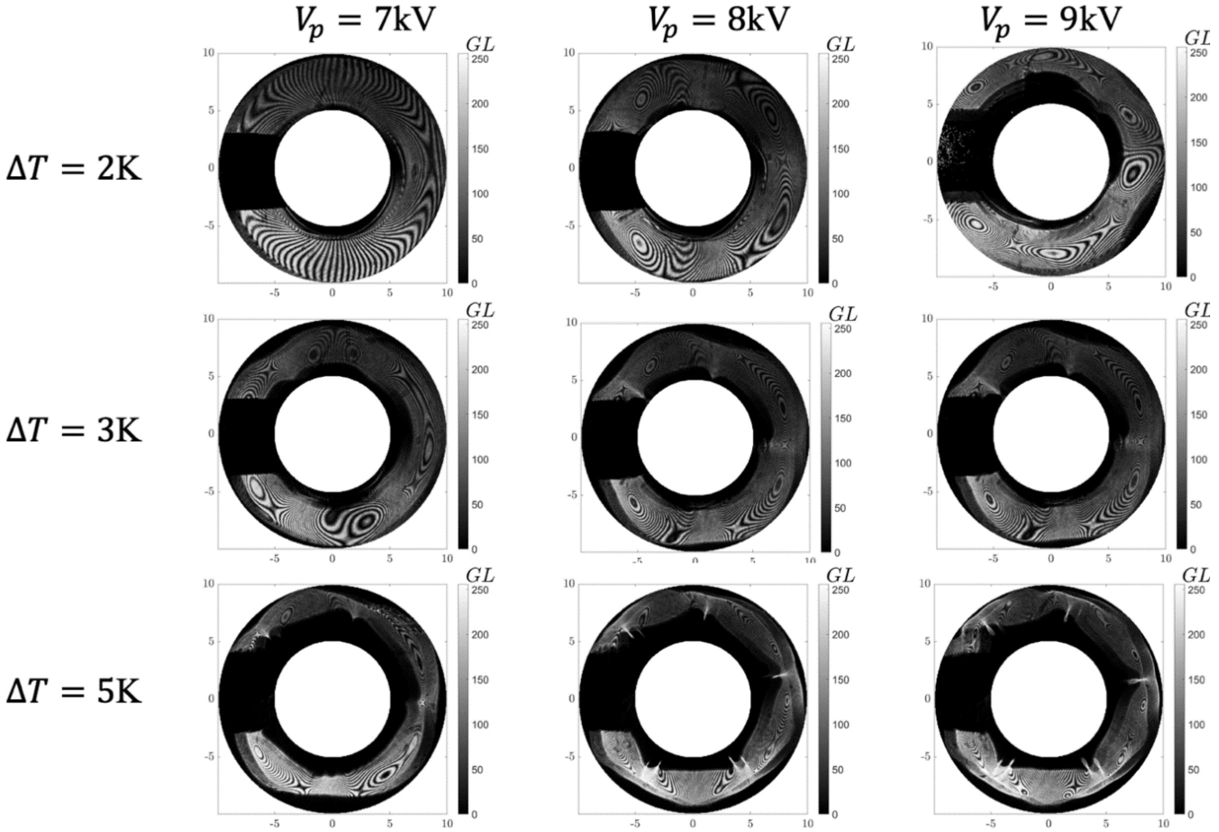

Figure 3: Interferograms of convective TEHD-development to visualise azimuthal modes for a set of three different electric field strength and three temperature differences with B5 as a working fluid.

subjected to a set of three different electric field stretch and three temperature differences. In the present study we repeated this particular experiment, however we use the above introduced WSI system to get a better spatial resolution of the temperature distribution that is proportional to the measured refractive index. Figure 3 shows a small selection of the conducted experiments. It is clearly visible that an onset of TEHD convection in azimuthal direction is observed for temperature differences above 5 K and a peak voltage of 7 kV. For smaller temperature differences a higher electric tension is of need to induce the azimuthal modes. The plots indicate that the mode number increase with electric tension and temperature difference with observed mode numbers of 4 to 6. The ability of the spatial resolved fringes that related to the refractive index, the focal length of the lens into the Wollaston prism may be utilised to recover the local temperature distribution in a 2-dimensional projection of the 3-dimensional temperature distribution in the experiment cell. The WSI system may therefore provide a better resolution of the refractive index distribution as e.g. the shadowgraph technique. Thus, the spatial fringe distance can be transferred to the local density distribution and thus to temperature. The results can provide an indication of how effective heat transfer is induced by TEHD-convection when observing the evolving convective patterns.

References

[1] A. O. Erdogdu, P.S.B. Szabo, R. Carter, M.-E. Gevrek, P. Haun, F. Zaussinger, B. Schulze, M. Meier, C. Egbers, Utilizing Wollaston Shearing Interferometry to investigate the double component density gradient in a differentially heated annulus, in: Experimentelle Strömungsmechanik: 28. Fachtagung, German Association for Laser Anemometry GALA e.V., Bremen, 7–9 September, 19.1–19.8 (2021).

[2] T. Seelig, A. Meyer, P. Gerstner, M. Meier, M. Jongmanns, M. Baumann, V. Heuveline, C. Egbers, Dielectrophoretic force-driven convection in annular geometry under Earth's gravity. International Journal of Heat and Mass Transfer, 139, 386-398 (2019).

Veröffentlichungen, Konferenzbeiträge und Vorträge/ Publications, contributions to conferences and invited lectures

Veröffentlichungen in reviewten Zeitschriften 2020

H. N. Yoshikawa, Ch. Kang, I. Mutabazi, F. Zaussinger, P. Haun, Ch. Egbers, 2020,
Thermoelectrohydrodynamic convection in parallel plate capacitors under dielectric heating conditions, Phys. Rev. Fluids **5**, 113503, DOI: 10.1103/PhysRevFluids.5.113503

W. Xu, U. Harlander, 2020,
Inertial mode interactions in a rotating tilted cylindrical annulus with free surface, Phys. Rev. Fluids **5**, 094801, DOI: 10.1103/PhysRevFluids.5.094801

G. Meletti, S. Abide, S. Viazzo, A. Krebs & U. Harlander, 2020,
Experiments and long-term high-performance computations on amplitude modulations of strato-rotational flows, Geophysical & Astrophysical Fluid Dynamics, 115:3, 297-321,
DOI: 10.1080/03091929.2020.1795647

Le Gal, P., Harlander, U., Borcia, I., Le Dizès, S., Chen, J., Favier, B., 2020,
Instability of vertically stratified horizontal plane Poiseuille flow, J. Fluid Mech., 907, R1,
doi:10.1017/jfm.2020.917

C. Rodda, U. Harlander, 2020
Transition from Geostrophic Flows to Inertia–Gravity Waves in the Spectrum of a Differentially Heated Rotating Annulus Experiment, Journal of the Atmospheric Sciences 77(8):2793-2806, DOI: 10.1175/JAS-D-20-0033.1

F. Zaussinger, P. Haun, P. Szabo, V. Travnikov, M. Alkawwas, C. Egbers, 2020,
Rotating spherical gap convection in the GeoFlow International Space Station (ISS) experiment, Phys. Rev. E 101, 05310, 063502 (June, 19 2020), DOI: 10.1103/PhysRevFluids.5.063502

V. Travnikov, F. Zaussinger, P. Haun, C. Egbers, 2020,
Influence of dielectrical heating on convective flow in a radial force field, Phys. Rev. E 101, 053106 (2020), DOI: 10.1103/PhysRevE.101.053106

G. Hasanuzzaman, S. Merbold, C. Cuvier, V. Motuz, J.-M. Foucaut & Ch. Egbers, 2020,
Experimental investigation of turbulent boundary layers at high Reynolds number with uniform blowing, part I: statistics, Journal of Turbulence, ISSN: (Print) 1468-524, Taylor & Francis

M. V. Kurgansky, T. Seelig, M. Klein, A. Will & U. Harlander, 2020
Mean flow generation due to longitudinal librations of sidewalls of a rotating annulus, Geophysical & Astrophysical Fluid Dynamics, ISSN: 0309-1929 (Print) 1029-0419 (Online), Taylor & Francis

V. Travnikov, Ch. Egbers, 2020,
Linear stability analysis of the convective flow in a spherical gap with rotating inner surface, Int. Journal of Heat and Mass Transfer, Elsevier Verlag, ISSN: 0017-9310

Veröffentlichungen, Konferenzbeiträge und Vorträge/ Publications, contributions to conferences and invited lectures

Veröffentlichungen in reviewten Zeitschriften 2021

E.-S. Zanoun, Ch. Egbers, Y. Dewidar, 2021,
Two-Point Velocity Correlations in Fully Developed Turbulent Pipe Flow at Shear Reynolds Number of $Re_{\tau} \approx 4000$, PAMM, Volume 20, Issue 1, Wiley-VCH GmbH, ISSN: 1617-7061, DOI: 10.1002/pamm.202000330

Z. Hallol, S. Merbold, Ch. Egbers, 2021,
Contribution of Large and Very Large Scale Motions to the Turbulent Kinetic energy in Turbulent Pipe Flow, PAMM, Volume 20, Issue 1, Wiley-VCH GmbH, ISSN: 1617-7061, DOI: 10.1002/pamm.202000330

St. Richter, E.-S. Zanoun, Ch. Egbers, 2021,
Investigation of Large Scale Motion Interaction with the Near-Wall Turbulence, PAMM, Volume 20, Issue 1, 91st Annual Meeting of the International Association of Applied Mathematics and Mechanics (GAMM), Wiley-VCH GmbH, ISSN: 1617-7061, DOI: 10.1002/pamm.202000330

E.-S. Zanoun, C. Egbers, H. Nagib, F. Durst, G. Bellani, A. Talamelli, 2021,
Wall friction relations in wall-bounded shear flows, European Journal of Mechanics - B/Fluids, Volume 89, September–October 2021, Pages 171-179

U. Harlander, M. Kurgansky, 2021,
Two-dimensional internal gravity wave beam instability. Linear theory and subcritical instability Geophysical and Astrophysical Fluid Dynamics, August 2021,
DOI: 10.1080/03091929.2021.1943379

P. S. B. Szabo, M. Meier, A. Meyer, E. Barry, V. Motuz, I. Mutabazi, Ch. Egbers, 2021,
PIV and shadowgraph measurements of thermo-electrohydrodynamic convection in a horizontal aligned differentially heated annulus at different gravity conditions, Experimental Thermal and Fluid Scienc, Elsevier Inc. 2021, DOI: 10.1016/j.euromechflu.2021.03.007

E. Johnston, P. S. B. Szabo, N. S. Bennett, 2021,
Cooling silicon photovoltaic cells using finned heat sinks and the effect of inclination angle, Thermal Science and Engineering Progress 23, 100902,

Vincze, M., Bozóki, T., Herein, M., Borcia, I., D., Harlander, U., Horicsányi, A., Nyerges, A., Rodda, C., Pál, A., Pálfy, J., 2021, The Drake Passage opening from an experimental fluid dynamics point of view. *Sci Rep* **11,** 19951 (2021).

G. Hasanuzzaman, S. Merbold,;,V. Motuz, Ch. Egbers, 2021,
Enhanced outer peaks in turbulent boundary layer using uniform blowing at moderate Reynolds number, Journal: Journal of Turbulence (TJOT), https://doi.org/10.1080/14685248.2021.2014058

Szabo, P. S. B., Meyer A., Meier, M., Motuz, V., Sliavin, Y., Egbers, C. “Simultaneous PIV and shadowgraph measurements of thermo-electrohydrodynamic convection in a differentially heated annulus”, Technisches Messen, published online December 21 (2021) https://doi.org/10.1515/teme-2021-0120

Veröffentlichungen, Konferenzbeiträge und Vorträge/ Publications, contributions to conferences and invited lectures

Veröffentlichungen in Büchern 2020/2021

A.O. Erdogdu, P.S.B. Szabo, R. Carter , M.-E. Gevre, P. Haun, F. Zaussinger B. Schulze, M. Meier, Ch. Egbers, Utilizing Wollaston shearing interferometry to investigate the refractive index gradient in a differentially heated annulus, Fachtagung "Experimentelle Strömungsmechanik", Universität Bremen, 2021, ISBN 978-3-9816764-7-1

M. Meier, P.S.B. Szabo, V. Motuz, Ch. Egbers, Flow field visualisation of thermo-electrodynamic convection utilising a combined PIV and Shadowgraph technique, Fachtagung "Experimentelle Strömungsmechanik", Universität Bremen, ISBN 978-3-9816764-7-1

Meier, M., Zaussinger, F. (2020) Abschlußbericht Projekt „Konvektion im konzentrischen Spalt (KIKS)", 50WM1644, 12. Oktober 2020, TIB Hannover

Veröffentlichungen, Konferenzbeiträge und Vorträge/ Publications, contributions to conferences and invited lectures

Veröffentlichungen in Tagungsbänden und Vorträge / Poster 2020/2021

P. Szabo, F. Zaussinger, P. Haun, V. Travnikov, M. Meier, Ch. Egbers, 2020,
Complementary numerical and experimental study in the baroclinic annulus for the microgravity experiment AtmoFlow, EGU General Assembly, EGU2020-20956, 4–8 May 2020

C. Rodda, U. Harlander, C. Savaro, A. Campagne, M. Calpe Linares, P. Augier, J. Sommeria, T. Valran, S. Viboud and N. Mordant, 2021,
Can Laboratory experiments help to explain the atmosphere and ocean's energetics?
Colaborative Research Center TRR 181, Energy transfers in Atmosphere and Oceans, 16th - 18th Mar. 2021, Universität Hamburg, Center for Earth System Research and Sustainability (CEN)

Z. Hallol, M. Yousry, S. Merbold, Ch. Egbers, 2021,
Time-resolved PIV measurements in fully developed turbulent pipe flow, 25th International Congress of Theoretical and Applied Mechanics Milan (Italy), 22-27 August 2021,
ISBN 978-83-65550-31-6

Meier, M., Meyer, A., Gerstner, P. Heuveline, H., Egbers, C.: Laboratory experiments on thermo-electro-hydrodynamic Convection, Int. Couette-Taylor Workshop (online, University of Twente, NL) 5.-9. July 2021

Master-, Bachelorarbeiten, Dissertationen, Habilitationen
Examinations, theses and habilitations

Dissertationen,

Gabriel Maltese Meletti de Oliveira
High-performance computing and laboratory experiments on strato-rotational instabilities,
Dissertationsschrift BTU Cottbus-Senftenberg, 2020,
https://opus4.kobv.de/opus4-btu/frontdoor/index/index/docId/5440

Wenchao Xu,
Experiments on nonlinear waves in homogeneous flows with free upper surface and time-dependent forcing
Dissertationsschrift BTU Cottbus-Senftenberg, 2020,
https://opus4.kobv.de/opus4-btu/frontdoor/index/index/docId/5386

Gazi Hasanuzzaman,
Experimental Investigation of Turbulent Boundary Layer with Uniform Blowing at Moderate and High Reynolds Number
Dissertationsschrift BTU Cottbus-Senftenberg, 2021

Mohamed Yousry,
On the influence of flow behaviorover structured surfaces,
Dissertationsschrift BTU Cottbus-Senftenberg, 2021

Zeinab Hallol
Behaviour of energetic coherent structures in turbulent pipe flow at high Reynolds numbers, Ph.D. thesis, Brandenburg University of Technology Cottbus-Senftenberg, Cuvillier Verlag, ISBN: 978-3-7369-7501-9, 2021

Habilitationen

Dr. rer. nat. Florian Zaussinger, 2021,
Modeling and Simulation of Thermo-Electro Hydrodynamics,
Habilitationsschrift BTU Cottbus-Senftenberg

Dr.Ing. Thomas Geyer, 2021,
Experimental Investigation of Methods for Cylinder Vortex Shedding Noise Reduction,
Habilitationsschrift BTU Cottbus-Senftenberg

Master-, Bachelorarbeiten, Dissertationen, Habilitationen
Examinations, theses and habilitations

Masterarbeiten (2020/2021)

M.Sc. Yasser Dewidar, 2021,
Two-Point Velocity Measurements in Pipe Flow at High Reynolds Numbers

Bachelorarbeiten (2020/2021)

B.Sc. Paul Abromeit, 2020,
Numerische Untersuchung zur Beeinflussung der Fahrbahngrenzschicht im Windkanal durch Mikroausblasen.

B.Sc Tark Raj Bista, 2020,
Mechanische Neukonstruktion eines Parabelflugexperimentaufbaus für thermoelektrische Untersuchungen.

B.Sc. Mert Edin Gevrek, 2021
Interferometriemessung der Temperaturverteilung in einem Zylinderspalt.

B.Sc. Oguzhan Bölük, 2021,
Untersuchung zur TEHD-Konvektion in einem Plattenspalt.

B.Sc. Robert William Kessler, 2021,
Charakterisierung der Strömung in der Messstrecke des LAS-Windkanals.

Anfahrt / How to get there?

Sie erreichen uns per

You can reach us by

Flugzeug:	über	Flughäfen Berlin (Tegel oder Schönefeld) Flughafen Dresden	**Airplane:**	via	Airports Berlin (Tegel or Schönefeld) Airport Dresden
Bahn:	über	Berlin Dresden Leipzig	**Train:**	via	Berlin Dresden Leipzig
Auto:	über	Berlin A10 Schönefelder Kreuz, A13 Richtung Dresden A15 Richtung Cottbus Abfahrt Cottbus-West	**Car:**	via	Berlin A10 Schönefelder Kreuz, A13 direction Dresden A15 direction Cottbus Exit Cottbus-West
	über	Dresden A4 Kreuz Dresden Nord A13 Richtung Berlin A15 Richtung Cottbus Abfahrt Cottbus-West		via	Dresden A4 Cross Dresden North A13 direction Berlin A15 direction Cottbus Exit Cottbus-West

Brandenburgische Technische Universität Cottbus - Senftenberg